

**On Coastlines and Climate:  
How Basin Geometry Shapes Ocean Circulation  
and Global Climate**

Zho Ragen

A dissertation  
submitted in partial fulfillment of the  
requirements for the degree of

Doctor of Philosophy

University of Washington  
2024

Reading Committee:  
Kyle Armour, Chair  
Luanne Thompson  
Andrew Shao

Program Authorized to Award Degree:  
School of Oceanography

©Copyright 2024  
Zho Ragen

University of Washington

## Abstract

### On Coastlines and Climate: How Basin Geometry Shapes Ocean Circulation and Global Climate

Zho Ragen

Chair of the Supervisory Committee:

Kyle Armour

School of Oceanography, Department of Atmospheric Sciences

This dissertation investigates the role of ocean basin geometry in the circulation of the ocean, of the atmosphere, and in shaping the global climate system as a whole. To explore this topic, a major component of this dissertation is the development of a novel coupled climate model with configurable bathymetry, orography, and coastline geometry.

Here I developed an ocean–atmosphere–sea-ice model that allows the testing of different theories for the development of major hemispheric asymmetries in the climate system. The model can be configured with a wide range of continental configurations. When configured with two ocean basins – one that is narrow and Atlantic-like and one wide and Pacific-like – and forced with zonally uniform atmospheric conditions in an ocean-only setup, the pole-to-pole, cross-equatorial meridional overturning circulation (MOC) and associated northern high latitude deep water formation localizes to the narrower of two ocean basins. This is similar to the ocean circulation in the real world, characterized by an Atlantic meridional overturning circulation (AMOC) and neither deep water formation nor cross equatorial overturning circulation in the Pacific. Widening the narrow basin increases the strength of the overturning circulation, in contrast to previous idealized geometry ocean-only studies. Also,

the shape with which the basin widens matters for the magnitude and pattern by which the MOC strengthens. For instance, maintaining straight, meridional coastlines and widening the ocean basins results in different changes to ocean circulation than widening the ocean basin by creating slanted coastlines.

I show that adding an atmosphere and a land model to form a fully-coupled model reveals vastly different results. Coupling the ocean–sea-ice model to an atmosphere–land model yields a surprising result of cross-equatorial MOC and northern deep water formation in the wide basin. MOC occurs in the wide basin, where negative surface buoyancy fluxes in the northern high latitudes allows for water transformation and deep water formation. Adding a subsurface zonal sill across the basin cuts off dense isopycnals that outcrop in the southern ocean from returning to the surface in the northern wide basin, forcing watermass transformation and deep sinking into the narrow basin.

Idealized continental configurations as explored in this dissertation also allow for the study of meridional heat transport by the ocean and the atmosphere. Differences in top of atmosphere radiation between different continental geometries drive different partitioning of poleward heat transport between the ocean and the atmosphere. The total climate system heat transport also can adjust, due to changes in planetary albedo driven by cloud distribution responses to ocean circulation changes.

We conclude that idealized modeling studies can illuminate key features of ocean and atmosphere circulation. These findings suggest that ocean basin geometry is of primary importance for ocean circulation and setting the mean climate state.

# Contents

<b>1</b>	<b>Background and Motivation</b>	<b>7</b>
<b>2</b>	<b>Methods</b>	<b>9</b>
2.1	Ocean-sea-ice Model . . . . .	10
2.2	Grid Creation . . . . .	10
2.3	Ocean-only Configuration . . . . .	11
2.4	Atmospheric Model . . . . .	11
2.5	Coupled MOM6-AM2 . . . . .	11
<b>3</b>	<b>The Impact of Atlantic Basin Geometry on Meridional Overturning Circulation</b>	<b>12</b>
3.1	Introduction . . . . .	12
3.2	Methods . . . . .	14
3.2.1	Model Description . . . . .	14
3.2.2	Atmospheric forcing . . . . .	16
3.2.3	Continental Configurations . . . . .	18
3.3	Results . . . . .	18
3.3.1	Response to Changes in Continental Configuration . . . . .	18
3.3.2	AMOC Density Scaling . . . . .	27
3.4	Discussion and Conclusions . . . . .	32
<b>4</b>	<b>Revisiting the Role of Ocean Basin Geometry in Atlantic Overturning: the Importance of the North Pacific Basin</b>	<b>36</b>
4.1	Introduction . . . . .	36
4.2	Methods . . . . .	39
4.2.1	Continental Configurations . . . . .	39
4.3	Results . . . . .	41
4.3.1	Localization of Meridional Overturning Circulation . . . . .	41
4.3.2	Comparison of Atmospheric and Oceanic Fields in Configurations with Different North Pacific Basin Geometries . . . . .	43
4.3.3	Moisture fluxes and freshwater transport . . . . .	47
4.3.4	Watermass transformation . . . . .	50
4.4	Discussion & Conclusions . . . . .	52
<b>5</b>	<b>The Impact of Continental Geometries on Mean State Climate and Heat Transport</b>	<b>54</b>
5.1	Model Configurations . . . . .	55
5.1.1	Coupled MOM6-AM2 . . . . .	55
5.1.2	Continental Configurations . . . . .	55
5.2	Results . . . . .	55
5.2.1	Surface Climate . . . . .	55
5.2.2	Overturning Circulation . . . . .	60
5.2.3	Heat Transport . . . . .	64

5.3 Discussion & Conclusions . . . . .	67
<b>6 Conclusions</b>	<b>69</b>

# 1 Background and Motivation

We owe so much to the motion of the ocean. Ocean circulation, as shaped by continental boundaries, imprints on global heat transport, hemispheric temperature asymmetries, cloud distribution and precipitation patterns, ocean basin salinity differences, and the rate and pattern of sea surface temperature (SST) changes under global warming. Moreover, Earth's climate is undergoing a period of rapid change, due primarily to anthropogenic greenhouse gas emissions. Earth's sensitivity to increasing atmospheric greenhouse gas concentrations is strongly mediated by both ocean heat uptake and the interactions between the ocean circulation and atmospheric radiative feedbacks. Thus, understanding the mechanisms by which ocean basin geometry shapes ocean circulation, hemispheric asymmetries in climate, and interactions with the atmosphere is critical for better understanding the global climate system and how it will change in the future.

The oceans play a primary role in shaping regional and global patterns of Earth's climate, particularly in creating large-scale hemispheric asymmetries. Examples of such asymmetries include: differences in the equator-to-pole temperature gradient in the Northern and Southern Hemispheres (Enderton and Marshall 2009); temperature and salinity differences across ocean basins; precipitation patterns (Enderton and Marshall 2009; Green et al. 2017; Donohoe et al. 2013; Frierson et al. 2013). Additionally, localization of deep water formation and meridional overturning in the Atlantic Ocean rather than the Pacific Ocean (Ferreira et al. 2010; Nilsson et al. 2013; Jones and Cessi 2017; Cessi and Jones 2017) creates asymmetries in meridional heat transport (Trenberth and Caron 2001; Enderton and Marshall 2009). Additionally, the climate is undergoing rapid changes due to rising anthropogenic CO<sub>2</sub> concentrations with implications for these climate asymmetries. These changes are modulated by the ocean through its ability to take up heat and carbon; transport and store heat below the surface; and impact global radiative feedbacks (Dong et al. 2019).

Much of the ocean's impact on climate is dependent on circulation patterns that transport ocean properties – such as heat and salt – both laterally and vertically. These circulation patterns are constrained by the geometry of the ocean basins. Previous studies have implicated several different features of ocean basin geometry as important for ocean currents and climate. Meridional boundaries to ocean flow are necessary for the formation of gyres and thus allow for zonal asymmetries and promote meridional heat transport in each ocean basin as well as influencing the partitioning of heat transport between the ocean and atmosphere (Enderton and Marshall 2009). The Drake Passage allows for the Antarctic Circumpolar Current and upwelling in the Southern Ocean, acting to isolate Antarctica from poleward ocean heat transport (Marshall and Radko 2003; Wolfe and Cessi 2011; Ferreira et al. 2010). The narrower width of the Atlantic basin than the Indo-Pacific basin and the shorter southern extent of the African continent compared to the South American continent allow for the development of a salinity gradient between the these two major ocean basins and help localize pole-to-pole cross-equatorial overturning to the Atlantic basin (Warren 1983; Cessi and Jones 2017; Jones and Cessi 2017; Nilsson et al. 2013; Ferreira et al. 2010). The location and shape of mountain ranges may also impact asymmetries in ocean circulation through their influence on surface wind and precipitation patterns (Sinha et al. 2012; Yang and Wen 2020).

Understanding how different features of the global distribution of continents impacts the ocean circulation is difficult. Climate models represent a complex coupled Earth system with rich dynamics and feedbacks. Nevertheless, there is still a gap between the complexity of the planetary system and the complexity possible in a numerical model. The most advanced climate models are still only analogues of the true climate system. It is important also to ensure that the scientific community recognizes the difference between simulating the climate system and understanding the climate system (Held 2005). To test whether climate models represent the physics of the climate system with fidelity, modelers employ a range of different models of varying complexity and spatial scale (Jeevanjee et al. 2017). In this way, it is possible to simplify the problem of understanding the climate system as well as test the robustness of our physical theories.

To ensure that we are moving towards a better understanding of the ocean circulation's role in climate, in this dissertation, we strip out some complexity from a fully coupled general circulation model. To do so, we use a state of the art ocean model coupled to a recent atmosphere model with symmetrized atmospheric aerosols, insolation, and greenhouse gasses, and we replace the land with idealized continents. Models with simplistic representations of the continents can reproduce key features of the global climate. For instance a narrow ridge from pole to pole (*Ridge*), a ridge with an Equatorial Passage (*EqPas*), or a ridge with a Drake Passage (*Drake*), each result in distinct temperature, precipitation, surface freshwater flux, wind stress, ice, and surface heat flux patterns (Enderton and Marshall 2009).

The previous studies investigating the role that ocean basin geometry plays in shaping the large-scale asymmetries in ocean circulation and climate generally use the same climate models. For instance, most of the studies listed above relied on similar components: MITgcm ocean run either on its own or coupled to an idealized atmospheric model, the Simplified Parameterization, Primitive Equation Dynamics (SPEEDY) atmospheric model (Molteni 2003). SPEEDY includes diagnostic cloud parameterizations that define cloud cover and thickness from relative and absolute humidity in the air column. This thesis explores the hypothesis that these prior results are sensitive to the complexity of the atmospheric models because clouds and various cloud feedbacks are a major source of uncertainty in climate models and climate feedbacks (Zhou et al. 2016; Zelinka et al. 2017; Armour 2017; Zelinka et al. 2020). Using an atmospheric model with a more sophisticated representation of clouds should yield further insights into how ocean and atmosphere dynamics create large-scale hemispheric asymmetries. Additionally, previous studies do not focus on the ocean circulation response to basin shape, just basin width and extent.

The goal of the work described in this dissertation is to increase understanding of how the climate system works by revisiting several of the results described above and performing novel studies, related to the role of ocean basin geometry in ocean and climate asymmetries within the framework of a more comprehensive climate model. As the dynamics in the oceans and atmosphere are incredibly complex, simplifying certain aspects of the Earth system can be useful to better understand the climate as a whole. This dissertation outlines a body of work which aims to help narrow this gap in understanding by contributing a model with simple ocean basin geometries in a climate model with state-of-the-art physics.

The overarching goal of this research is to develop a deeper understanding of the role of

oceans in climate by identifying mechanisms through which ocean circulation contributes to major asymmetries in the climate system. To do so, we developed framework for modifying continental configurations in a comprehensive coupled atmosphere–ocean–sea-ice general circulation model (GCM). The main aim is to study how climate depends on the geometry of ocean basins. Questions that guide the research outlined in this dissertation are as follows:

1. How does continental configuration impact the major asymmetries in ocean circulation and global climate? What is the role of ocean circulation in setting global climate? How do clouds and cloud feedbacks influence the global climate?
2. What sets the partitioning of meridional heat transport between the ocean and atmosphere, and how does this partitioning depend on continental configuration?

Additionally, a major goal of this work is to provide the ocean and climate community a new modeling tool that can be used in projects beyond those listed in this dissertation. In the next sections, I will describe the modeling framework developed for this research before outlining the research projects designed to address these questions.

## 2 Methods

The gap between simulation and understanding in climate modeling can be narrowed by creating models of intermediate complexity between simple theoretical models and full global climate models (Held 2005). It is thus useful to employ a range of models of increasing complexity with which to test our understanding of the phenomena at work. Previous work, using idealized GCMs, suggests that modifying continental barriers significantly changes ocean heat transport, atmospheric circulation, and climate (Enderton and Marshall 2009; Ferreira et al. 2010; De Boer et al. 2008; Nilsson et al. 2013; Cessi and Jones 2017; Jones and Cessi 2017). Such idealized GCMs employ simplified representations of the continents in order to test the impacts on ocean circulation of the distribution of barriers to flow in the ocean. In contrast, the GCMs used for climate prediction have been built to include a comprehensive set of physical, chemical, and biological processes and thus include immense levels of complexity that require an enormous amount of computing power for simulations. This complexity is needed to resolve emergent properties of the climate system that emerge from as feedbacks among different components of the climate system. The cost is an inability to develop or test our understanding of the deeper workings of the climate system as it can be difficult to tease apart physical drivers of key features of global circulation.

Previous work using MITgcm coupled to SPEEDY includes a comprehensive ocean model but an atmospheric model with very few vertical layers and simplified clouds compared to modern GCMs. The advantage of this model setup is computational efficiency, but the disadvantage is unrealistic atmospheric responses to changes in ocean circulation. Here we use a comprehensive, fully-coupled GCM that includes components for the ocean, sea-ice, land, and atmosphere. The atmosphere model used here is an older generation than current state of the art versions for the sake of computational efficiency, but, importantly, it includes more vertical levels and more sophisticated cloud processes than SPEEDY. In this dissertation, I employ a relatively under-exploited step in the hierarchy of climate models,

which spans the range of complexity and realism, to examine how continental configuration shapes the ocean’s circulation and, in turn, how ocean circulation governs Earth’s climate and its response to greenhouse gasses. Much of the work for this dissertation has focused on development of a new coupled atmosphere–ocean–sea-ice climate model that uses state-of-the art model components but simplified representations of the continents and ocean basin geometry.

## 2.1 Ocean–sea-ice Model

For the ocean component, I use the Modular Ocean Model version 6 (MOM6) (Adcroft et al. 2019), an open-development project originally written by the Geophysical Fluid Dynamics Laboratory (GFDL). The model is configured with a  $2^\circ$  degree horizontal resolution, 31 vertical levels using a geopotential depth coordinate and a uniformly spaced, bipolar Arakawa C-grid. Seawater density is calculated with the Wright equation of state (Wright 1997).

To balance the momentum input by the wind, a strong bottom drag is applied as a turbulent viscosity in the bottom boundary layer by increasing the non-dimensional drag coefficient by a factor of ten (I use a value of 0.03) over the standard value to account for the lack of bathymetry. Additional vertical turbulence parameterizations include the energetic planetary boundary layer scheme (Reichl and Hallberg 2018) and a small-scale, shear-driven mixing scheme (Jackson et al. 2008). An additional constant background diapycnal diffusivity of  $2.0 \times 10^{-5} \text{ m}^2 \text{ s}^{-1}$  is applied to all simulations. Horizontal eddy effects are parameterized using a uniform background Laplacian horizontal viscosity of  $20,000 \text{ m}^2 \text{ s}^{-1}$ , an eddy isopycnal thickness diffusivity coefficient (after Gent and McWilliams 1990) of  $1,000 \text{ m}^2 \text{ s}^{-1}$ , and an iso-neutral diffusion diffusivity (Shao et al. 2020) of  $1,200 \text{ m}^2 \text{ s}^{-1}$ .

I include interactive sea-ice using the GFDL Sea Ice Simulator version 2 (SIS2) (Adcroft et al. 2019). SIS2 includes full ice dynamics with an elastic-viscous-plastic rheology and calculates the concentration, thickness, brine content, and snow cover of sea ice.

## 2.2 Grid Creation

Model grids for the different continent configurations are generated using a Python script developed for this research (Ragen et al. 2024).

There are land caps at both poles down to  $70^\circ$  to avoid the convergence of longitude lines in the ocean and, as such, preserve numerical stability. The ocean is of uniform depth with vertical sidewall boundaries. In coupled runs, the ocean is 4000 m deep. These specific conditions were chosen for these projects, but are all configurable. For instance, the model does support a tripolar grid and the ocean can support more complex bathymetry or sidewall shapes.

The topography and bottom bathymetry are prescribed by choosing a uniform depth for the ocean and designating latitude and longitude ranges for land, which has a depth of 0 m, but which can be customized. Running this script generates ocean, atmosphere, and land grids, as well as the topography. A critical step executed during the running of this bash script is

the use of GFDL’s FMS NC-Tools to create grid mosaics so fluxes can be exchanged between different model components.

Using this script allows us to set up novel model configurations with a wide range of idealized continental geometries.

### 2.3 Ocean-only Configuration

In Chapter 3, I run MOM6 in an ocean-only mode with atmospheric forcing that is derived from the Coordinated Ocean-ice Reference Experiments (CORE) corrected normal year of forcing version 2.0 (CNYF2) for ocean-ice simulations (Large and Yeager 2004). Land points in the CNYF2 dataset are masked before a zonal average is taken. To ensure that the forcing is hemispherically symmetric, I mirror the Southern Hemisphere data across the equator but maintain a seasonal cycle by lagging the Northern Hemisphere by 6 months. I apply this same procedure to all surface fields: shortwave radiation, longwave radiation, precipitation, 10-m meridional wind speed, and 10-m air temperature. The surface forcings are calculated using bulk formulae (Fairall et al. 2003) from the modified atmosphere fields. The ocean is 5000 m deep, whereas in the coupled model the ocean is 4000 m deep, but this does not significantly impact the model results.

### 2.4 Atmospheric Model

The atmospheric model used in these simulations is GFDL’s AM2 (GFDL et al. 2004). This model has a resolution of  $2^\circ$  latitude  $\times 2.5^\circ$  longitude. AM2 uses a hybrid vertical coordinate; sigma surfaces near the ground continuously transform to pressure surfaces above 250 hPa. There are 24 vertical levels with the lowest model level about 3.5 m above the surface.

Atmospheric gasses and aerosols are symmetrized about the equator to ensure that hemispheric asymmetries are a result of model dynamics rather than atmospheric forcing. CO<sub>2</sub> is set to pre-industrial levels (284 ppm). AM2 includes a fully prognostic cloud scheme with cloud microphysics (Rotstayn 1997) and cloud macrophysics (Tiedtke 1993) parameterizations. AM2 differentiates between cloud liquid and cloud ice and also considers convective effects.

The GFDL land model, LM2, is included in the coupled model (GFDL et al. 2004). I modified LM2’s river-routing scheme to direct excess water to the nearest ocean grid point (following Maroon 2016).

### 2.5 Coupled MOM6-AM2

In Chapters 4 and 5, I run MOM6-SIS2 coupled to AM2-LM2. In these simulations, the atmosphere is allowed to respond to changes in the ocean which result from different continental geometries. This is a significant departure from the ocean-only model configuration, in which climatological differences between the distinct continental geometries arise solely from changes in ocean circulation. In the coupled configuration, climatological differences between continental geometries are influenced by changes in both the ocean and atmosphere

circulation as well as feedbacks between the two. Fluxes are exchanged between the ocean–sea-ice and atmosphere-land component models by the GFDL Flexible Modeling System (FMS) coupler (Balaji 2012). FMS allows for conservative exchange of information between separate model components and parallel processing of inputs and outputs as well as across multiple computers. For the coupled model, the ocean depth is uniformly 4000 m.

### 3 The Impact of Atlantic Basin Geometry on Meridional Overturning Circulation

This chapter has been published as: Ragen, S., Armour, K. C., Thompson, L., Shao, A., & Darr, D. (2022). The Role of Atlantic Basin Geometry in Meridional Overturning Circulation. *Journal of Physical Oceanography*, 52(3), 475-492.

#### 3.1 Introduction

The global ocean circulation exhibits several large-scale hemispheric asymmetries, including, perhaps most notably, the deep water formation and ventilation down to 2000 m at northern high latitudes that is present in the North Atlantic but absent in the North Pacific (Ganachaud and Wunsch 2000; Lumpkin and Speer 2007; Talley 2008; Buckley and Marshall 2016; Ferreira et al. 2018). The deep water formation in the North Atlantic is linked to the large-scale overturning circulation that crosses the equator in the Atlantic. In the high-latitude North Atlantic, shallow warm, salty water is cooled at the surface and sinks, forming North Atlantic Deep Water, which flows southward at depth. This water upwells in the Southern Ocean, drawn up by westerlies (see Marshall and Speer 2012; Buckley and Marshall 2016, for reviews). Some of the upwelled water flows northward across the equator in the Atlantic, sustaining the Atlantic Meridional Overturning Circulation (AMOC). In contrast, the Pacific is characterized by an absence of deep ventilation, a weak abyssal overturning circulation, and shallow wind-driven subtropical cells (Ganachaud and Wunsch 2000).

Northward heat transport occurs at all latitudes in the Atlantic basin and peaks at about 1.2 PW near 20°, over half of which is accomplished by AMOC, defined as the zonally-integrated meridional currents in the Atlantic (Trenberth and Caron 2001; Talley 2003; Ferrari and Ferreira 2011). This northward heat transport is partially responsible for the warmer average temperature of the Northern Hemisphere as compared to the Southern Hemisphere (Vellinga and Wood 2002; Kuhlbrodt et al. 2007) and for the peak in zonal-mean rainfall residing north of the equator (Frierson et al. 2013; Marshall et al. 2014). It also influences regional climates of North America and Europe (Sutton and Hodson 2005; Kaspi and Schneider 2011; Woollings et al. 2012). Thus, AMOC plays a key role in setting up hemispheric asymmetries in climate. AMOC strength is linked to the warming hole in the North Atlantic (Drijfhout et al. 2012) as well as to the depth of ocean heat storage and the global transient response to climate change (Winton et al. 2013; Kostov et al. 2014). Moreover, AMOC is also important for the distribution of carbon and nutrients in the ocean (Sabine et al. 2004; Watson et al. 2015; Smethie Jr and Fine 2001) that are linked to the geography of marine ecosystems in

the Atlantic (Schmittner et al. 2005).

Despite the prominent role large-scale meridional overturning plays in the global climate system, consensus has yet to emerge regarding its controlling mechanisms or the reason for its localization to the Atlantic basin (Ferreira et al. 2018). The deep ventilation in the Atlantic is linked to the higher salinity of the Atlantic basin (Warren 1983), explanations for which fall into two broad categories: atmosphere-driven salinity asymmetries due to differences in net surface freshwater fluxes (precipitation minus evaporation) and ocean-driven salinity asymmetries due to circulation and salt transport. Smaller atmospheric freshwater input is thought to account for about half the difference in the mean sea-surface salinity between the Atlantic and the Pacific (Ferreira et al. 2018). The narrower width of the Atlantic relative to the rainfall fetch for water evaporated over both ocean basins leads to higher precipitation over the Pacific than over the Atlantic (Ferreira et al. 2010). The Atlantic basin also has more evaporation per unit area than the Pacific basin (Warren 1983; Nilsson et al. 2013). Ocean circulation may also play a role in the higher salinity, and thus localization of AMOC, in the Atlantic basin. These studies have predominantly explored the sensitivity to basin width (zonal extent) and basin length (meridional extent) using idealized continents with straight coastlines to separate a narrower, Atlantic-like basin from a wider Pacific-like basin. Such a configuration leads to a saltier Atlantic-like basin, which in turn leads to the localization of meridional overturning to the Atlantic, both in coupled (Ferreira et al. 2010; Nilsson et al. 2013) and in ocean-only simulations using zonally-uniform atmospheric forcing (Cessi and Jones 2017; Jones and Cessi 2017). Moreover, the wider the basin, the smaller the meridional gradient in evaporation minus precipitation must be to shut off northern high latitude convection, thus making a narrower basin more likely to support deep convection than a wider basin (Youngs et al. 2020).

Changing the width of the Atlantic-like basin in simulations with idealized forcing and geometry has been shown to change the the strength of AMOC. Ocean-only simulations using zonally-uniform atmospheric forcing suggest that widening the Atlantic-like basin leads to a weaker AMOC (Jones and Cessi 2017; Youngs et al. 2020). Jones and Cessi 2017 hypothesize a mechanism for this result: because gyre transport scales with basin width (Sverdrup 1947), narrower basins have weaker southward flowing subpolar western boundary currents than wider basins do. There is also a northward component of the western boundary velocity associated with the meridional overturning circulation, the strength of which is independent of basin width. In a narrower basin, the wind-driven subpolar western boundary component is weaker than the northward AMOC-associated velocities, allowing salty subtropical water to flow north into the subpolar gyre, which acts to weaken stratification in the northern subpolar region, allowing deep ventilation in the narrow basin.

A different theoretical argument suggests that widening the basin could lead to larger meridional ocean transport since wider basins have a larger effective isopycnal diffusivity associated with wind-driven gyre and mesoscale eddy transport (Wang et al. 1995; Rose and Marshall 2009; Nilsson et al. 2021). Thus, in a wider basin, the northward eddy-induced transport of heat and salt across the boundary between the subtropical and subpolar gyre causes competing effects on the high latitude surface density by allowing relatively warm, salty water to flow farther north than in a narrow basin. If the surface temperatures are low in the

northern sinking region, the salinity effects can dominate the temperature effects, increasing the density of the surface water and increasing the overturning strength.

Additionally, the meridional extent of the continents favors salt transport into the Atlantic basin from the Indian Ocean, increasing the salinity of the Atlantic over the Indo-Pacific and thus contributing to a preference for deep convection in the Atlantic (Reid Jr 1961; Sijp and England 2009; Nilsson et al. 2013; Cessi and Jones 2017).

As reviewed above, theories exist that predict both an increase and a decrease in AMOC strength in response to a widening of the Atlantic-like basin. It is also reasonable to expect that the shape of the Atlantic as a function of latitude could impact the structure and strength of AMOC through interactions with the Sverdrup gyre transport at different latitudes. That is, the structure and strength of AMOC could depend on basin width at different latitudes – the shape of the basin. Additionally, widening the ocean basin by a constant number of degrees longitude (as in Jones and Cessi 2017) results in a larger increase in width in the tropics as compared with higher latitude regions, thus increasing the Sverdrup transport in the subtropical and subpolar regions unequally. This raises a key question: how does the AMOC depend on the shape of the Atlantic basin coastlines?

Here, we explore this question using a state-of-the-art ocean–sea-ice model with idealized, zonally-symmetric surface forcing under a range of idealized continental configurations with different Atlantic coastlines. Following previous studies, we examine the ocean circulation within an ocean-only simulation that has a large Pacific-like basin and a small Atlantic-like basin. However, we go beyond these previous studies by exploring five different coastline geometries that impart different shapes to the Atlantic basin (Fig. 3.1). Using these simulations, we examine how Atlantic basin geometry influences the strength and structure of AMOC. While sensitivity of AMOC to the shape of the coastlines in our simulations is observed, no clear mechanisms emerge that link the two. In the later half the study, we thus evaluate a scaling for AMOC based on the meridional density gradient along the western boundary and use this scaling to understand the causes of the AMOC changes.

## 3.2 Methods

This section describes the physical configuration of the model components, the atmospheric forcing, and the five different continental configurations used (Fig. 3.1).

### 3.2.1 Model Description

We use the most recent version of the Modular Ocean Model (MOM6) (Adcroft et al. 2019), an open-development project originally developed by the Geophysical Fluid Dynamics Laboratory (GFDL). The model is configured with a  $2^\circ$  degree horizontal resolution, 31 vertical levels using a geopotential, or  $z^*$  coordinate, and a uniformly spaced, bipolar grid. There are land caps at both poles from  $70^\circ$  to  $90^\circ$  to avoid the convergence of longitude lines in the ocean. The ocean is uniformly 5000m deep with purely vertical sidewall boundaries. Our MOM6 configuration uses the Wright equation of state to calculate seawater density (Wright 1997). The model does not form Antarctic Bottom Water in these idealized configurations, rather the deepest mixed layers are in the northern Atlantic-like basin.

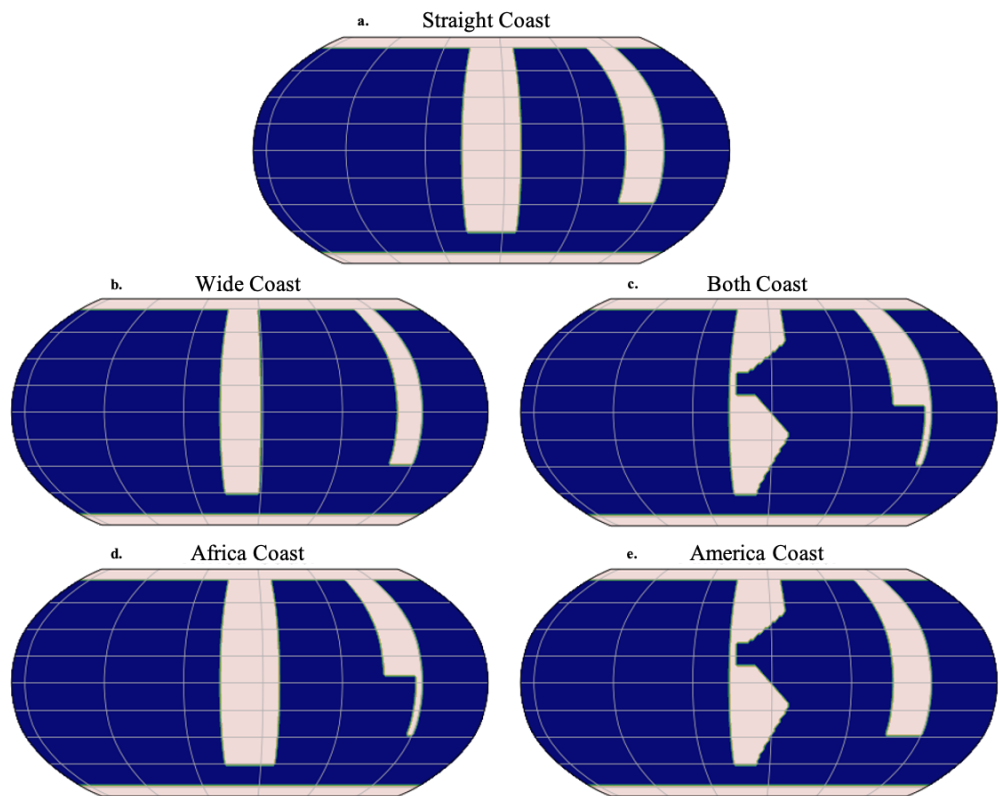


Figure 3.1: Continental configurations for each of the simulations. Grey regions indicate land, blue indicates ocean. The land boundaries are vertical and the ocean is everywhere 5000 m deep and devoid of bathymetry.

To balance the momentum input by the wind, a strong bottom drag is applied as a turbulent viscosity  $\nu_{BBL}$  in the bottom boundary layer according to  $\nu_{BBL} = c_d |u| u$ , where  $c_d$  is a non-dimensional drag coefficient (we use a value of 0.03, a ten-fold increase over the standard value to account for the lack of bathymetry) and  $u$  is the velocity in the bottom boundary layer. Additional vertical turbulence parameterizations include the energetic planetary boundary layer scheme (Reichl and Hallberg 2018) and a small-scale, shear-driven mixing scheme (Jackson et al. 2008). A constant background diapycnal diffusivity of  $2.0 \times 10^{-5} \text{ m}^2 \text{ s}^{-1}$  is equal across simulations. Horizontal eddy effects are parameterized using a uniform background Laplacian horizontal viscosity of  $20,000 \text{ m}^2 \text{ s}^{-1}$ , an eddy isopycnal thickness diffusivity coefficient (after Gent and McWilliams 1990) of  $1,000 \text{ m}^2 \text{ s}^{-1}$ , and an iso-neutral diffusion diffusivity (Shao et al. 2020) of  $1,200 \text{ m}^2 \text{ s}^{-1}$ .

Unlike in previous idealized studies of the dependence of AMOC on basin geometry, here we include interactive sea-ice using the GFDL Sea Ice Simulator version 2 (SIS2) (Adcroft et al. 2019). SIS2 includes full ice dynamics with an elastic-viscous-plastic rheology and calculates the concentration, thickness, brine content, and snow cover of sea ice.

### 3.2.2 Atmospheric forcing

We run the ocean-sea-ice model with atmospheric forcing that is derived from the Coordinated Ocean-ice Reference Experiments (CORE) corrected normal year of forcing version 2.0 (CNYF2) for ocean-ice simulations (Large and Yeager 2004). In order to guarantee that asymmetries between basins and differences between model simulations arise solely from ocean circulation and sea ice, we mask out land points in the CNYF2 dataset then perform a zonal average across all longitudes. To ensure that the forcing is hemispherically symmetric, we mirror the Southern Hemisphere data across the equator but maintain a seasonal cycle by lagging the Northern Hemisphere by 6 months. We apply this same procedure to all surface fields: shortwave radiation, longwave radiation, precipitation, 10-m meridional wind speed, and 10-m air temperature (all shown in Fig. 3.2). The surface forcings are calculated using bulk formulae (Fairall et al. 2003) from the modified atmosphere fields.

Sea level pressure is taken to be a constant, globally uniform value of 101 kPa. Wind speed is purely zonal in direction with meridional wind speeds set to zero everywhere. From the land caps to  $50^\circ$  N and S, the wind speed profiles are smoothed with a Savitsky-Golay filter using a 5th-order polynomial to allow wind speed to go smoothly to zero at the edge of the polar land caps.

Surface salinity flux adjustment is necessary to account for net nonzero freshwater flux at the surface arising from nonzero global precipitation minus evaporation ( $P - E$ ). To maintain conservation of fresh water,  $P - E$  is adjusted by scaling with a virtual precipitation at each coupling timestep to ensure a globally-integrated net zero freshwater flux while maintaining the correct pattern of global  $P-E$ .

The simulations (Fig. 3.1) start from rest and are integrated for 1,000 365-day years to equilibrium. Temperature and salinity are initiated from zonally-averaged fields derived from a MOM6 aquaplanet simulation without continents. We perform all analyses on model climatologies produced by the last 100 years of the runs, and as such, we do not discuss

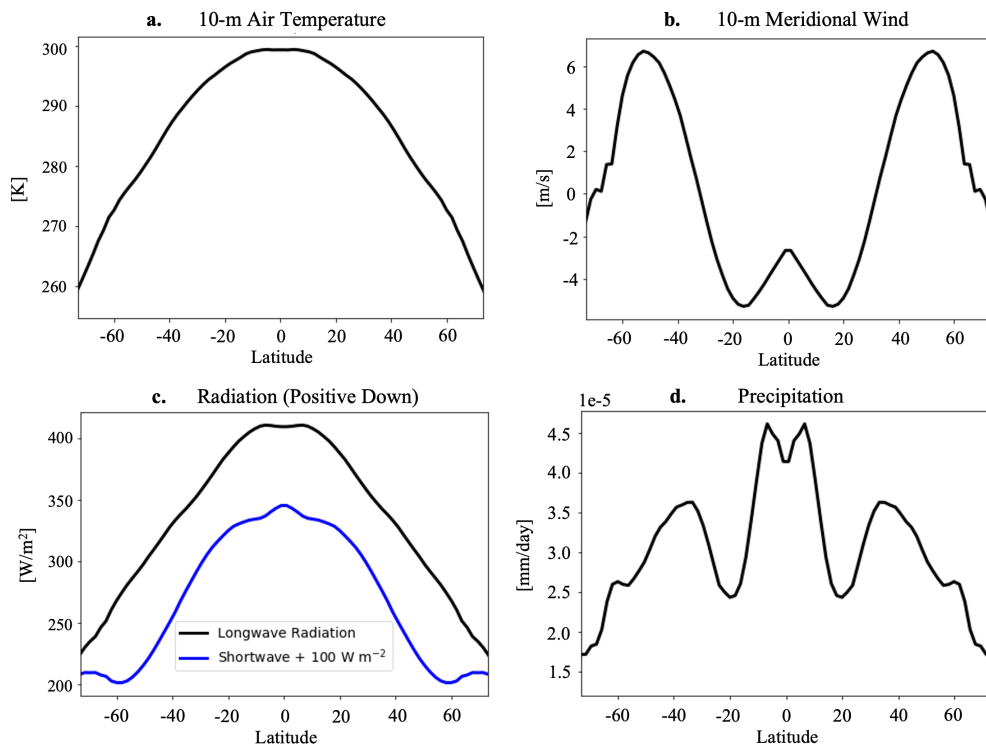


Figure 3.2: Annual mean values of the modified CORE Normal Year Forcing 2.0 used to force the ocean – sea-ice model. (a) 10-m air temperature, (b) 10-m meridional wind speed, (c) downwelling shortwave radiation and downwelling longwave radiation, and (d) precipitation.

Simulation	Mean Atlantic Width	Mean North Atlantic Width 20- 60°N ( $L_x$ )	Atlantic Basin Area	Global Ocean Area
Straight Coast	7200 km	6700 km	$0.87 \times 10^8 \text{ km}^2$	$4.0 \times 10^8 \text{ km}^2$
Both Coast	9400 km	8200 km	$1.1 \times 10^8 \text{ km}^2$	$4.3 \times 10^8 \text{ km}^2$
Wide Coast	9300 km	8700 km	$1.1 \times 10^8 \text{ km}^2$	$4.3 \times 10^8 \text{ km}^2$
America Coast	8500 km	8200 km	$1.0 \times 10^8 \text{ km}^2$	$4.2 \times 10^8 \text{ km}^2$
Africa Coast	8100 km	6700 km	$0.98 \times 10^8 \text{ km}^2$	$4.1 \times 10^8 \text{ km}^2$

Table 3.1: List of model configuration names, average Atlantic-like basin width from the southern tip of the African continent, average Atlantic-like basin width between 20°N and 60°N ( $L_x$  in Eqn. 3), and Atlantic-like basin area, and Global Ocean Area.

variability in the runs. The only difference between each model simulation is the continental geometry along the Atlantic basin.

### 3.2.3 Continental Configurations

Each of the five simulations has two meridional continents and two ocean basins: one wide, Pacific-like basin and one narrow, Atlantic-like basin (Fig. 3.1). In all cases, the western boundary of the Atlantic-like basin terminates at 55°S and the eastern boundary of the Atlantic-like basin terminates at 35°S. The simplest of our basin configurations, *Straight Coast*, features straight, meridional coastlines (Fig. 3.1a). *Wide Coast* widens the Atlantic-like basin while keeping the boundaries strictly meridional (Fig. 3.1b). *Both Coast* widens the Atlantic-like basin by the same average area as *Wide Coast* but does so by cutting out idealized shaped coastlines on both sides of the basin to resemble the east coast of the Americas and the west coast of Africa. *Africa Coast* has an Eastern boundary shape that is modified to resemble the African west coast to explore the effect of changing only the shape of the eastern boundary (Fig. 3.1d). *America Coast* has a Western boundary shape that is modified to resemble the east coast of the Americas to explore the effect of changing only the shape of the western boundary (Fig. 3.1e). The average width and area of the Atlantic-like basin for each configuration is listed in Table 3.2.3.

## 3.3 Results

### 3.3.1 Response to Changes in Continental Configuration

The *Straight Coast* is chosen as our reference case experiment because its average Atlantic-like width and area are similar to the real Atlantic ocean while the other configurations represent a widening of the Atlantic-like basin compared to *Straight Coast*. *Straight Coast* shows patterns of sea-surface temperature (SST) and sea-surface salinity (SSS) that are similar to what is observed in the world oceans: SST is highest in the tropics and decreases

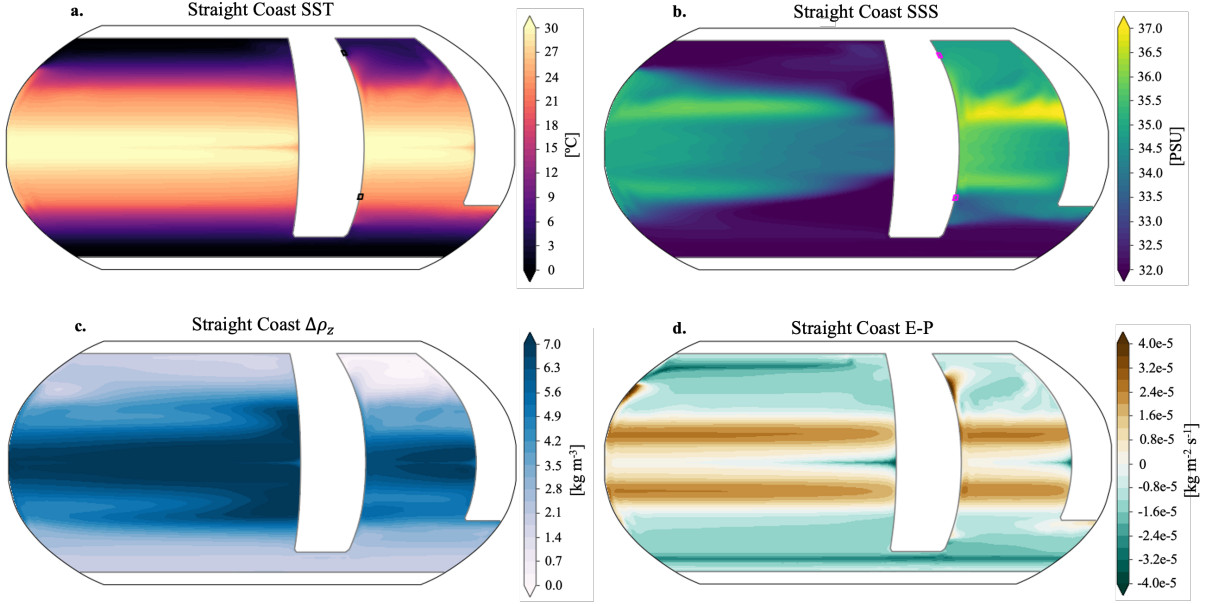


Figure 3.3: Maps of (a) sea surface temperature, (b) sea surface salinity), (c) difference in density between 1000m and the surface,  $\Delta\rho_z$ , and (d) evaporation minus precipitation for the *Straight Coast* continental configuration.

towards the poles; there is an equatorial cold tongue where water upwells to the surface; and SSTs in the northern high latitudes are higher in the small, Atlantic-like basin than in the large, Pacific-like basin by about 5°C (Fig. 3.3a). The salinity has maxima in the subtropical regions and minima in the tropics and subpolar to polar regions (Fig. 3.3b) and is elevated in the small Atlantic-like basin by about 3 PSU compared to the large basin at 60°N. The north Atlantic-like basin is also less stratified than the north Pacific-like basin. The difference in density between 100m and the surface,  $\Delta\rho_z$  is smaller in the narrow basin than the large basin (Fig. 3.3c). While the precipitation is supplied as a boundary condition (Fig. 3.2d), the evaporation is allowed to evolve and follows a similar pattern to the SST. The evaporation minus the precipitation (Fig. 3.3d) highlights the subtropics as a region of excess evaporation while the subpolar regions and the equatorial cold tongues have more precipitation.

Consistent with previous studies (e.g. Ferreira et al. 2010; Nilsson et al. 2013; Cessi and Jones 2017; Jones and Cessi 2017), we find deep water formation in the northern Atlantic-like basin (Fig. 3.4a) but not in the Pacific-like basin. A strong cross-equatorial meridional overturning circulation exists in the small, Atlantic-like basin, while a weaker, counter-rotating deep cell penetrates into the large, Pacific-like basin (Fig. 3.4b). Sea-ice is present year-round in the Southern Ocean and in the Northern Pacific-like basin, while in the Northern Atlantic-like basin a negligible amount of sea ice forms during the winter.

To compare sea-surface properties across cases, we subtract the zonal mean of SST and SSS for *Straight Coast* from each configuration. The *Both Coast* Atlantic-like basin SST is warmer than *Straight Coast* by about 3°C (Fig. 3.5a) and the northern high latitude SSS in

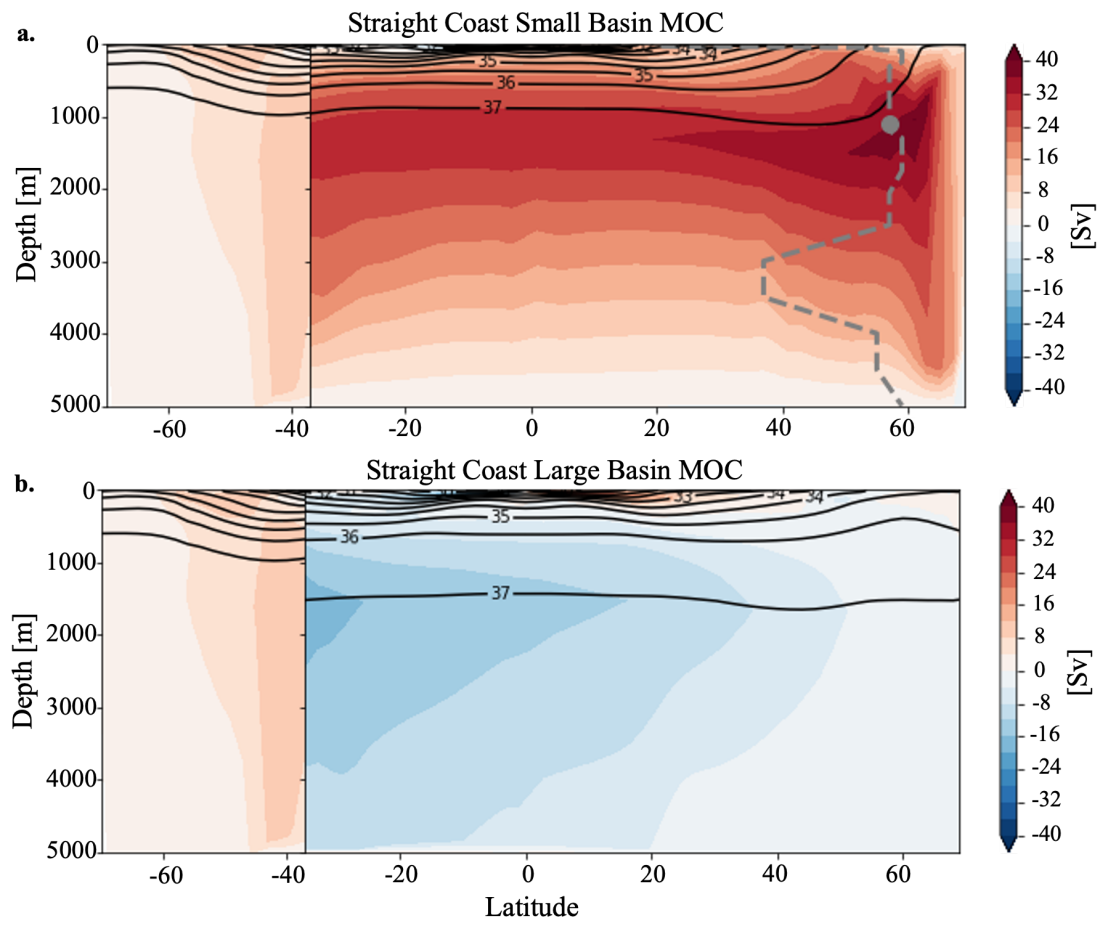


Figure 3.4: Meridional overturning circulation (MOC) for the Straight Coast case in (a) the small, Atlantic-like basin and (b) the large, Pacific-like basin. The southern ocean region in both plots shows the streamfunction integrated over all longitudes.

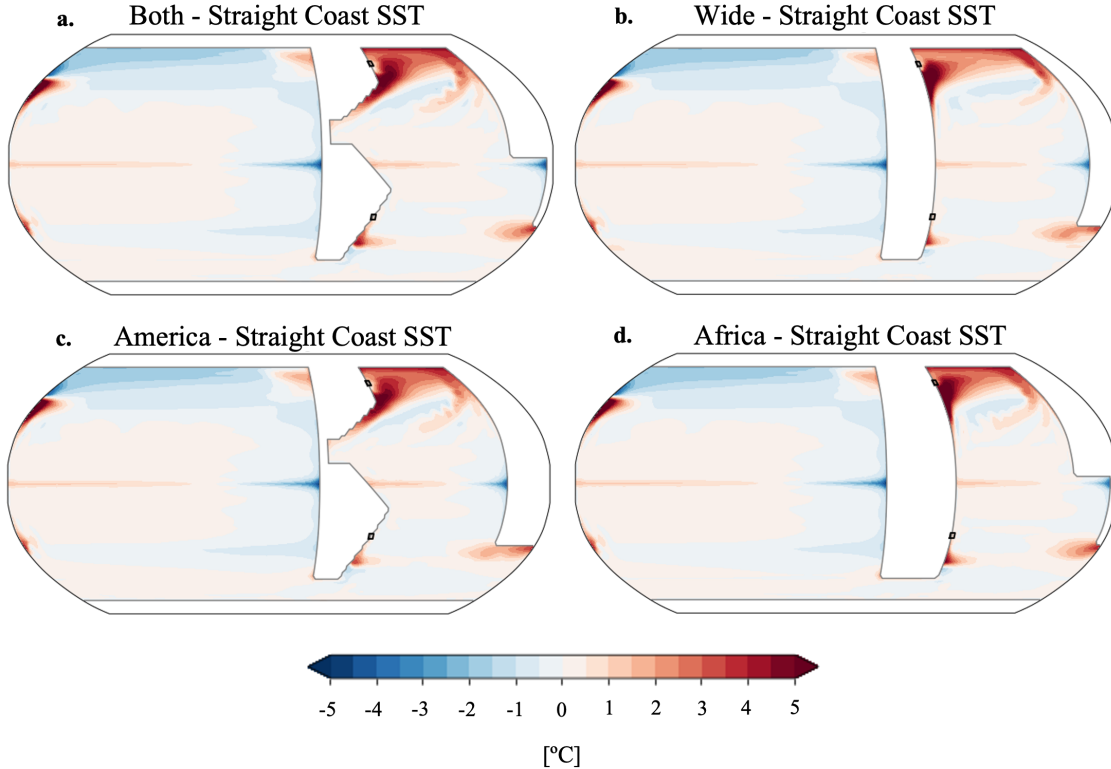


Figure 3.5: Climatological SST anomalies from *Straight Coast* global zonal mean SST for (a) *Both Coast*, (b) *Wide Coast*, (c) *America Coast*, and (d) *Africa Coast*.

the Atlantic-like basin is 2 psu larger than *Straight Coast* (Fig. 3.6a). For *Wide Coast*, the northern Atlantic-like basin SST is about 2°C warmer than for *Straight Coast* (Fig. 3.5b) and the basin SSS is about 2 psu larger (Fig. 3.6b). Cases with shaped western boundaries results in lower eastern equatorial SSS than cases without.

The *Both Coast*, *America Coast* and *Africa Coast* simulations all show similar SST and SSS anomalies (taken relative to *Straight Coast*). In the narrow basin, *America Coast* and *Africa Coast* have warmer SSTs than *Straight Coast* and show a pattern of zonal mean differences in SST from *Straight Coast* that is very similar to *Both Coast* (Fig. 3.5c,d). The pattern of SSS changes in *America Coast* are similar to the changes in *Both Coast* with decreases in the eastern tropics and increases in the northern subpolar region (Fig. 3.6c). The SSS in *Africa Coast* shows a similar pattern to *America Coast*, but with a smaller decrease in SSS in the eastern tropics than *America Coast* and *Both Coast* (Fig. 3.6d). These changes in SST and SSS result in a small density increase in the northern high latitudes in the narrow basin.

The changes between configurations can be seen deeper in the water column as well. Changes in the zonal mean density difference between 1000m and the surface,  $\Delta\rho_z$ , relative to what is seen in *Straight Coast* reveal differences in stratification between configurations (Fig. 3.7). The stratification in *Straight Coast* is weakest in the northern part of the basin, near 60°N

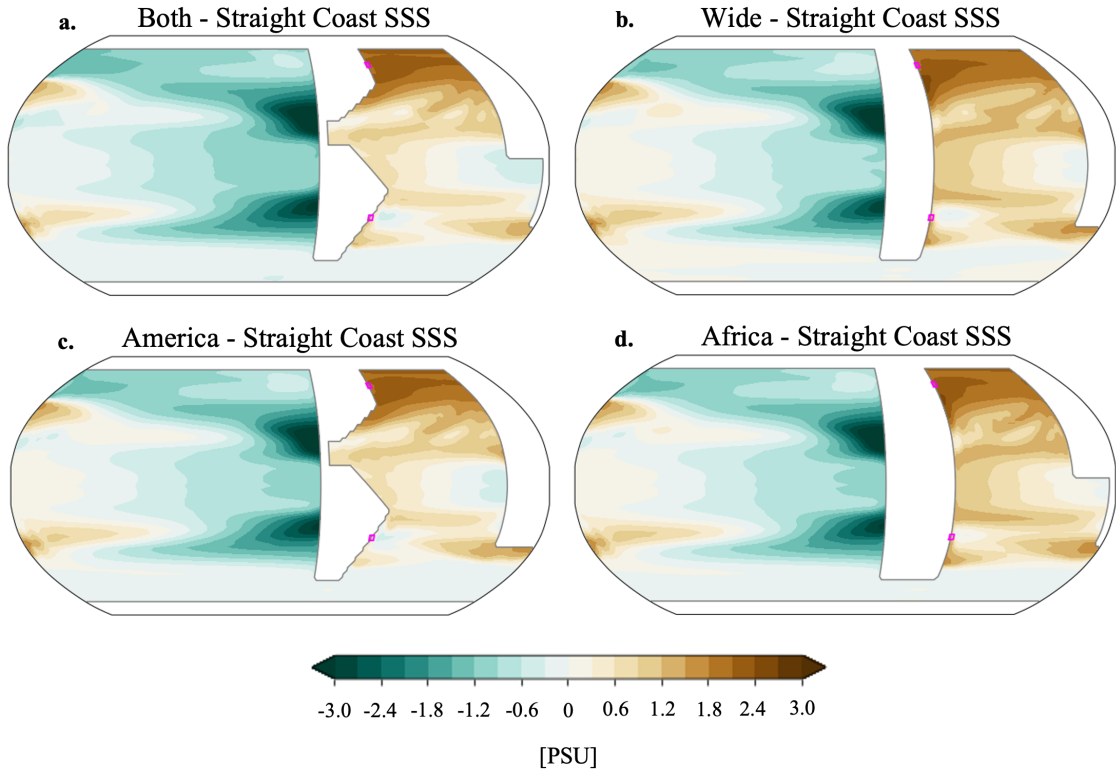


Figure 3.6: Climatological sea surface salinity (SSS) anomalies from zonal mean *Straight Coast SSS* for (a) *Both Coast*, (b) *Wide Coast*, (c) *America Coast*, and (d) *Africa Coast*.

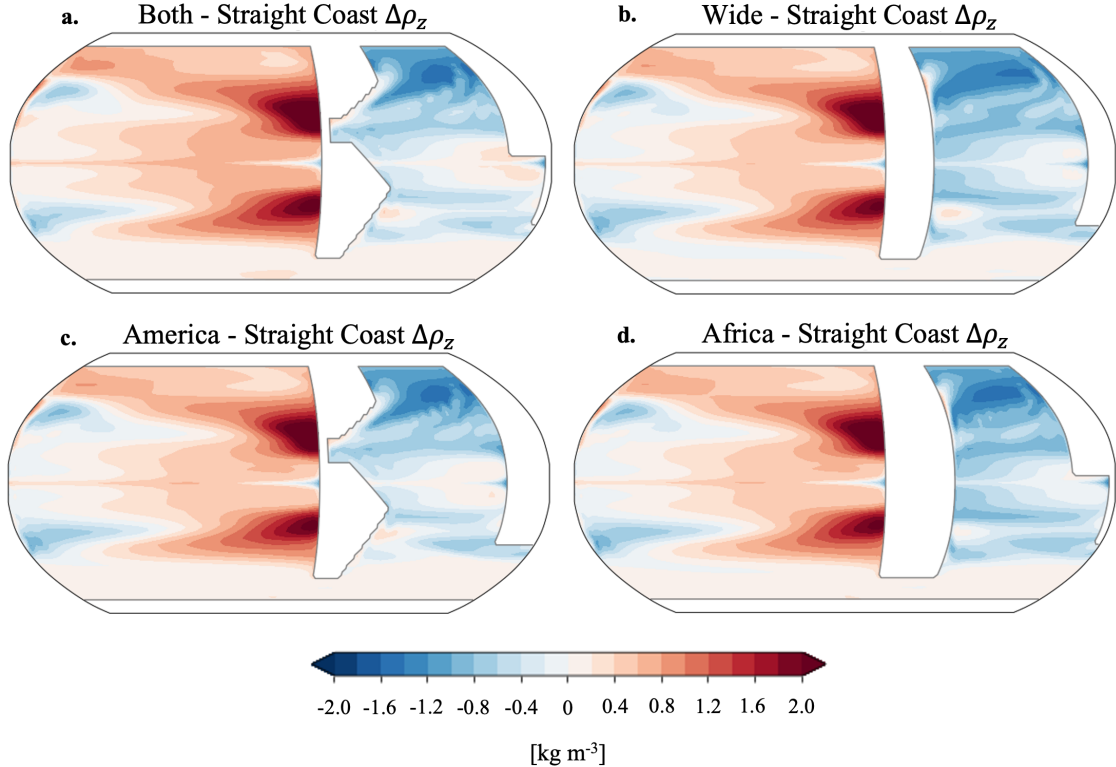


Figure 3.7: Climatological  $\Delta\rho_z$  (differences in density between 1000m and the surface) anomalies from zonal mean *Straight Coast* SSS for (a) *Both Coast*, (b) *Wide Coast*, (c) *America Coast*, and (d) *Africa Coast*.

(Fig. 3.7a). In all of the other configurations (Fig. 3.7b-e), the stratification decreases over the majority of the Atlantic-like basin, with the largest differences in the subpolar regions just south of  $60^{\circ}\text{N}$ . Generally, each of the other cases is warmer, saltier, and more weakly stratified than *Straight Coast*, making the northern Atlantic-like basin more favorable for deep ventilation.

In each of the configurations, deep ventilation and cross-equatorial model meridional overturning circulation (MOC) are confined to the Atlantic-like basin. Deep water formed at the northern edge of the basin flows southward at depth. It upwells in the Southern Ocean and is replenished by northward flowing shallow water (Fig. 3.4). MOC is calculated on isopycnal surfaces and remapped to depth space for plotting purposes. As in previous studies, the MOC is localized to the narrower basin with a eastern boundary that terminates north of the zero wind stress line in the Southern Hemisphere (Ferreira et al. 2010; Nilsson et al. 2003; Cessi and Jones 2017; Jones and Cessi 2017; Youngs et al. 2020). This can be attributed to the higher salinity of the narrow basin driven by higher evaporation over the warmer SSTs in our simulations. In turn, the warmer SSTs in the narrow basin are due to changes in ocean circulation from changing the geometry of the ocean basin.

While surface conditions look similar across each configuration, small changes in stratification

in the northern Atlantic-like basin (Fig. 3.7) are enough to drive significant changes in the meridional overturning circulation (Fig 3.8). In *Both Coast*, the overturning in the Atlantic-like basin shoals compared to *Straight Coast* (Fig. 3.8a) with MOC increasing near the surface and decreasing at depth. At 1000 m and 60°N, *Both Coast* MOC is larger by about 6 Sv. In addition, the MOC in *Both Coast* (which has more realistic coastlines than *Straight Coast*) more closely represents the canonical AMOC – the model MOC shoals to allow for a deep, counter-clockwise overturning cell. The increase in MOC for both *Wide Coast* and *Both Coast* differs from Jones and Cessi 2017 who found an increase in basin width resulted in an overall decrease in AMOC strength (see Discussion and Conclusions). MOC in *Wide Coast* is larger than in *Straight Coast*, particularly below 1500 m, with the exception of a small region of weaker circulation at the northern edge of the basin near the surface (Fig. 3.8b). At 1000 m and 60°N, the depth and latitude of maximum MOC, the *Wide Coast* MOC is larger than *Straight Coast* MOC by 10 Sv (Table 3.2, Fig. 3.9).

Changing the shape of the western boundary, as represented by *America Coast*, results in an increased MOC strength and a MOC deepening (Fig. 3.8c). However, changing the eastern boundary, as in *Africa Coast*, results in a shoaling of the MOC (Fig. 3.8d) and larger changes in the abyssal ocean circulation than in the upper ocean. The changes in MOC in *Both Coast* reflect the impact of a shaped western boundary and a shaped eastern boundary. The simple linear summation of the magnitudes of the maximum MOC anomaly (relative to *Straight Coast*) from *Africa Coast* and *America Coast* is similar to that of *Both Coast* – 6.6 Sv versus 6.3 Sv, respectively. This linearity also holds for the vertical and meridional structure of MOC, which allows us to attribute anomalies in the *Both Coast* simulation to either one coastline or the other. Changing the western boundary shape results in much larger differences in MOC strength than changing the eastern boundary shape.

As the overturning circulation in the small, Atlantic-like basin responds to changes in coastline shape, the overturning in the abyssal large, Indo-Pacific-like basin acts to compensate those changes, such that as AMOC increases, the deep Indo-Pacific overturning decreases (Sun et al. 2020). Here, in response to a strengthening of MOC in the Atlantic-like basin, the deep overturning streamfunction associated with upwelling in the large, Indo-Pacific-like basin intensifies, bringing more deep water northward and more intermediate water southward (Fig. 3.8e-h).

Widening the Atlantic-like basin with straight coastlines (*Wide Coast*), results in a different change in MOC than widening the Atlantic-like basin by changing the shape of the coastlines (*Both Coast*), despite equal basin-average widths over the length of the basin (between 35°S and 70°N). Thus, changes in MOC strength cannot be predicted based on changes in average basin width alone – the shape of the basin boundaries also matters. Differences in coastline shape along the Atlantic-like basin lead to distinct sea-surface properties and meridional overturnings in each experiment. Moreover, widening the Atlantic by changing the shape of the eastern boundary of the basin results in distinct impacts on sea-surface properties, MOC, and abyssal circulation as compared to widening the Atlantic by changing the shape of the western boundary. Indeed, the shape of the basin, or more specifically the shape of the western and eastern coastlines along the basin, is just as important if not more important than the width of the basin, even when taking into account the change in width

with latitude. We performed an additional simulation in which we mirrored the realistic American coastline onto the African continent (while leaving a straight western boundary); this configuration (not shown) produces a vastly different AMOC than the *America Coast* configuration, consistent with our above findings that the shape of the coastlines – rather than simply the basin width – influences the structure and strength of AMOC.

Deep ventilation and associated MOC are localized to the narrow basin due to its elevated salinity compared to the wide basin. At equilibrium, the transport of freshwater into an ocean basin must balance the total integrated surface freshwater flux over the basin. Thus, to examine the drivers of salinity differences between runs with different continental configurations, we calculate the freshwater transport into the Atlantic-like basin by integrating the surface freshwater terms:  $F = \int_{y_S}^{y_N} \int_{x_W}^{x_E} (E - P) dx dy$ , where  $E - P$  is the net surface freshwater balance including evaporation, precipitation, runoff, and ice melt in units of  $\text{m s}^{-1}$ . The integral extends from the western ( $x_W$ ) to the eastern ( $x_E$ ) boundaries of the Atlantic-like basin and from the southern boundary of the basin ( $y_S = 30^\circ\text{S}$ ) to the northern ( $y_N$ ) continental boundary, as it is the freshwater transport at the southern boundary of the basin which is most relevant for the stability of MOC (Rahmstorf 1996).

Values for the Atlantic-like basin freshwater transport at  $30^\circ\text{S}$  are listed in Table 3.2. While configurations with narrower mean Atlantic widths and smaller Atlantic areas generally have larger values for freshwater transport, there are exceptions. For instance, *Wide Coast* has a wider basin than *Both Coast* and *America Coast*, but has a smaller freshwater transport. A larger freshwater transport into the Atlantic-like basin is generally correlated with larger values of maximum AMOC across configurations. This arises because a larger AMOC corresponds to higher SSTs in the basin, which in turn corresponds to higher evaporation rates requiring larger freshwater transport to balance at equilibrium. Note that this is different from the simulations of Jones and Cessi 2017 who prescribe a zonally-uniform net freshwater flux at the surface which cannot change with basin geometry, thus requiring no net change in freshwater input into the Atlantic-like basin to balance.

To summarize, the structure and strength of the MOC depend on the details of the Atlantic-like basin geometry, rather than simply the average width of that basin. A larger MOC corresponds to higher SST in the Atlantic-like basin which, via enhanced evaporation, causes higher salinity in that basin and thus larger surface density at high latitudes. The causal role of ocean transport of freshwater in MOC changes is complex, however, since the ocean actually transports more freshwater into the Atlantic-like basin when MOC is stronger and the basin is saltier (as is required to balance the salinity budget at equilibrium in these simulations). Any analysis to compare the relative roles of ocean circulation and surface freshwater forcing in setting the Atlantic-like basin's salinity would be purely diagnostic. In the next section, we instead attempt to better understand MOC changes by evaluating their relationship to the changes in basin-scale meridional density gradients that have resulted from the changes in coastline shape.

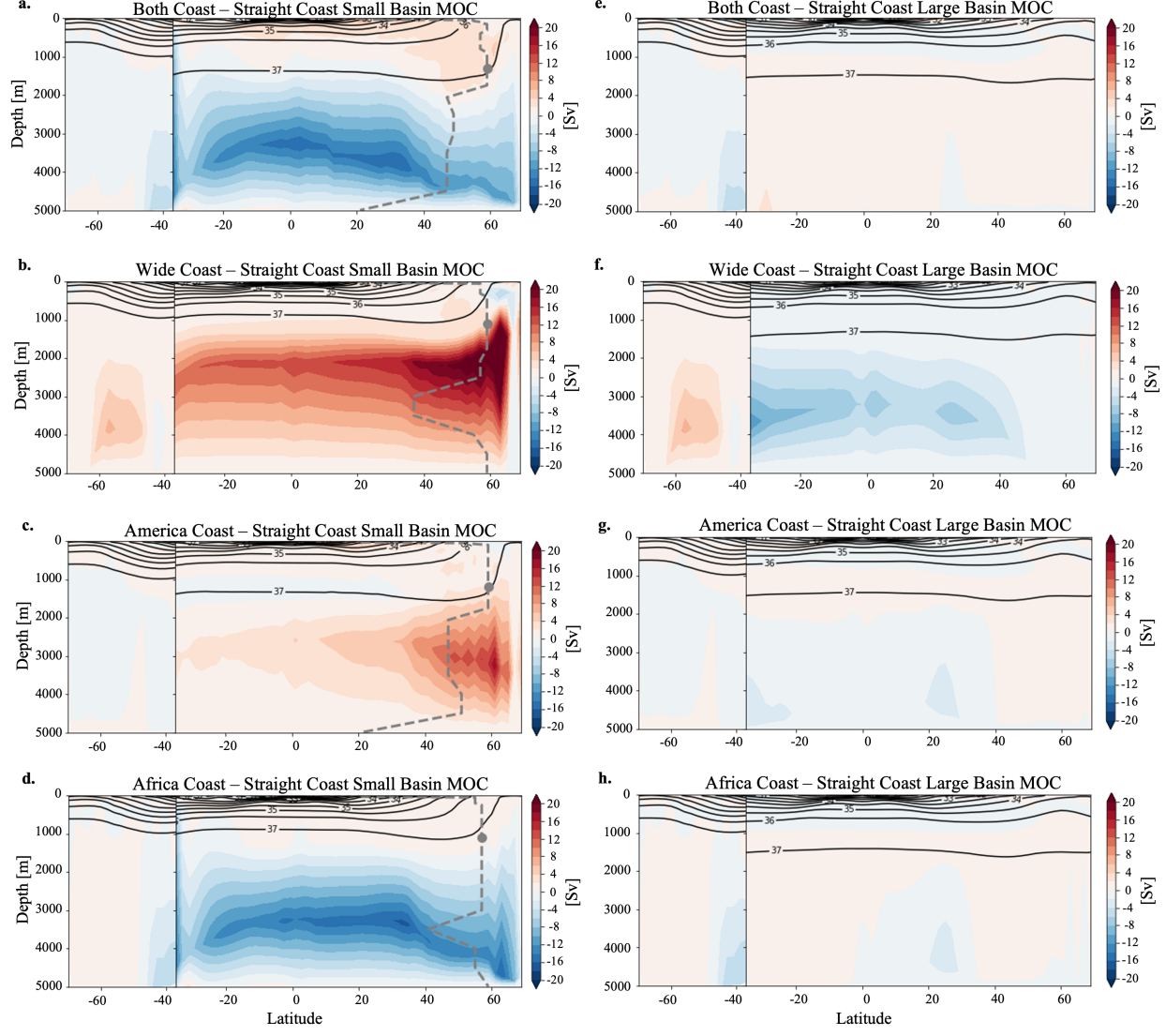


Figure 3.8: Meridional overturning circulation (MOC) anomaly from *Straight Coast* in the Atlantic-like basin for (a) *Both Coast*, (b) *Wide Coast*, (c) *America Coast*, and (d) *Africa Coast*. Meridional overturning circulation (MOC) anomaly from *Straight Coast* in the Pacific-like basin for (e) *Both Coast*, (f) *Wide Coast*, (g) *America Coast*, and (h) *Africa Coast*. The grey dashed line indicates the latitude of the maximum MOC at each depth plotted in Fig. 3.9 and the grey circle indicates the depth and latitude of the maximum MOC. Black contours indicate density surfaces.

### 3.3.2 AMOC Density Scaling

The similar surface conditions across continental configurations (Figs. 3.5, 3.6, and 3.7) belie the large differences in MOC strength and structure that occur when coastline shape is changed (Fig. 3). To investigate the relationship between basin geometry and meridional overturning circulation, we employ previously developed theory that relates AMOC to the basin-scale meridional density gradient. Theoretical approaches for understanding controls on overturning strength have been framed in terms of density gradient-driven gravity currents and have sought to relate the strength of meridional overturning in the Atlantic to the meridional density gradient (Thorpe et al. 2001; Delworth and Dixon 2006; Straneo 2006). Previous studies derived similar density scalings for AMOC (Robinson and Stommel 1959; Bryan 1987; Marotzke 1997; Gnanadesikan 1999; Thorpe et al. 2001; Griesel and Maqueda 2006). De Boer et al. 2010 explore several different variations of the relationship between MOC strength (denoted by  $\Psi$ ) and the meridional density gradient (denoted by  $\Delta\rho_y$ ):  $\Psi \propto \Delta\rho_y H^2$ , where  $H$  is a vertical scale depth. The most appropriate scale depth (as determined by De Boer et al. 2010) is that derived from the meridional density gradient in the western boundary, where  $H$  is taken to be the depth at which the depth-integrated meridional density gradient equals the vertical mean of the depth-integrated meridional density gradient. This scale depth is linked to isopycnal slopes near the northern boundary of the basin and the available potential energy in the region, as well as to processes in the Southern Ocean (Gnanadesikan 1999; Wolfe and Cessi 2010; Sijp et al. 2012). We adopt this interpretation here while retaining a depth dependence, following a method described by Butler et al. 2016.

We apply theory developed by Butler et al. 2016 as a framework for comparing the results of the different simulations. Butler et al. 2016 makes the following assumptions: 1) the large-scale ocean circulation is geostrophic; 2) thermal wind balance holds over the entire area and depth range of interest; and 3) the meridional density gradient is proportional to the zonal density gradient, such that  $\frac{\Delta\rho_x(z)}{L_x} = c \frac{\Delta\rho_y(z)}{L_y}$ , where  $c$  is some dimensionless constant of proportionality,  $\Delta\rho_x$  is the zonal density gradient,  $L_x$  is the zonal width of the basin between 20°N and 60°N,  $\Delta\rho_y$  is the meridional density gradient, and  $L_y$  is the meridional length. Zonal and meridional pressure and density gradients are closely related provided that the large-scale circulation is geostrophic. This relationship is found to hold at equilibrium in an idealized modeling study (Park and Bryan 2000). Moreover, meridional pressure gradients drive zonal eastward flows, which converge at the eastern boundary of the ocean basin, propping up a zonal pressure gradient. This zonal gradient in turn, sets up a meridional flow (Marotzke 1997; Kuhlbrodt et al. 2007). Another theory justifying the proportionality between zonal and meridional density gradients involves the propagation of fast boundary waves southward along the western boundary and across the equator to the eastern boundary; these waves are produced by a meridional density gradient along the western boundary of the basin (Johnson and Marshall 2002; Bell 2015; Johnson et al. 2019, and references therein).

By relating the zonal and meridional density gradient, the thermal wind relation can be scaled and rewritten to relate typical values for meridional velocity,  $V$ , to the meridional density difference,  $\Delta\rho_y$  (Butler et al. 2016):

$$\frac{\partial V}{\partial z} = \frac{cg}{f_0 \rho_0} \frac{\Delta \rho_y(z)}{L_y}, \quad (1)$$

where  $g$  is the gravitational acceleration,  $f_0$  is a typical value for the Coriolis parameter, and  $\rho_0$  is the reference density. Eq. 1 can then be integrated with respect to depth to find an expression for the characteristic meridional velocity and still retain the depth dependence of the meridional density difference (Butler et al. 2016):

$$V(z) = \frac{cg}{f_0 \rho_0 L_y} \left( \frac{1}{D} \int_{-D}^0 \left( \int_{z'}^0 \Delta \rho_y(z'') dz'' \right) dz' - \int_z^0 \Delta \rho_y(z') dz' \right), \quad (2)$$

where  $D$  is the ocean depth. The constant of integration is constrained by the fact that there is no net meridional flow and, as such, cannot be zero. Butler et al. 2016 show that the constant of integration is  $\frac{cg}{f_0 \rho_0 L_y} \left( \frac{1}{D} \int_{-D}^0 \left( \int_{z'}^0 \Delta \rho_y(z'') dz'' \right) dz' \right)$ .

Integrating Eq. 2 and assuming vertical side-walls results in an expression for the meridional overturning circulation,  $\Psi$ .

$$\Psi(z) = L_x \int_z^0 V(z) dz \quad (3)$$

As defined by Eq. 3, there is a positive relationship between the magnitude of the twice-integrated density difference between northern and southern points in the Atlantic-like basin ( $\iint \Delta \rho_y dz dz$ ) and MOC (Fig. 3.10c). As the meridional density difference increases, so too does the meridional overturning. The derivation of Eq. 3 assumes straight meridional boundaries along the basin and excludes any consideration of coastline shape. Applying the scaling to the configurations in this study tests how well the relationship between MOC and meridional density gradient holds when the assumption of straight coastlines is relaxed and gives insight into how the meridional density structure is linked to MOC.

Unlike other AMOC scalings that rely on the density at specific depths, the Butler et al. 2016 relationship (Eq. 3) uses the entire vertical structure of density and results in an estimate of MOC as a function of depth. Here, we interpret this as the structure of the maximum MOC at each depth within the Atlantic Basin. The density structure can be influenced by both changes in ocean circulation and surface freshwater forcing, both of which are driven by changes in basin geometry.

We use the scaling described in Eq. 3 to calculate the MOC in the narrow basin of each simulation. Maximum MOC predicted from the Butler et al. 2016 scaling (hereafter  $\Psi_B$ ) for each case are shown in Fig. 3.9. Here, the meridional density difference,  $\Delta \rho_y$ , is taken as the difference in density between 60°N and 30°S one grid point away from the western boundary of the Atlantic-like basin. The locations from which the density differences are calculated are indicated with gray and pink boxes in Figs. 3.3, 3.5, and 3.6. The basin width,  $L_x$ , is taken as the average basin width between 20°N and 60°N for each configuration. Values for  $L_x$  are listed in Table 3.2.3. The constant of proportionality,  $c = 0.96$ , used to calculate  $\Psi_B$  is the same value across all of the simulations and is the value reported in Butler et al. 2016.

Simulation	Max MOC	Max MOC Depth	Predicted MOC	Predicted MOC Depth	Subtropical Barotropic Stream-function	Subpolar Barotropic Stream-function	Atlantic Fresh-water Transport, $F$
<b>Straight Coast</b>	28.3 Sv	1100 m	25.6 Sv	1000 m	22.1 Sv	21.5 Sv	0.44 Sv
<b>Both Coast</b>	34.6 Sv	1300 m	38.6 Sv	1000 m	24.2 Sv	21.8 Sv	0.64 Sv
<b>Wide Coast</b>	38.5 Sv	1100 m	41.1 Sv	1200 m	31.5 Sv	26.6 Sv	0.54 Sv
<b>America Coast</b>	34.4 Sv	1200 m	37.4 Sv	1100 m	23.9 Sv	21.9 Sv	0.56 Sv
<b>Africa Coast</b>	28.8 Sv	1100 m	27.6 Sv	900 m	22.1 Sv	21.0 Sv	0.53 Sv

Table 3.2: List of model output maximum MOC values and associated depths for each simulation, along with maximum MOC and depth predicted from the meridional density difference scaling. Also included are the maximum barotropic streamfunction values for the northern subtropical and subpolar gyres in the Atlantic-like basin. The final column lists values of the inferred freshwater transport at 30°S in the Atlantic-like basin,  $F$ , calculated by integrating the surface freshwater balance as described in section 3.33.3.1.

While the values of the maximum model MOC (hereafter  $\Psi_{max}$ ) and  $\Psi_B$  differ somewhat, the ranking of  $\Psi_{max}$  and  $\Psi_B$  from weakest to strongest agree well (Table 3.2). This suggests that Eq. 3 can provide insight into how MOC depends on basin shape. Further examination of the relative vertical structures of  $\Psi_{max}$  and  $\Psi_B$  shows qualitative agreement as well (Fig. 3.9):  $\Psi_{max}$  and  $\Psi_B$  for *Straight Coast* and *Africa Coast* are similar to each other, as are  $\Psi_{max}$  and  $\Psi_B$  for *America Coast* and *Both Coast*. This suggests that the shape of the North American coast is particularly important in the vertical structure of MOC via changes in meridional density gradient along the western boundary of the basin, while the shape of the African coast plays a smaller role.

What causes changes in meridional density gradients, and thus  $\Psi_B$ , between the different continental configurations? Changes in the twice-integrated density at either the northern or southern end of the Atlantic-like basin are similar to each other across continental configurations, and much larger than the changes across configurations in twice-integrated density differences themselves (Fig. 3.10a, b). Thus, changes in meridional density gradients cannot be explained by changes at surface in the northern end of the Atlantic-like basin.

Moreover, changes in meridional density gradients cannot be described by changes in temperature or salinity alone. We calculate  $\iint \Delta\rho_y dz dz$  using a fixed-temperature meridional density gradient and a fixed-salinity meridional density gradient, but find little correlation between the double-integral and MOC strength. Changes in both temperature and salinity contribute to the changes in density between the experiments in complex ways.

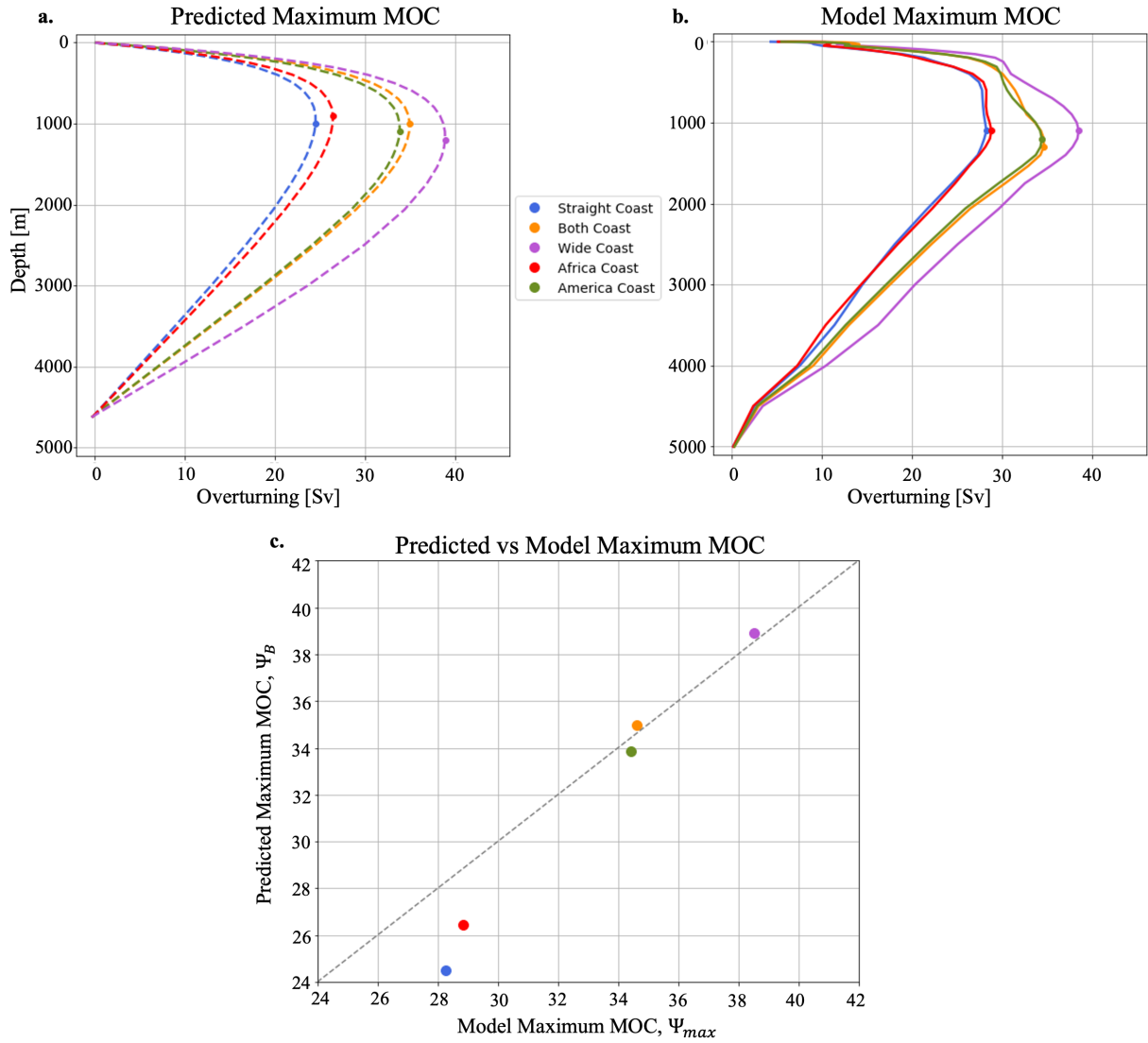


Figure 3.9: (a) Maximum MOC calculated from the model,  $\Psi_{max}$ , at each depth level between  $30^{\circ}\text{S}$  and  $50^{\circ}\text{N}$  for each case. (b) Maximum MOC predicted by the Butler scaling, Eq. 3,  $\Psi_B$ , strength at each depth calculated by twice-integrating the meridional density difference. (c)  $\Psi_B$  plotted against  $\Psi_{max}$ .

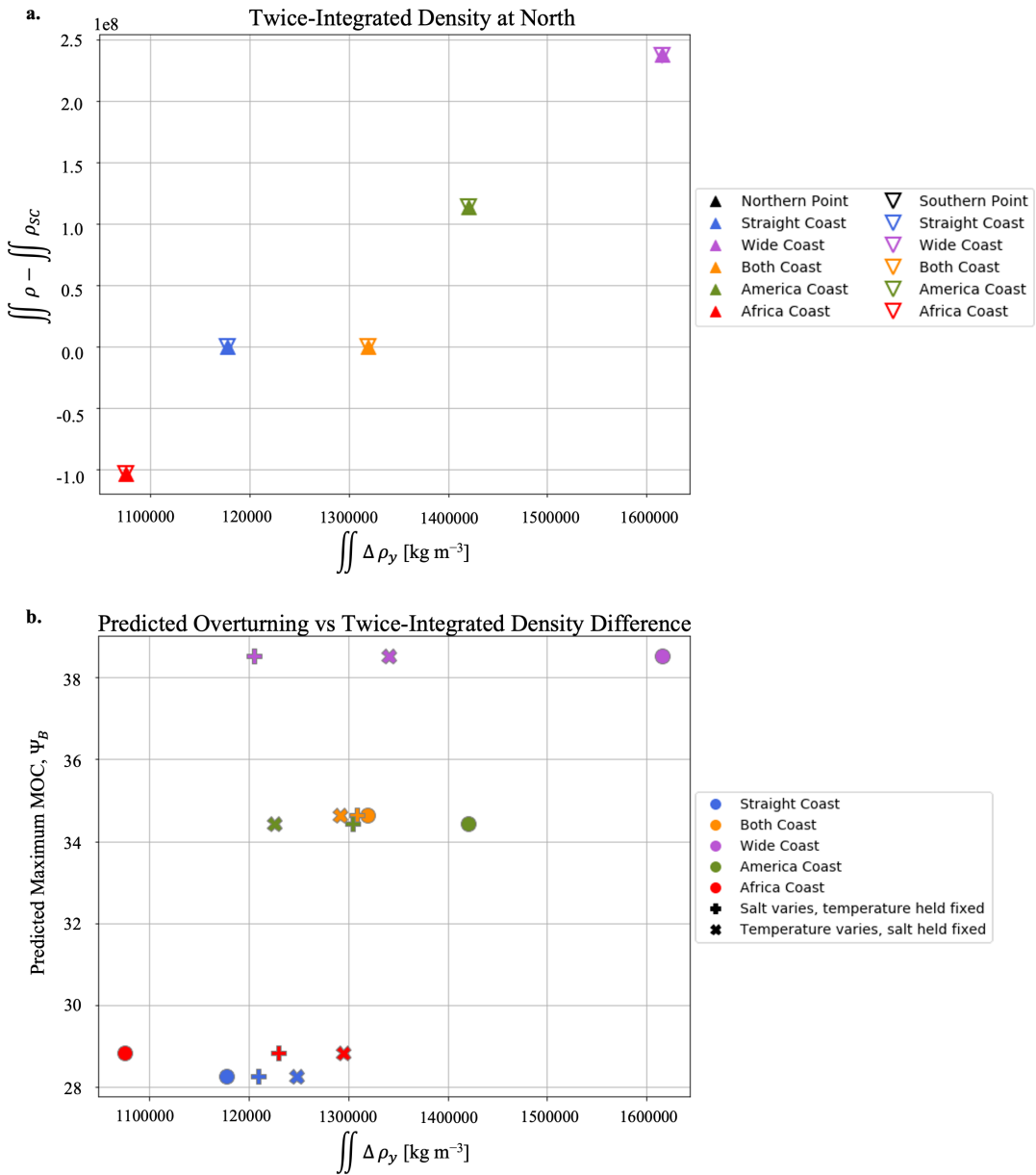


Figure 3.10: (a) Twice-integrated density anomaly from *Straight Coast*,  $\iint \rho_{sc}$ , at both the northern and southern ends of the domain is plotted against the twice-integrated meridional density difference,  $\iint \rho_y$ . (b) Predicted overturning plotted against twice-integrated meridional density difference is plotted with circles. Also shown is predicted overturning plotted against twice-integrated meridional density difference calculated with fixed temperature,  $\Theta_0$ , or fixed salinity,  $S_0$ . Density differences calculated with fixed temperature are indicated with a '+' while density differences calculated with fixed salinity are indicated with an 'x'.

Sensitivity tests reveal that the MOC scaling (Eq. 3) is relatively unaffected by changes in latitude for both the northern and southern regions used to calculate the meridional density difference (not shown). Moreover, the basin width,  $L_x$ , that produces the best fit to the model output MOC is the average width between 20°N and 60°N, rather than the average width of entire basin. While the Butler model assumes straight boundaries, it can in fact predict overturning in basins with shaped sidewalls, provided the choice of  $L_x$  describes the width of the northern basin. This indicates that shape, and not only basin width, matters for the meridional density gradient and thus the overturning strength.

### 3.4 Discussion and Conclusions

Previous studies have shown that the relatively narrow basin width and the southern extent of the continents provide important geometric constraints on the localization of deep water formation in the Atlantic Ocean (Ferreira et al. 2010; Nilsson et al. 2013; Jones and Cessi 2017; Cessi and Jones 2017; Youngs et al. 2020). Here we examine the impacts of coastline geometry on meridional overturning circulation in a narrow, Atlantic-like basin in five ocean-only idealized continental configurations that range from coastlines that are straight to coastlines shaped like the American and African continents.

A primary finding is that overturning circulation changes that occur when widening the Atlantic basin by changing the coastline shape (*Both Coast*) are distinct from those that arise when widening the Atlantic basin without modifying the coastline shape (*Wide Coast*), even when the average basin widths and areas increase by the same amount (Table 1). While generally we see an increase in MOC strength with basin width, this relationship is not linear; configurations with the same western boundary shape have similar MOC strengths despite differences in mean basin width (with the exception of *Wide Coast*, which has a stronger MOC than all other cases).

Note that because our atmospheric forcing is zonally-symmetric and constant across configurations, any asymmetries that arise between basins or between configurations must be due to differences in ocean circulation driven by changes in the coastline geometry of the Atlantic basin. Freshwater forcing at the ocean surface can drive differences between configurations but the evaporation responds to SST changes that are due to circulation changes (while precipitation is zonally uniform and constant across configurations). While the basin width and shape as well as the basin evaporation minus precipitation both impact the oceanic freshwater transport, the changes all arise due to the change in coastline geometry between simulations. The freshwater transport at the south of the Atlantic-like basin is controlled both by basin size and by the surface freshwater balance, and is not perfectly correlated with the MOC strength. Moreover, the freshwater balance at the surface is influenced by the SSTs, which are influenced by ocean circulation changes that arise from changing the shape of the coastline.

Each of the *Wide Coast*, *Both Coast*, *America Coast*, and *Africa Coast* cases represents a widening of the Atlantic-like basin with respect to the *Straight Coast* control case. Widening the basin results in warmer northern Atlantic-like basin SSTs (Fig. 3.5). Moreover, simulations with shaped western boundaries (*Both Coast* and *America Coast*) and those that do

not (*Wide Coast* and *Africa Coast*) show different patterns of SST anomalies. Widening the Atlantic-like basin also results in higher basin-average SSS (Fig. 3.6). Stratification in the subpolar region of the Atlantic-like basin decreases in strength when the western boundary along the basin is shaped, rather than purely meridional (Fig. 3.7).

Both the western coastline and the eastern coastline play important roles in modulating the overturning circulation (Fig. 3.8). The simulations with shaped western coastlines (*America Coast* and *Both Coast*) show increased shallow overturning streamfunctions above about 1500m compared to *Straight Coast*. This demonstrates that the *shape* of the American coast along the Atlantic basin is important for MOC vertical structure and strength. Simulations with shaped eastern coastlines (*Both Coast* and *Africa Coast*) show decreased abyssal overturning streamfunction and shoaled MOC compared to *Straight Coast*. Changes in abyssal circulation seen in *Africa Coast* highlight an apparent link between Atlantic abyssal circulation and the width of the Agulhas region. The shape of the African coast along the Atlantic is important for the abyssal Atlantic circulation and the vertical structure of MOC but not for MOC strength.

Generally our results confirm the findings of previous studies that find that northern deep ventilation and associated cross-equatorial overturning circulation is confined to the narrower of two ocean basins. In our simulations, we see an increase in MOC strength with an increase in basin width. This is inconsistent with the results of Jones and Cessi 2017, who found that widening the Atlantic-like basin leads to a small decrease in MOC strength. This could, in part, be explained by differences in experimental design: the Jones and Cessi 2017 continental boundaries are thin, meridional ridges whereas ours are wider strips of land, some of which have more complex coastline shapes and could impact the relative contributions of “Warm Route” and “Cold Route” transport into the basin; their model does not include sea ice while ours does; they prescribe P-E through a surface freshwater flux whereas our model allows evaporation to evolve with changing SST; and the surface forcings they use are constant in time and include a SST relaxation, which could constrain the SST more strongly. The simulations presented here include seasonality and use surface forcings calculated with bulk formulae from atmospheric products (CNYF2). Moreover, Jones and Cessi 2017 use a linear equation of state while MOM6 uses the non-linear Wright equation of state (Wright 1997), which makes temperature less important for density at low temperature compared to a linear equation. One final difference is that in Jones and Cessi 2017, the total global ocean area remains constant while here, the different coastline configurations do have different global ocean areas (Table 3.2.3), providing a larger area over which water can upwell and which can allow for a larger MOC (Jones and Cessi 2016). Interestingly, AMOC strength (Table 3.2) does not scale linearly with narrow basin width, narrow basin area, total global ocean area, or freshwater transport into the narrow basin (Table 3.2.3), allowing for the possibility of the existence of the salt-advection feedback (Stommel 1961).

Jones and Cessi 2017 argue that an increase in basin width results in a larger Sverdrup gyre transport (Sverdrup 1947), and thus a stronger subpolar western boundary current. This acts to oppose the northward MOC component of the western boundary velocities. The MOC-associated subtropical transport can be modulated by non-local effects (Gnanadesikan 1999; Jones and Cessi 2017), and thus does not strengthen with increased basin width as the wind-

driven subpolar western boundary current does. As such, in a narrower Atlantic basin, the subtropical western boundary current can flow farther north, bringing salty water with it. As this salty water flows north and cools, it increases in density, decreasing stratification and increases MOC. Other studies suggest that a wider basin could result in a larger magnitude in MOC due to a larger effective meridional diffusivity in wider basins (Wang et al. 1995; Nilsson et al. 2021). In a wider basin, the gyre and mesoscale eddy driven transport of salinity from the subtropical to subpolar gyre is larger, increasing northern salinity and density, thus creating favorable conditions for deep sinking. This transport also brings heat into the northern high latitudes, allowing for more evaporation, further increasing the northern high latitude salinity.

The results presented here suggest that the relationship between basin width, salt transport, and deep ventilation are complex. Meridional density differences are driven by density changes at both the north or south of the Atlantic basin (Fig. 3.10a) and also by changes in both temperature or salinity (Fig. 3.10b). This is in contrast to results in Jones and Cessi 2017, where salinity in the North Atlantic dominates de-stratification and deep water formation. Moreover, while basin width certainly controls the barotropic circulation, the details by which the transport of salinity and temperature around the Atlantic basin and how that impacts the overturning circulation are not straightforward. In our simulations, the *Wide Coast* subpolar and subtropical gyre barotropic circulations are largest among the simulations (Table 3.2, Fig. 3.11). *Both Coast*'s subpolar gyre is of similar strength to that of *Straight Coast*, but *Both Coast* has a much stronger subtropical gyre than *Straight Coast*, consistent with predicted increase in Sverdrup transport with basin width (Jones and Cessi 2017; Sverdrup 1947). However, Jones and Cessi 2017's argument is not consistent with the larger MOC strength in *Wide Coast* as compared to *Straight Coast*.

While the MOC response to changes in basin shape is complicated, the MOC for each simulation is well predicted by the scaling derived by Butler et al. 2016. MOC scales with twice-integrated meridional density difference along the western coastline and with average basin width for ocean basins with both shaped and straight coasts. Moreover, the scaling is not sensitive to the choice of latitude for either the northern or the southern point for calculation of the the meridional density difference. The density at only two locations in the ocean – one point at the north and one at the south of the basin – can provide a good estimate of MOC. Applying the Butler et al. 2016 scaling to several different continental configurations demonstrates the robustness of the scaling to different basin geometries that lead to large changes in MOC, despite the fact that the scaling was derived for a case with straight coastlines.

Salinity and temperature differences between simulations influence the stratification and meridional density gradient along the western boundary in the Atlantic-like basin, allowing the scaling developed by Butler et al. 2016 to accurately predict MOC strength. Causality in the relationship between meridional density gradient and MOC is difficult to ascribe due to the influence of remote Southern Ocean forcing on overturning (De Boer et al. 2010). Moreover, the meridional velocity is proportional to zonal pressure gradients, which are then related to meridional density differences through fast boundary waves (Johnson and Marshall 2002), so the relationship between meridional density gradient and MOC is not

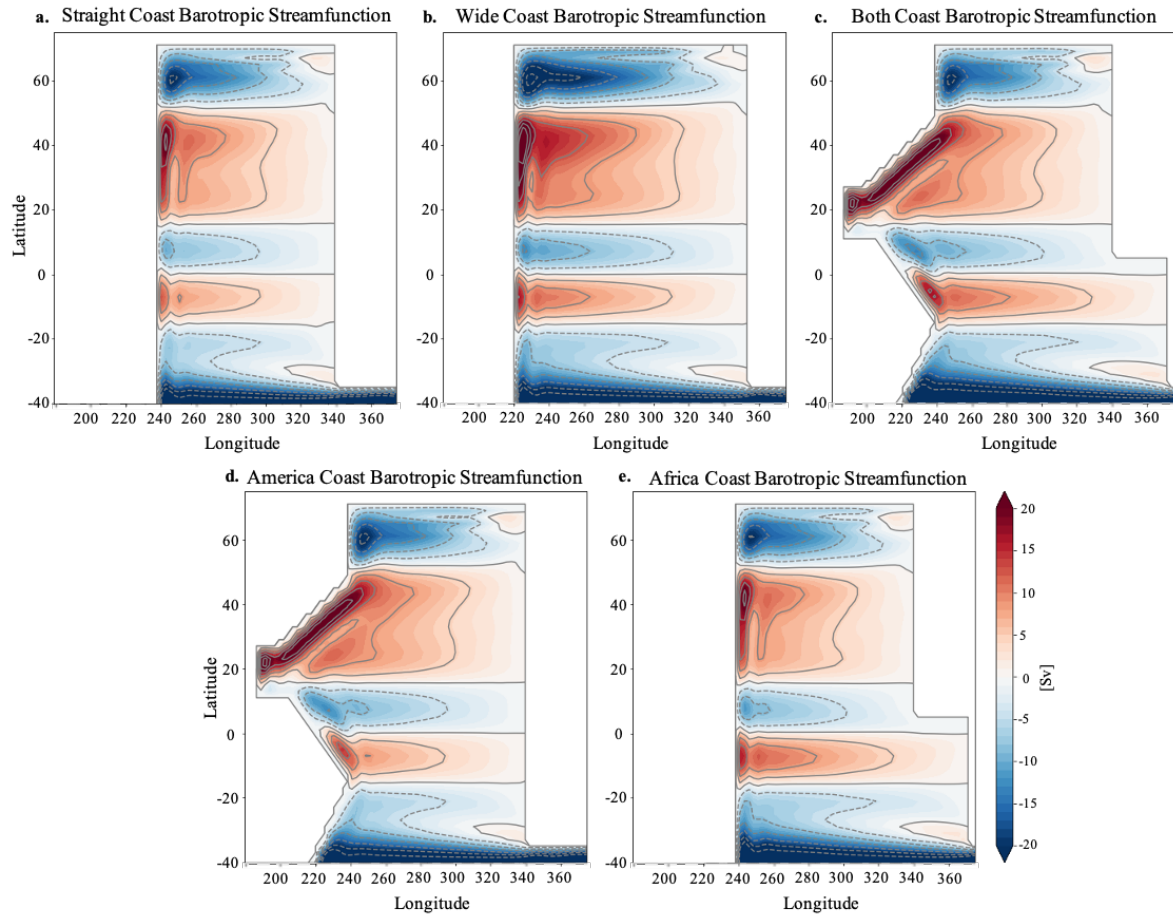


Figure 3.11: The barotropic streamfunction for (a) Straight Coast, (b) Wide Coast, (c) Both Coast, (d) America Coast, and (e) Africa Coast. Red shading indicates clockwise circulation whereas blue shading indicates counter-clockwise circulation. Contours are every 5 Sv.

direct. Butler et al. 2016 posit that the MOC responds to the meridional density gradient through the creation of zonal pressure gradients or through ageostrophic flow. Thus, the differences in both temperature and salinity at the north and the south of the Atlantic-like basin across simulations act to cause meridional density gradient changes and in turn changes to MOC. The success of the Butler et al. 2016 scaling demonstrates its versatility in reproducing MOC given density profiles at only two points in the Atlantic. While Butler et al. 2016 does not directly invoke the coupling of the barotropic circulation and the baroclinic structure of the gyres, inspection of the density difference between the surface and 1000m (Fig. 3.7, and the barotropic circulation (Fig. 3.11 suggest that this coupling likely plays a large role in setting the density structure along the western boundary. This in turn suggests that basin geometry influences MOC through its influence on barotropic circulation.

Our model configurations represent a simplification of realistic continental configurations. However, they represent an increase in basin geometry complexity compared to past aqua-planet and other simulations with idealized continental configurations studies (such as Ferreira et al. 2010; Nilsson et al. 2013; Cessi and Jones 2017; Jones and Cessi 2017. As such, this study serves as an intermediate step in a hierarchy of ever more realistic idealized models aimed at better understanding the role of ocean basin geometry on ocean circulation. It is important to note that even the more realistically shaped coastlines in our model simulations are low-resolution simplifications of the real ocean boundaries. Also, by employing purely vertical, rather than sloping, ocean sidewalls and flat bottom bathymetry, we ignore the effects of topographically-enhanced mixing and form drag as well as the role of bathymetry in steering abyssal flow. Despite these limitations, the continental configurations in this study demonstrate the importance of coastline shape on meridional overturning circulation and raise further questions about the role of interplay between meridional overturning and gyre transports for ocean stratification and circulation.

## 4 Revisiting the Role of Ocean Basin Geometry in Atlantic Overturning: the Importance of the North Pacific Basin

### 4.1 Introduction

The modern ocean is marked by a cross-equatorial, pole-to-pole overturning in the Atlantic Ocean, known as the Atlantic Meridional Overturning Circulation (AMOC). The general flow of AMOC transports warm surface waters northward where they release heat to the atmosphere near Greenland, gaining density and sinking to the intermediate and deep ocean. This newly transformed water, which is cold relative to the surface waters in the Atlantic Ocean, flows southward at depth. There is no corresponding cross-equatorial overturning circulation associated with deep sinking of water in the Northern Hemisphere of the Indo-Pacific Ocean. Instead, the water in the Indo-Pacific flows northward at depth into the Northern Hemisphere where it upwells diffusively and flows southward at intermediate depths. The asymmetry in the circulation patterns between the Atlantic and the Indo-Pacific ocean basins generates several important asymmetries in Earth's climate. For instance, by bringing heat

northward, AMOC creates an asymmetry in sea surface temperature (SST) at equivalent latitudes between the Atlantic and the Pacific, contributing to a milder climate in Europe than in Canada (Palter 2015). This northward heat transport is also important for setting the mean location of the Inter-Tropical Convergence Zone, the global rainfall maximum, north of the equator (Marshall et al. 2014; Frierson et al. 2013). Thus, AMOC is a key feature of the climate system, but a fundamental question remains: why does deep sinking and its associated large-scale meridional overturning exist in the Atlantic and not the Pacific?

The localization of this meridional overturning circulation in the Atlantic basin has widely been attributed to the higher salinity relative to that in the North Pacific (Warren 1983; Jones and Cessi 2017; Ferreira et al. 2018). Saltier water is denser, and the water at the ocean surface must be dense enough in regions of cold surface temperatures so that, with cooling, the water can lose enough buoyancy to sink to the deep ocean. Previous work highlights several theories for why this salinity contrast exists between the Atlantic and the Pacific, many of which are summarized in Ferreira et al. 2018. Two particular features of the geometry of Earth’s ocean basins identified as important for creating circulation asymmetries between the Atlantic and the Indo-Pacific are the basin width and the southern extent of the continents.

The narrow width of the Atlantic basin as compared to the Indo-Pacific impacts both atmospheric and oceanic freshwater pathways. Ferreira et al. 2010 and Nilsson et al. 2013 note the rainfall fetch of water evaporated over the Atlantic is long enough for it to precipitate over the Indo-Pacific while the water that evaporates over the Indo-Pacific is likely to precipitate before being transported into the Atlantic sector. Jones and Cessi 2017 isolate an oceanic mechanism for elevated salinity in the northern narrow, Atlantic-like basin compared to the wide, Indo-Pacific-like basin. The western boundary current in the subtropical gyre of the narrow ocean basin with northern deep sinking is composed of a wind-driven component, which scales with basin width, and a MOC-associated component, which is width-independent; whereas the subpolar western boundary current is primarily wind-driven. In a narrow basin, the northward flowing subtropical (high salinity) western boundary current is opposed by a weaker southward flowing subpolar (low salinity) western boundary current resulting in a saltier northern basin. In a wide basin, the subtropical western boundary current is opposed by a subpolar western boundary current of a similar magnitude, resulting in a fresher northern basin.

Previous idealized ocean model simulations suggest that the southern extent of continents is a second proposed feature of model ocean basin geometry that results in deep sinking in the Atlantic. The African continent terminates at a lower latitude than South America. For instance, in a continental configuration similar to that of modern Earth, where the western boundary of the Atlantic extends farther south than the eastern boundary, the wind-driven gyre circulation imports warm, salty subtropical Indo-Pacific surface water into the Atlantic (Nilsson et al. 2013). This source of salty water into the Atlantic, termed the warm route, is diminished when the eastern boundary of the Atlantic is extended to the same latitude as the western boundary (Nilsson et al. 2013). When the continent on the western side of the Atlantic terminates farther north than the eastern boundary, fresher water from the Southern Ocean is imported into the Alantic which destabilizes AMOC.

Continental orography has also been implicated as an explanation for the elevated salinity of the Atlantic compared to the Indo-Pacific. Sinha et al. 2012 illustrate a key role for mountains. In a model simulation without any mountains, AMOC collapses fully and the global ocean circulation develops a PMOC instead. The Rocky Mountains divert the Northern Hemisphere midlatitude atmospheric jet to the North over the Atlantic. Over the North Pacific, the jet stream is much more zonal in character, whereas over the North Atlantic, the presence of the Rockies causes the jet to flow towards the north east. This results in a tilted barotropic ocean gyre circulation pattern in the subtropical North Atlantic. High salinity water is thus transported further north compared to when the winds are oriented towards the northeast (Emile-Geay et al. 2003; Czaja 2009).

Much of the previous work on the topic of how continental geometry shapes ocean circulation and confines Northern Hemisphere deep convection and large-scale overturning to the Atlantic Basin has used either ocean-only configurations of the Massachusetts Institute of Technology General Circulation Model (MITgcm) (Marshall et al. 1997; 1998) or the MITgcm coupled to an idealized atmospheric model, Simplified Parametrizations, primitive-Equation DYnamics (SPEEDY; Molteni 2003) (as in Enderton and Marshall 2009; Ferreira et al. 2010; Nilsson et al. 2013). Ocean-only aquaplanet simulations show that purely zonal boundary conditions produce overturning in the narrower ocean basin (Jones and Cessi 2017; Chapter 3).

Here we revisit this topic using a coupled model that has a more-sophisticated representation of atmospheric processes while still remaining computationally cheap enough to perform the long simulations required to achieve a stable climate under different continental configurations. Here we use the NOAA/GFDL Modular Ocean Model version 6 (MOM6; Adcroft et al. 2019), with sea ice, coupled to the NOAA/GFDL Atmosphere Model 2 (AM2; GFDL et al. 2004), as described in Chapter 2.

In Chapter 3, we examined ocean circulation in MOM6 run with idealized basin geometry – with straight or shaped continents producing a wide (Indo-Pacific-like) and narrow (Atlantic-like) basin – forced by zonally-symmetric atmospheric-forcing that is derived from observed atmospheric fields. For these simulations deep sinking and large-scale overturning occurs in the narrow (Atlantic-like) basin, consistent with previous studies. However, in this chapter, we investigate whether the results of ocean-only studies (i.e., Jones and Cessi 2016; Jones and Cessi 2017) hold when an ocean is coupled to an atmosphere.

As we will show below, the coupled MOM6-AM2 model run with a similar continental configuration produces deep sinking and large-scale overturning in the wide (Indo-Pacific-like) basin – at odds with previous studies that use a different ocean model and a simplified atmospheric model. This suggests that (i) the importance of continental configuration for ocean circulation depends on whether ocean-only or coupled model configurations are used, and (ii) that the location of deep sinking may not be as robust as previously thought and instead maybe sensitive to atmospheric model complexity.

We examine what aspects of ocean basin geometry and bathymetry control localization of Northern Hemisphere deep convection. In particular, we explore the impact of asymmetries in the latitudinal extent of the Indo-Pacific and Atlantic basins with a focus on the role

of the Aleutian Islands. We will show that the presence of the Aleutians in the northern Indo-Pacific-like basin precludes deep convection to isopycnal surfaces that connect to where dense water is upwelled in the Southern Ocean, thus preventing large-scale overturning in that basin. Moreover, without overturning in the Indo-Pacific-like basin, the atmospheric circulation adjusts to favor deep convection in the Atlantic-like basin.

In what follows, we introduce this MOM6-AM2 coupled model and describe the model setup and the continental configurations used in the simulations. In Chapter 4, we focus on two configurations: a configuration with a wide (Indo-Pacific-like) basin and a narrow (Atlantic-like) basin and a configuration with the same land geometry except with a sill rising to 1000 meters depth across 55°N in the Indo-Pacific-like basin which produces deep convection and large-scale overturning localized in the narrow Atlantic-like basin.

## 4.2 Methods

We use the ocean–atmosphere–sea-ice model developed in Chapter 2 to explore different continental configurations. Throughout this Chapter, we compare our MOM6-AM2 model results to those of a pre-industrial control simulation of GFDL’s CM4 (Adcroft et al. 2019; Held et al. 2019). CM4 consists of AM4 atmosphere at 1° resolution and 33 levels, LM4 land with dynamic vegetation, MOM6 ocean at 1/4° resolution with 75 vertical levels, and SIS2 sea ice.

### 4.2.1 Continental Configurations

We present five different idealized continental configurations, each with one narrow, Atlantic-like basin and one wide, Indo-Pacific-like basin. In each configuration there are two ‘continents,’ one America-like continent to the west of the narrow basin and one Africa-like continent to the east of the narrow basin, which have straight meridional coastlines. These ridge ‘continents’ are two grid cells wide and do not protrude into the atmosphere. Each of these continental geometries is shown in the left column of Fig. 4.1. All configurations have land caps over the poles, which are necessary to preserve numerical stability in the ocean model. *Double Drake* is a configuration with two ocean basins, one three times wider than the other, with two ridges that extend from the northern land cap to 55°S (Fig. 4.1b). *Short Africa* is similar to *Double Drake* but one of the ridges extends to only 35°S (Fig. 4.1c). *Short Africa Wideland* is similar to *Short Africa* but the continents are 20 grid cells wide (Fig. 4.1d). *Rockies Wideland* is similar to *Short Africa Wideland* but with a Gaussian mountain on the longer continent (Fig. 4.1e). *Double Drake Sill* is similar to *Double Drake* but there is a zonal sill in the Pacific-like basin centered on 55°N which extends from the sea floor to 1000 m below the sea surface (Fig. 4.1f).

Initial conditions for the model runs are derived from zonal mean temperature and salinity after 1000 years of integration of an ocean-only MOM6 simulation forced with zonally symmetric atmospheric conditions (*Both Coast* configuration in Chapter 3). Each configuration is run for about 1000 years, with the exception of *Double Drake* and *Double Drake Sill*, which were run for 2000 years. The climatologies are calculated from the last 100 years of the simulations.

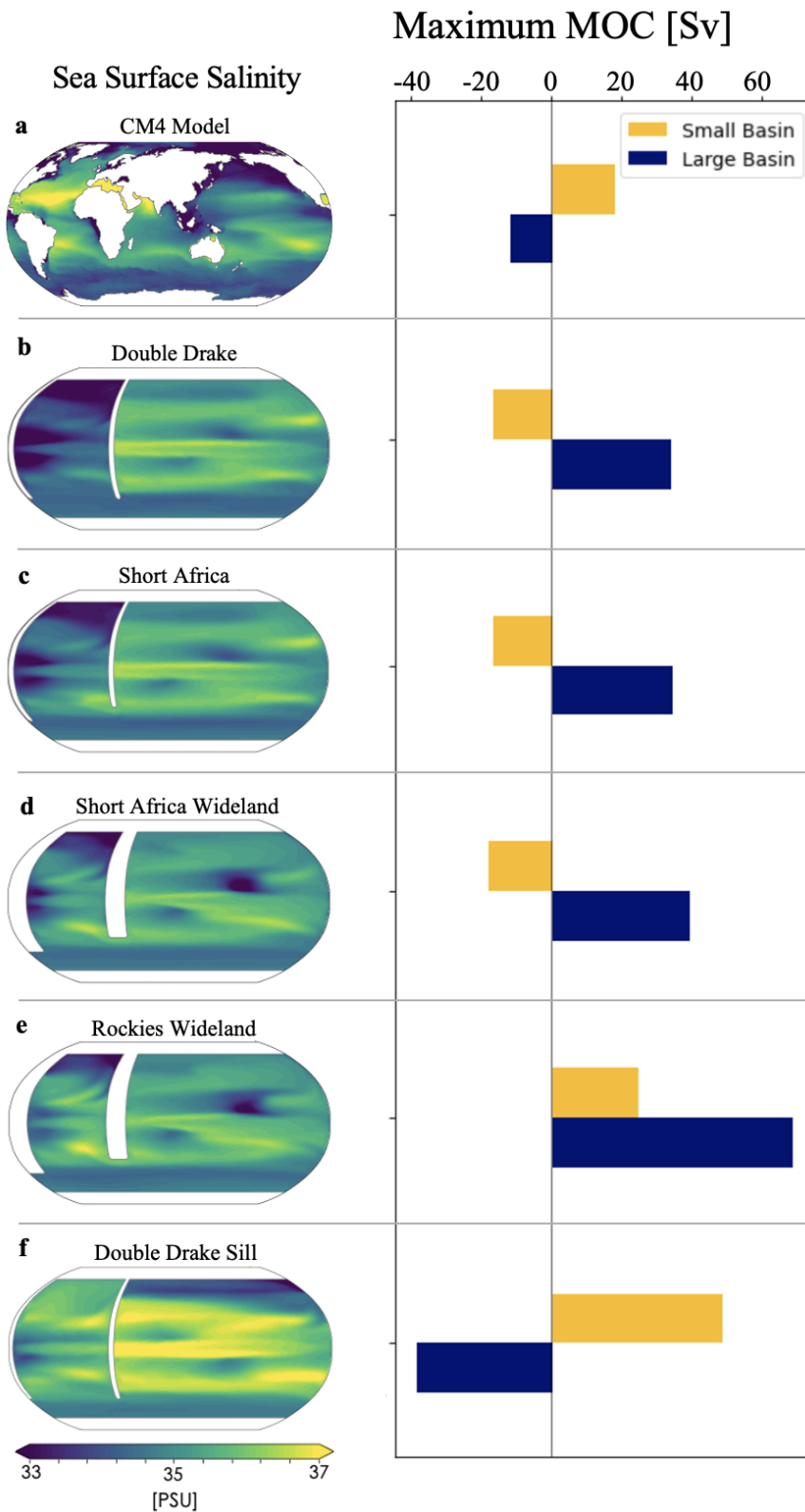


Figure 4.1: Maximum MOC strength in each ocean basin (bar graph on right) with associated sea surface salinities (maps on left) for CM4 and each idealized continental configuration.

## Meridional Overturning Circulation on Depth Coordinates

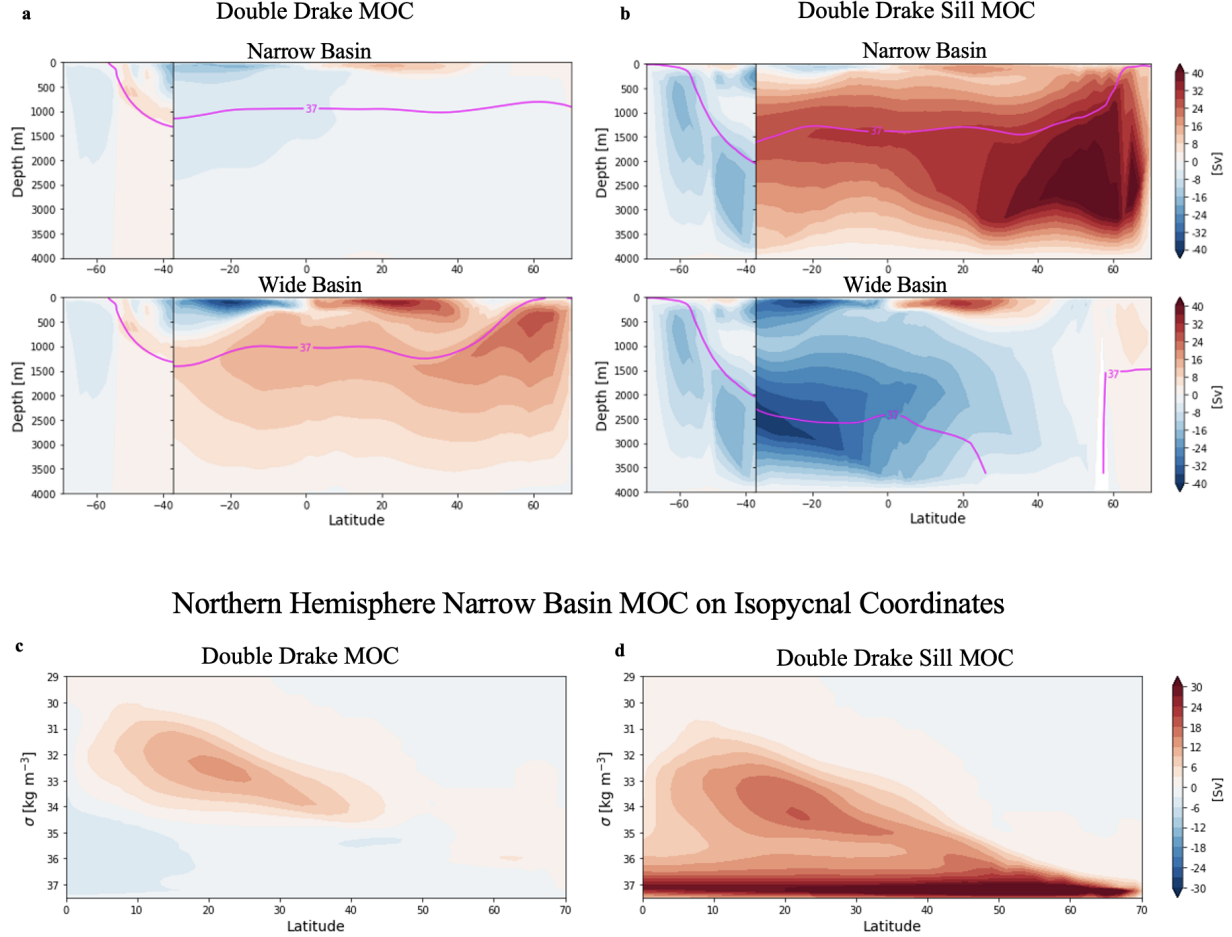


Figure 4.2: Meridional overturning circulation for the narrow and wide basins of (a) *Double Drake* (b) *Double Drake Sill* on depth levels. Northern Hemisphere narrow basin overturning circulation on isopycnal levels for c) *Double Drake* and d) *Double Drake Sill*.

## 4.3 Results

### 4.3.1 Localization of Meridional Overturning Circulation

We begin by examining the GFDL CM4 pre-industrial control climatology (Fig. 4.1a). Notably, the Atlantic ocean is saltier than the Indo-Pacific. The global ocean circulation is broadly characterized by a pole-to-pole, cross equatorial overturning circulation in the Atlantic with northward flowing surface waters, deep water formation in the northern high latitudes, and southward flow at depth. This is balanced by a deep northward flow in the Indo-Pacific that upwells diffusively before slowly returning southward. This flow is indicated by positive values for a circulation that is Atlantic-like and negative values for a circulation that is Pacific-like (Fig. 4.1a, bar chart).

In stark contrast, when using the idealized *Double Drake* basin geometry, an AMOC-like circulation forms within the wide (Indo-Pacific-like) basin, rather than the narrow (Atlantic-

like) basin, as would be inferred from the results of previous studies and Chapter 3 (Fig. 4.1b). Meanwhile, the narrow, Atlantic-like basin is characterized by a deep northward flow that upwells and flows southward at intermediate depths. Moreover, the wide basin is saltier (more Atlantic-like) than the narrow basin (more Pacific-like). In the simulations presented here, deep water formation occurs in the wide basin rather than the narrow basin (Fig. 4.2a), contradicting the results of previous idealized studies. Those studies posit that atmospheric moisture transport and the wider fetch over the wider basin (which act to depress the salinity of the wide basin compared to the narrow basin) is the primary mechanism that drives deep sinking preferentially in the narrow basin (Ferreira et al. 2010). Our results, with a more complex model, suggests that there may be more factors that drive deep sinking to the Atlantic basin than explored in previous idealized studies (Ferreira et al. 2018).

The length of the African continent has also been shown to impact the localization of deep water formation to the Atlantic rather than the Indo-Pacific. The southern extent of the African Continent is thought to assist in the import of high salinity water to the Atlantic (Nilsson et al. 2013). We test this theory with a configuration that shortens the Africa-like continent (*Short Africa*). However, this continental arrangement also fails to generate an AMOC and leaves the Atlantic fresher than the Pacific (Fig. 4.1c). While the sea-surface salinity (SSS) of the narrow basin increases in Short Africa compared to *Double Drake*, the intrusion of saline water to the narrow basin is mainly confined to the Southern Hemisphere, leaving the northern high latitudes – the regions of deep watermass transformation – relatively fresh. Thus, an increase in transport of relatively high salinity water into the Atlantic-like basin in the Southern Hemisphere does not guarantee dense water formation in the northern high latitudes.

Another theory for MOC localization invokes the differences in zonal extent of the rainfall fetch over the Atlantic compared to the Indo-Pacific, which leads to higher precipitation and thus fresher conditions in the Indo-Pacific region (Ferreira et al. 2010). We test this theory by increasing the width of the continents, creating more separation between the two ocean basins (*Short Africa Wideland*). Widening the meridional ridges acts to increase the salinity of the Atlantic basin, but the increase is not large enough to promote deep sinking (Fig. 4.1d). Instead, deep sinking is confined to the wide, Indo-Pacific-like basin.

Prior work shows that the presence of orography can impact the strength of meridional overturning and deep water formation by changing the orientation of the jet stream over the Atlantic, thus impacting the structure of the North Atlantic gyres (Sinha et al. 2012). We test this theory by adding an idealized Gaussian bump for the Rocky Mountains (*Rockies Wideland*). This configuration allows for dual sinking with a strong PMOC and a weak AMOC (Fig. 4.1e). The MOC in the narrow basin is much weaker than that in the wide basin, but the dual sinking points to the importance of land orography in determining the strength and location of deep water formation in the global ocean.

Other differences in Atlantic Ocean and Pacific Ocean basin geometries may influence the localization of deep sinking to the North Atlantic as well. For instance, the deep sinking occurs in the Atlantic Ocean much further north than the Pacific extends. The latitude of the Labrador Sea and the Greenland, Icelandic, Norwegian Seas connect the circulation in the mid-latitude Atlantic to almost 80 °N. In the Pacific, on the other hand, the Bering

Strait is located at 65°N and the Aleutian islands at 55°N. The Aleutians act as significant barriers to the meridional flow of dense waters (Reed and Stabeno 1997). To reflect these asymmetries, in previous work with idealized ocean basin geometries, Nadeau and Jansen 2020 used idealized continental geometry with the northern boundary of the wide, Pacific-like basin farther south than that of the narrow basin. Motivated by these factors, we altered *Double Drake* by adding a submarine zonal sill in the wide, Indo-Pacific-like basin at the approximate latitude of the Aleutian Islands (*Double Drake Sill*). The sill consists of a ridge three grid cells on either side of the peak elevation centered on 55°N and increases linearly in height from the sea floor to 1000 m below the surface.

Adding a sill in the northern wide basin results in higher salinity in the northern subpolar gyre region of the Atlantic than at comparable latitudes in the Indo-Pacific (Fig. 4.1f). In this configuration, the Indo-Pacific-like basin is, on the whole, still saltier than the Atlantic-like basin, suggesting that what matters for deep water formation is the surface salinity in the subpolar regions in particular, not the average basin salinity. The meridional mean overturning circulation is substantially different in *Double Drake* from that in *Double Drake Sill* (compare Fig. 4.2a,c and Fig. 4.2b,d respectively). In the *Double Drake Sill* configuration, the deep convection and cross-equatorial meridional overturning shift to the narrow basin, generating a global ocean meridional overturning circulation that looks most similar to that of CM4's a realistic continental geometry (Fig. 4.2a,f).

To our knowledge, previous studies have not explored how the latitude of the northern boundary of the Indo-Pacific as a key feature of global ocean basin geometry that leads to the confinement of northern deep water formation to the Atlantic.

In the following sections, we will focus on the *Double Drake* and *Double Drake Sill* configurations to uncover how the addition of a sill from sea floor to 1000m depth in the northern portion of the wide, Indo-Pacific-like basin can shift the location of deep water formation and large-scale overturning to the narrow, Atlantic-like basin.

#### 4.3.2 Comparison of Atmospheric and Oceanic Fields in Configurations with Different North Pacific Basin Geometries

To better understand the geometric drivers of ocean circulation that lead to deep water formation and associated cross equatorial meridional overturning, we compare climatological fields in the Northern Hemisphere of *Double Drake* and *Double Drake Sill* to the more realistic CM4 model. In general, changing the geometry of the northern Indo-Pacific-like basin by adding a sill at 55°N (*Double Drake Sill*) results in fields in both the ocean and atmosphere that are similar to GFDL CM4 (Figs. 4.3, 4.4, 4.5). The addition of the sill in the northern wide basin precludes watermass transformation of water that sinks to dense isopycnals that outcrop at the surface in the Southern Ocean, suppressing the MOC in the wide basin. This results in less heat transported to the subpolar wide basin, so the subpolar region of the Pacific-like basin fills with sea ice. The presence of this sea ice rearranges the atmospheric circulation and increases the turbulent fluxes over the subpolar Atlantic-like basin, driving deep sinking and the formation of a MOC in that basin.

In CM4, the sea-surface temperature (SST) is warmer in the northern Atlantic-like basin than

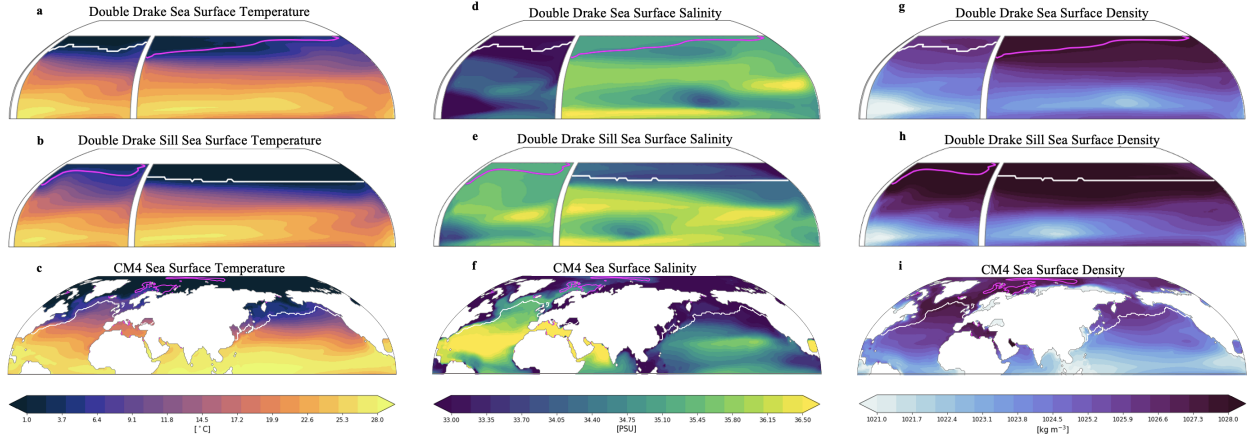


Figure 4.3: Northern Hemisphere SST for (a) *Double Drake*, (b) *Double Drake Sill*, and (c) CM4. Northern Hemisphere sea surface salinity for (d) *Double Drake*, (e) *Double Drake Sill*, and (f) CM4. Northern Hemisphere sea surface density for (g) *Double Drake*, (h) *Double Drake Sill*, and (i) CM4. Magenta contour lines show the location of where the  $\sigma = 37$  isopycnals outcrop at the surface. White contour lines show the maximum sea ice extent for 15% of the averaging period. Figures show 30 year means.

in the northern Indo-Pacific-like basin (Fig. 4.3c). In *Double Drake*, the SST is colder in the narrow North Atlantic-like basin than in the wide North Indo-Pacific-like basin (Fig. 4.3a). The SST increases in the northern narrow basin of the *Double Drake Sill* configurations by upwards of 10°C in some regions compared to the SST in *Double Drake* (Fig. 4.3b,c). The northern wide basin also cools with the addition of a zonal subsurface sill at 55°N. While the resulting SST field in *Double Drake Sill* does not look the same as that in CM4, it does represent a marked improvement in reproducing the temperature differences between basins in CM4 compared to the SST in *Double Drake*.

Sea-ice cover asymmetry between the basins is also improved in *Double Drake Sill* compared to *Double Drake*. Sea ice cover extends farther south in the Pacific than the Atlantic in CM4 (white contour, Fig. 4.3c). The sea ice extent in *Double Drake Sill* is confined to the wide basin, whereas in *Double Drake*, the sea ice is in the narrow basin.

Sea surface salinity in CM4 is higher at all latitudes in the North Atlantic than the North Pacific by upwards of 3 PSU in many regions (Fig. 4.3f). The average SSS in *Double Drake* north of 45°N is lower in the Atlantic-like basin than in the Indo-Pacific-like basin by about 2 psu (Fig. 4.3d). SSS in *Double Drake Sill* in the narrow basin is 2-3 psu higher than *Double Drake* (Fig. 4.3e). While the Indo-Pacific-like basin does not experience a noticeable decrease in SSS averaged over the entire basin, the northern subpolar region (north of 50°N) does freshen. By this measure, the SSS in the *Double Drake Sill* configuration is much more similar to the CM4 SSS than the SSS in *Double Drake* is, particularly north of 50°N, though the Indo-Pacific is fresher and the Atlantic is saltier in CM4 than in any of our idealized configurations.

In CM4, the sea surface density is lowest in the high latitude North Atlantic (Fig. 4.3i).

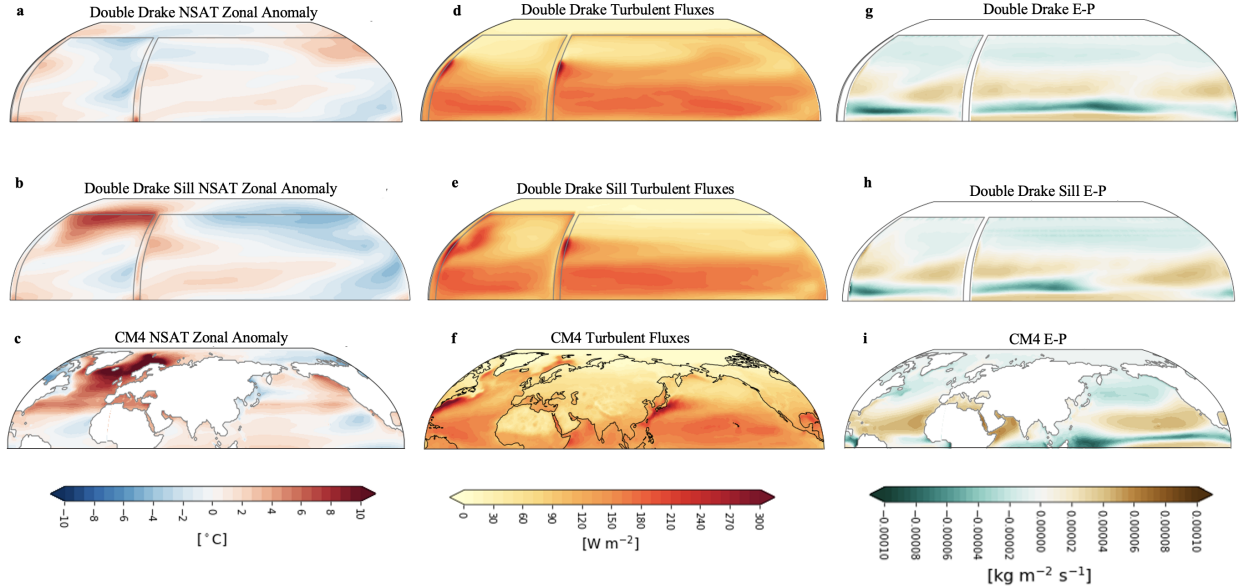


Figure 4.4: Northern Hemisphere near surface air temperature anomaly from the zonal mean for (a) *Double Drake*, (b) *Double Drake Sill*, and (c) CM4. Northern Hemisphere turbulent fluxes (positive indicates fluxes out of the ocean) for (d) *Double Drake*, (e) *Double Drake Sill*, and (f) CM4. Northern Hemisphere evaporation minus precipitation for (g) *Double Drake*, (h) *Double Drake Sill*, and (i) CM4. Figures show 30 year means.

Sea surface density in *Double Drake* is highest in the northern Pacific-like basin (Fig. 4.3g), which aligns with where the deep water formation occurs (Fig. 4.8a). However, density in the narrow basin of *Double Drake Sill* is higher than in the wide basin (Fig. 4.3k). The surface density of *Double Drake Sill* is more similar to that of CM4 than *Double Drake*, which is larger at comparable latitudes in the Atlantic than the Pacific.

Atmospheric fields in *Double Drake Sill* are also more similar to that found in CM4 than that found in *Double Drake*. In the North Atlantic region, the anomaly from the zonal mean temperature is much warmer than that found in the North Pacific in CM4 (Fig. 4.4c). Anomalous zonal near surface air temperature values in *Double Drake* are close to 0°C in the northern narrow basin and are slightly negative in the northeast region of the narrow basin (Fig. 4.4a), which looks markedly different from the values in CM4. The anomaly of near surface air temperature from the zonal mean is upwards of 10°C in the North Atlantic in CM4 (Fig. 4.4a). *Double Drake Sill*, on the other hand, exhibits a much more similar distribution of zonal anomalies in near surface air temperature to CM4 (Fig. 4.4b).

In CM4, turbulent fluxes are larger over the North Atlantic than over the North Pacific (Fig. 4.4f). Turbulent fluxes in *Double Drake* are larger in the high latitudes of the northern wide basin than over the narrow basin by about 100  $\text{W m}^{-2}$ . Heat fluxes are similar between *Double Drake* and *Double Drake Sill* over the wide, Indo-Pacific-like basin, but there are increases by about 150  $\text{W m}^{-2}$  out of the narrow Atlantic-like basin north of 40°N in *Double Drake Sill* compared to *Double Drake*. This is evident in Fig. 4.4d and 4.4e. The region

north of the subsurface zonal sill of *Double Drake Sill* fills with sea ice, reducing surface heat fluxes in the northern wide basin of *Double Drake Sill* compared to *Double Drake*. Thus, the northern wide basin sea surface in *Double Drake Sill* looks more like snow-covered land in the winter.

None of the idealized model configurations considered here capture in detail the pattern of E-P present in CM4, though they do capture the magnitude and general pattern of larger magnitudes of precipitation in the tropics and high latitudes and larger values of evaporation in the subtropics (Fig. 4.4g). E-P is larger over the northwest narrow basin in *Double Drake Sill* than in *Double Drake*, indicating that interrupting the connectivity of waters in the northern wide basin to high latitude regions results in patterns of E-P more similar to CM4 (Fig. 4.4g-i).

The structure of the geopotential height anomaly in CM4 is more complex than that of any of the idealized continental configurations, but the magnitude and position of the trough and the crest over the North Atlantic is more similar to that over the northern narrow basin in *Double Drake Sill* than *Double Drake*. Atmospheric stationary waves over the Northern Hemisphere, particularly over the North Atlantic, are better in *Double Drake Sill* than in *Double Drake* (Fig. 4.5a,b) when compared to the stationary waves in CM4. In *Double Drake*, there is a high in the 300 hPa zonal geopotential height anomaly over the northwestern narrow basin and a low in the northeast. In *Double Drake Sill* and CM4, the high sits over the northeastern part of the Atlantic (Fig. 4.5b,c). These atmospheric circulation structures are driven by the strong contrast in surface turbulent fluxes between *Double Drake* and *Double Drake Sill*. In *Double Drake Sill*, the sea ice acts like snow-covered land, reducing the surface fluxes in the northern wide basin compared to the northern narrow basin. The contrast in surface fluxes in the northern high latitudes drives at atmospheric stationary wave response, which manifests as an eastward shift and a strengthening of the high geopotential height anomaly over the northern narrow basin in *Double Drake Sill* compared to *Double Drake*.

The surface zonal wind speed in the North Atlantic basin of CM4 blows diagonally towards the northwest while the westerlies across the North Pacific are more zonal in character (Fig. 4.5f). There are two zonal wind speed maxima over the northern narrow basin in *Double Drake*, one in the west and one in the east (Fig. 4.5d). Surface zonal wind patterns in CM4 are not well captured by our idealized simulations, however, in *Double Drake Sill* and CM4 there is only one maximum in zonal surface winds in the west of the North Atlantic (Fig. 4.5e,f). Thus we conclude that changes in ocean geometry in the northern Indo-Pacific-like basin result in changes in zonal wind speeds over the northern Atlantic-like basin.

The barotropic streamfunction in CM4 shows a relatively strong subpolar gyre in the North Atlantic and a weak one in the North Pacific (Fig. 4.5i). In contrast, the subpolar gyre in the narrow basin of *Double Drake* is much weaker than the subpolar gyre in the wide basin (Fig. 4.5g). In *Double Drake Sill* the wide basin subpolar gyre is weak and deviates from a characteristic Sverdrup gyre shape, due to the presence of the zonal submarine sill (Fig. 4.5h). The subpolar gyre in the narrow basin is stronger by about 20 Sv compared to *Double Drake* (Fig. 4.5h). The gyre circulation in *Double Drake Sill* is much more similar to that of CM4 than *Double Drake*'s does. This change in barotropic streamfunction arises due to a strengthening of the surface winds over the narrow basin and reduced surface wind stress

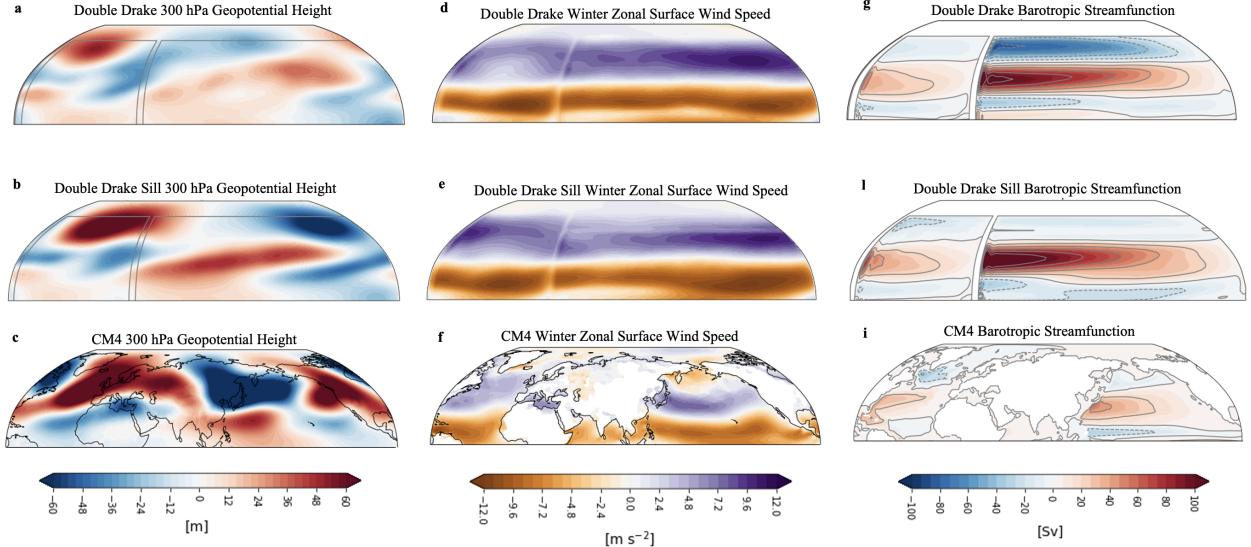


Figure 4.5: Northern Hemisphere Geopotential height anomaly from the zonal mean at 300hPa for (a) *Double Drake*, (b) *Double Drake Sill*, and (c) CM4. Northern Hemisphere surface zonal wind speed for (d) *Double Drake*, (e) *Double Drake Sill*, and (f) CM4. Northern Hemisphere barotropic streamfunction for (g) *Double Drake*, (h) *Double Drake Sill*, (i) CM4. Figures show 30 year means.

from sea ice cover over the wide basin of *Double Drake Sill* compared to *Double Drake*. The stronger subpolar gyre in the narrow basin of *Double Drake Sill* brings salty, subtropical water farther north where it is exposed to cold air temperatures, loses buoyancy, and sinks.

#### 4.3.3 Moisture fluxes and freshwater transport

Positive values of moisture transport indicate export of freshwater out of the Atlantic by the atmosphere. The zonal atmospheric moisture transports for *Double Drake* and *Double Drake Sill* generally favor the export of moisture over the Pacific to the Atlantic in the low latitudes (Fig. 4.6). With a barrier to ocean flow by the sill in the North Pacific, the atmosphere exports more freshwater out of the Atlantic basin. The largest changes in atmospheric moisture transport occur in the tropics, where *Double Drake Sill* import less atmospheric freshwater into the Atlantic-like basin than *Double Drake* does, contributing to the higher salinity in the Atlantic-like basin in *Double Drake Sill* compared to *Double Drake*.

Both idealized configurations' zonal atmospheric moisture transport deviate significantly from that of CM4. In the Northern Hemisphere mid-latitudes, however, the export of moisture is qualitatively similar in CM4 and *Double Drake Sill* (Fig. 4.6). Both exhibit a maximum in export out of the narrow basin at around 35-40°N and moisture import north and south of this export maximum. This indicates that atmospheric moisture transport and basin salinity are not primary drivers of MOC localization to the narrow basin in *Double Drake Sill*.

The ocean imports less freshwater in the Northern Atlantic basin in *Double Drake Sill* than

### Atmospheric Moisture Transport (Eastern-Western Boundary)

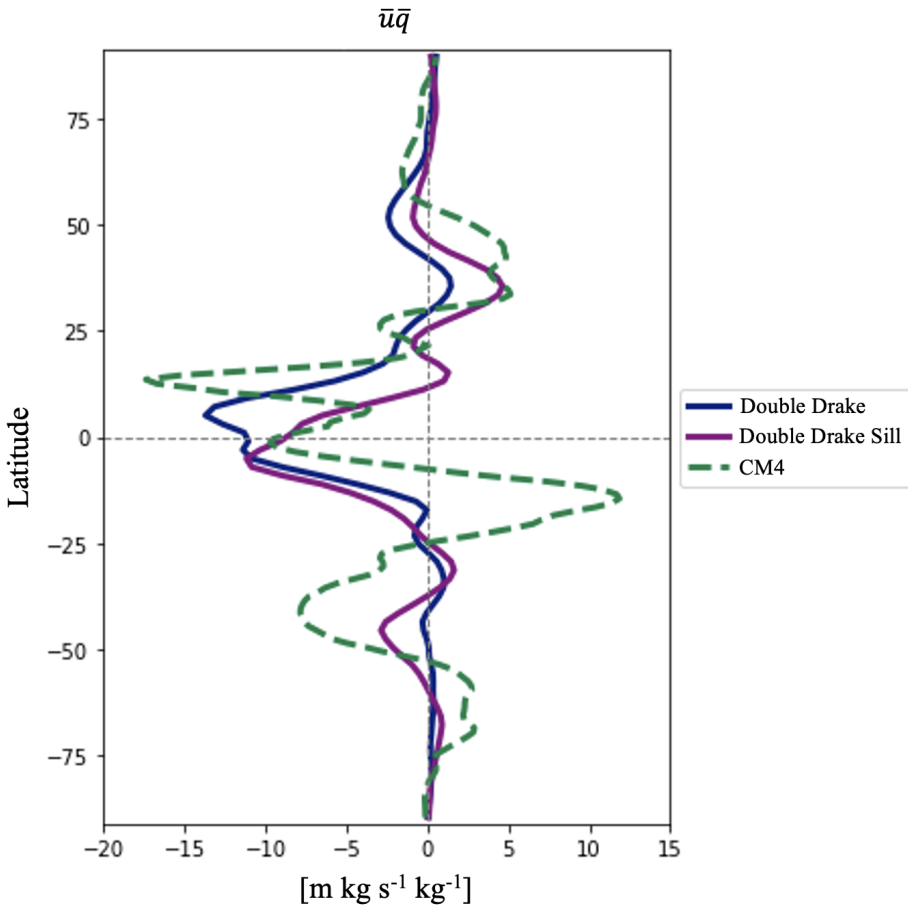


Figure 4.6: Atmospheric moisture transport across basin boundaries. Net zonal transport,  $\bar{u}\bar{q}$ , for *Double Drake*, *Double Drake Sill*, and CM4

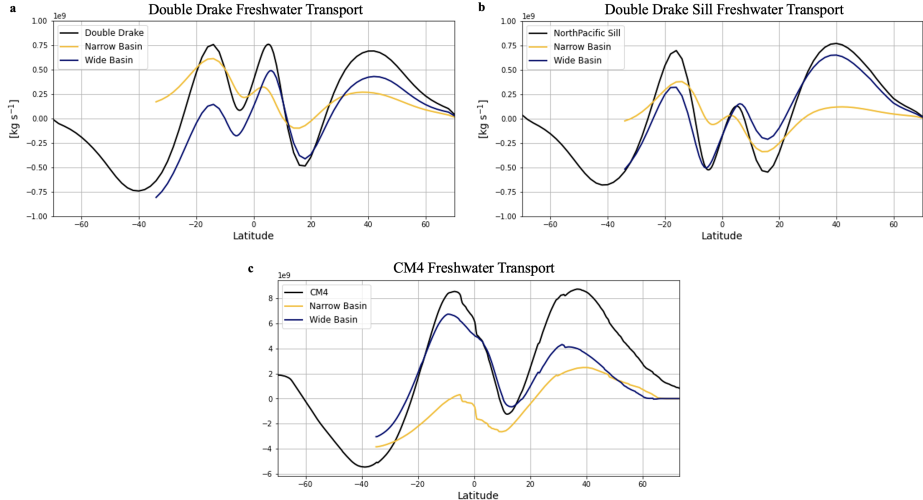


Figure 4.7: Implied freshwater transport for both basins calculated from surface freshwater fluxes ( $P+R-E$ )

in *Double Drake* (Fig. 4.7). This is indicative of the salt advection feedback (Stommel 1961), which attributes the relatively high salinity in the North Atlantic to the northward flowing AMOC that brings warm, salty subtropical water to the northern subpolar region. The Atlantic exports fresher water than it imports (Weiher et al. 1999; Wolfe and Cessi 2014), indicating a positive salt-advection feedback in which the ocean circulation exports freshwater from the Atlantic basin, which in combination with the net evaporation over the Atlantic (Wijffels et al. 1992), acts to strengthen AMOC. Here, in the Atlantic-like basin deep ventilation and associated cross-equatorial MOC, the ocean imports saltier water than in the basin in which deep convection is absent. Qualitatively, the freshwater flux in *Double Drake Sill* looks more similar to that in CM4 (Fig. 4.7). While the northward freshwater transport at all latitudes in both *Double Drake* and *Double Drake Sill* is not present in CM4, the narrow basin transports less freshwater northward in the Northern Hemisphere in *Double Drake Sill* than in *Double Drake*, which aligns with the interpretation that saltier water is transported northward in the basin to which MOC localizes.

For this coupled general circulation model, higher basin-average sea surface salinity of an ocean basin is not a necessary condition for the localization of deep sinking to that basin. The *Double Drake Sill* configuration is marked by a cross-equatorial meridional overturning circulation in the narrow basin, even as the mean salinity of the wide basin is similar to that of the narrow basin. Of note, however, is that the subpolar salinity is higher in the narrow sinking basin of *Double Drake Sill* than in the wide basin. Thus, surface salinity does matter for deep sinking, but the focus should be on the contrast in subpolar salinity between ocean basins, rather than the contrast in basin-average salinity. This also suggests the salt-advection feedback is not a necessary condition for the development and maintenance of a MOC. Further, the AMOC may not be as sensitive to the import of salty water into the Atlantic as previous theory suggests. The salt advection feedback - and thus the freshwater transport in the ocean - is not necessarily a precursor to MOC development, and the

simulations here suggest that it is not required for the localization of deep water formation.

#### 4.3.4 Watermass transformation

To examine how the different continental configurations impact the interior density fields, we examine the watermass transformation rates following Speer and Tziperman 1992 and Oldenburg et al. 2021. The surface density flux,  $D(x, y, t)$  is calculated by considering both heat and freshwater fluxes via:

$$D(x, y, t) = \frac{\alpha(x, y, t)Q_H(x, y, t)}{c_w} - \beta(x, y, t)S(x, y, t)Q_F(x, y, t), \quad (4)$$

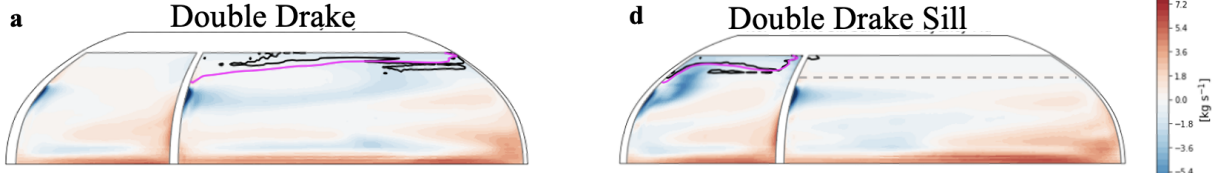
where  $\alpha$  is the thermal expansion coefficient,  $Q_H$  is the surface heat flux into the ocean,  $c_w$  is the specific heat capacity of water,  $\beta$  is the haline contraction coefficient,  $S$  is the absolute salinity, and  $Q_F$  is the freshwater flux into the ocean.

The surface buoyancy flux in the Northern Hemisphere in *Double Drake* is most negative (making surface water parcels denser) in the northern Indo-Pacific basin where the densest isopycnals and the deepest wintertime mixed layers occur (Fig. 4.8a). The presence of the zonal sill in the northern wide basin of *Double Drake Sill* means dense isopycnals that outcrop in the Southern Ocean cannot connect to the surface at high northern latitudes (Fig. 4.2b). As such, deep convection and associated cross-equatorial overturning is not supported in the basin with the sill. This leads to a shutdown of PMOC-like overturning, and less ocean heat transport to the northern subpolar wide basin, causing cooling and sea ice expansion. In turn, surface heat fluxes are reduced resulting in less watermass transformation compared to the corresponding region in *Double Drake*.

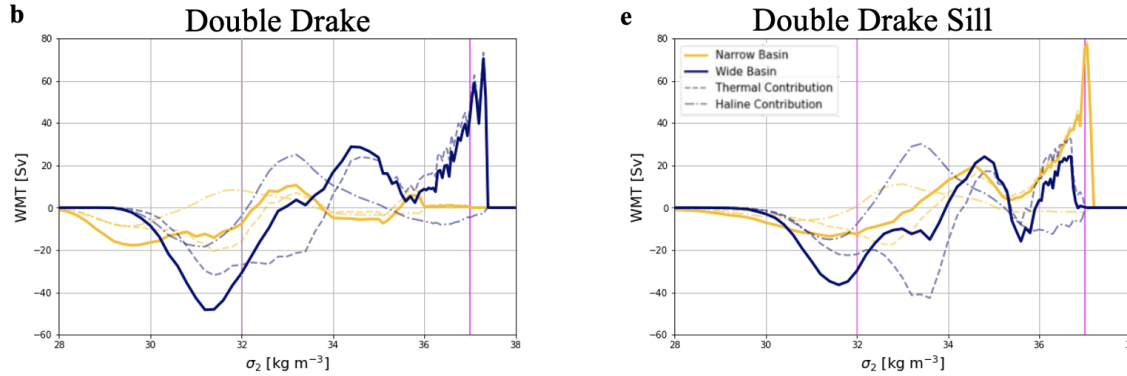
In nature, dense isopycnals cannot outcrop in the northern Indo-Pacific basin due to the presence of the Aleutians. Additionally, the surface buoyancy fluxes in the North Pacific are less negative than in the North Atlantic. The combination of these two factors prevents deep water formation and large scale meridional overturning from occurring in the Pacific Ocean. The isopycnals and surface buoyancy fluxes in *Double Drake Sill* exhibit a similar behavior. In *Double Drake*, however, the regions of densest water and most negative surface buoyancy flux are in the northern Indo-Pacific-like basin (Fig. 4.8b). The subpolar gyres in both the Atlantic and the Indo-Pacific are associated with wind-driven upwelling, which is altered by the presence of the northern zonal subsurface sill. In *Double Drake Sill*, while the North Pacific extends far enough north to experience cold atmospheric temperatures, the dense interior isopycnals cannot connect to the surface owing to the presence of the zonal sill at 55° (Fig. 4.8c).

While wide basin overturning and deep convection decrease with the addition of a sill in the northern wide basin, they increase in the narrow basin. The increase in magnitude of negative surface buoyancy fluxes in *Double Drake Sill* indicate that the ocean transports heat that it takes up at low latitudes to high latitudes where it can lose heat in order to balance the surface buoyancy budget. AMOC with deep sinking occurs in *Double Drake Sill* suggests that the primary reason cross equatorial MOC localizes to the narrow basin is because dense isopycnals are not allowed to outcrop in the northern wide basin.

## Surface Buoyancy Fluxes



## Watermass Transformation Rates



## Narrow Basin Surface-Forced MOC

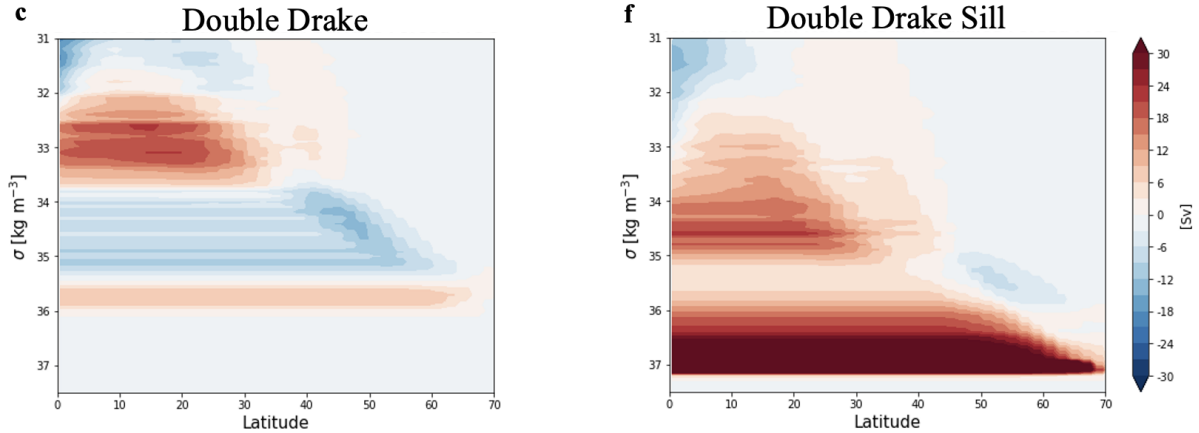


Figure 4.8: Surface buoyancy fluxes for the Northern Hemispheres of (a) *Double Drake* and (d) *Double Drake Sill* are plotted in filled contours. The  $\sigma = 37$  isopycnal is contoured in magenta. The black contour indicates regions where the wintertime mixed layer depth is greater than 600m. The second row of plots show (b) *Double Drake* and (e) *Double Drake Sill* watermass transformation rates for each ocean basin as well as their thermal and haline components. The bottom row of plots shows surface-forced MOC plotted on isopycnal layers calculated from the watermass transformation rates for (c) *Double Drake* and (f) *Double Drake Sill*.

The greatest watermass transformation rates occur in regions of deep ventilation all of the simulations. In the highest density classes, namely  $\sigma \geq 37 \text{ kg m}^{-3}$ , transformation of water into higher density occurs in the wide basin in *Double Drake* (Fig. 4.8d). For *Double Drake Sill*, however, the transformation of these dense waters into higher density classes occurs in the narrow basin (Fig. 4.8b,c). These watermass transformation rates are driven primarily by thermal effects, rather than the impact of salinity differences between configurations.

From the surface buoyancy in *Double Drake* and *Double Drake Sill*, we calculate the implied meridional overturning circulation driven by surface fluxes,  $F(\sigma)$ . This is done by binning the surface density flux into density classes and integrating over the surface area of each density bin:

$$F(\sigma) = \frac{1}{\Delta\sigma} \int \int_{\sigma}^{\sigma+\Delta\sigma} D(x, y, t) dA, \quad (5)$$

where  $\sigma = \rho - 1000$  is the potential density referenced to 2000 m, and  $\Delta\sigma$  is the width of each density bin. The surface forced MOC in the narrow, Atlantic-like basin for *Double Drake* and *Double Drake Sill* are plotted in Fig. 4.8g-i. As with the MOC calculated directly from volume transport (Fig. 4.2), the narrow basin in *Double Drake* does not contain an AMOC (Fig. 4.8g), while the narrow basin in *Double Drake Sill* does (Fig. 4.8h,i).

#### 4.4 Discussion & Conclusions

Previous studies implicate the narrow width of the Atlantic compared to the Indo-Pacific and the shorter southern extent of the African continent compared to the South American continent as the primary factors of ocean basin geometry that lead to AMOC localization (Ferreira et al. 2010; Nilsson et al. 2013). These geometric features lead to ocean and atmospheric circulations that act to elevate the salinity of the Atlantic over that of the Pacific. The higher salinity of the Atlantic contributes to the localization of deep sinking by increasing the surface density and decreasing the stratification of the North Atlantic. However, in the coupled model discussed in this chapter, the reasons for why AMOC localizes to the Atlantic Ocean cannot be explained by the conclusions of previous studies that used MITgcm and SPEEDY. The root cause of MOC localization in the simulations discussed here using MOM6-AM2 is the ability for isopycnals in the ocean interior to outcrop at northern high latitudes where there are negative surface buoyancy fluxes. Thus, in the configurations presented here, the primary reason the global ocean circulation is marked by an AMOC rather than a PMOC is the northern extent of the wide basin, not the width or southern extent of the narrow basin as suggested by previous idealized modeling studies (Ferreira et al. 2010; Jones and Cessi 2017; Nilsson et al. 2013; Ferreira et al. 2018).

Restricting the ocean's access to the northern high latitudes in the wide, Pacific-like basin forces deep ventilation into the northern high latitudes in the Atlantic-like basin. While this has not explicitly been explored in previous idealized configurations, a more southward northern boundary in the Indo-Pacific-like basin is employed in some previous studies (i.e. Nadeau and Jansen 2020). Additionally, Hu et al. 2015 note a strengthening of AMOC with a closure of the Bering Strait, indicating a link between deep water formation in the

Atlantic and the connectivity between waters in the North Indo-Pacific and Arctic ocean basins. Our study does not test the impact of the Bering Strait on AMOC localization. The simulations illustrate a role for limiting access to high latitude waters in the North Pacific for determining the strength and location of northern deep water formation and the localization of deep sinking in the Atlantic.

Surface turbulent fluxes over the North Atlantic respond to atmospheric conditions that result from warm North Atlantic SSTs and the relatively cooler North Pacific. Atmospheric stationary wave response leads to increased turbulent fluxes over the North Atlantic, particularly over the western part of the basin, which leads to an increase in the negative surface buoyancy fluxes over the North Atlantic basin (Fig. 4.4e-g). Turbulent fluxes out of the ocean increase over North Atlantic, which generates a stationary wave response. This in turn strengthens the zonal surface winds over the North Atlantic and further increases turbulent fluxes over North Atlantic. The changes in surface winds drives a strengthening of North Atlantic subpolar gyre, which brings more warm water to North Atlantic, again further increasing turbulent fluxes over North Atlantic. The increased turbulent fluxes over the North Atlantic, particularly over the western part of the basin, lead to an increase in the negative surface buoyancy fluxes over the North Atlantic basin.

In the coupled idealized GCM employed in this study, the narrow width of the Atlantic and the shorter extent of the African continent are not sufficient to localize deep sinking and MOC to the Atlantic basin. We found that the higher surface salinity of the Atlantic compared to the Indo-Pacific is a diagnostic that is intimately connected to the AMOC, but does not explain the cause of MOC localization to the narrow basin. It is not necessary for the Atlantic to be saltier than the Pacific for deep sinking and associated cross-equatorial MOC to occur in the Atlantic. For example, in the realistic continental geometry of the CM4 simulation, the Indo-Pacific is fresher and the Atlantic is saltier than in any of our idealized configurations, even the ones that have an AMOC (Fig. 4.1).

Sinking occurs in the densest water classes, thus it is simply necessary for the densest water to be in the northern subpolar region of the Atlantic. As such, the surface salinity in the subpolar regions is key. Deep sinking occurs in the saltier subpolar gyre, not the basin with a higher basin-average salinity. This is a surprising result; in our configurations, the primary reason the global ocean circulation is marked by an AMOC rather than a PMOC is the northern extent of the wide basin, not the width or southern extent of the narrow basin as implicated in previous idealized modeling studies (Ferreira et al. 2010; Jones and Cessi 2017; Nilsson et al. 2013; Ferreira et al. 2018). This is due to changes in ocean and atmosphere circulation which result in a higher salinity in the subpolar region of the narrow basin with the addition of a zonal sill in the northern wide basin. The salinity in the Atlantic basin does increase after the AMOC develops, which is caused by the salt-advection feedback (Stommel 1961). This suggests that an ocean basin geometry that does not allow for dense isopycnals that outcrop in the Southern Ocean to return to the surface in the North Pacific cannot sustain deep sinking in the Pacific.

The density of the North Atlantic does not necessarily need to be significantly higher than that of the North Pacific to localize AMOC, particularly when ocean basin geometry interrupts dense interior isopycnals from reaching the surface in the North Pacific, as in *Double*

*Drake Sill.* When dense isopycnals are not allowed to reach the surface in the North Pacific, that shuts off northward heat transport, leads to sea ice formation in the northern Indo-Pacific basin.

The ocean takes up heat at low latitudes and must deliver it to high latitudes. It is indiscriminate about the region where heat loss occurs, but in order to balance the buoyancy budget, watermass transformation that creates denser water must occur to oppose the addition of buoyancy near the equator (Newsom and Thompson 2018). Restricting the ocean’s access to the northern high latitudes in the wide, Pacific-like basin by adding a subsurface zonal sill at the latitude of the Aleutians forces deep ventilation into the northern high latitudes in the Atlantic-like basin. The sill cuts off dense isopycnals in the ocean interior from outcropping at the surface, keeping the surface watermass transformation from forcing a meridional overturning circulation in the wide ocean basin and instead requiring a meridional overturning in the narrow basin.

As a result of changes in ocean circulation in response to the addition of a sill in the northern Indo-Pacific-like basin, the region north of the sill fills with sea ice. This sea ice cover acts to reduce the surface fluxes over the subpolar wide basin. The contrast in surface turbulent fluxes between the northern wide basin and the northern narrow basin leads to an atmospheric stationary wave response that drives a strengthening of the subpolar gyre in the narrow basin. This brings more salty, subtropical water to high latitudes where it is exposed to cold enough air temperatures for watermass transformation, deep-sinking, and generates a MOC in the Atlantic-like basin.

## 5 The Impact of Continental Geometries on Mean State Climate and Heat Transport

Total meridional heat transport from the equator to the poles is relatively insensitive to different oceanic and atmospheric circulations, except as they influence the planetary albedo (Enderton and Marshall 2009). This implies that if the ocean heat transport changes with climate forcing or differs among models, we expect compensation from atmospheric heat transport (Stone 1978). Moreover, the partitioning of the total poleward heat transport in the climate system between the ocean and the atmosphere is robust over a range of continental geometries (Czaja and Marshall 2006). However, continental configuration directly impacts the ocean currents, which transport heat in the ocean. This heat transport in turn exerts direct control on sea ice and the meridional surface albedo gradient (Enderton and Marshall 2009). For instance, adding narrow meridional continents to an aquaplanet model modifies the ocean circulations by allowing the creation of zonal pressure gradients and western boundary currents, which promotes larger poleward transport of heat in the ocean. The opening of a Drake Passage allows for the formation of an Antarctic Circumpolar Currents which isolates the South Pole from southward heat transported from low latitudes. Thus ocean circulation changes that result from modification of ocean basin geometries generate a large range of different atmospheric heat transports and climates.

Previous work demonstrates that different ocean basin geometries and thus different ocean

circulation patterns result in vastly different climates in otherwise similar model simulations (De Boer et al. 2008; Enderton and Marshall 2009; Ferreira et al. 2010; Nilsson et al. 2013). However, much of the previous work investigates ocean heat transport in simple ocean basin geometries used MITgcm coupled to SPEEDY, which lacks accurate simulations of cloud processes.

In this study, we compare four different continental geometries, all of which have polar land caps for numerical stability, discussed further in chapter 2, consistent with the configurations explored in chapters 3 and 4.

## 5.1 Model Configurations

### 5.1.1 Coupled MOM6-AM2

We use a fully coupled, global circulation model with an ocean–sea-ice model (MOM6-SIS2) coupled to an atmosphere–land model (AM2-LM2). This is a novel model configuration developed for this thesis work, and is described fully in Chapter 2.

### 5.1.2 Continental Configurations

For this Chapter, we run the same coupled model as in Chapter 4, but we consider a more idealized set of ocean basin geometries. These geometries are designed to create ocean planets with incrementally increasing complexity and increasing similarity to the modern ocean. The first configuration is an aquaplanet without any meridional barriers to ocean flow (*Aqua*). This ocean configuration does not support gyre circulation or a pole-to-pole cross equatorial meridional overturning circulation in the ocean. The second is a planet with a single narrow meridional ridge from the northern to the southern boundary (*Ridge*), which supports planetary scale barotropic gyres. The third is a planet with a single narrow meridional ridge from the northern boundary to 55°S to mimic the Drake Passage (*Drake*), which has gyres and a global scale cross-equatorial meridional overturning circulation. The fourth is a planet with two narrow meridional ridges forming two ocean basins, one three times wider than the other (*Double Drake Sill*). We place a zonal, Gaussian sill rising to 1000 meters depth centered on 55°N. This configuration supports gyres in both ocean basins and a meridional overturning circulation localized to the narrower ocean basin (Chapter 5).

Each model configuration is run for 2000 years. The results are shown for averages of the last 100 years of each simulation. The ocean is 4000 m in depth. The meridional barriers are all 4° of latitude wide and do not extend into the atmosphere.

## 5.2 Results

### 5.2.1 Surface Climate

The gyre circulation in the ocean helps explain many of the sea surface salinity and sea ice differences between configurations. Without any meridional boundaries to ocean flow, as in *Aqua*, the ocean the barotropic streamfunction is much stronger than any gyres observed in the nature. Without any barriers in the ocean, there is no mechanism to support Sverdrup

### Sea Surface Salinity and Barotropic Streamfunction

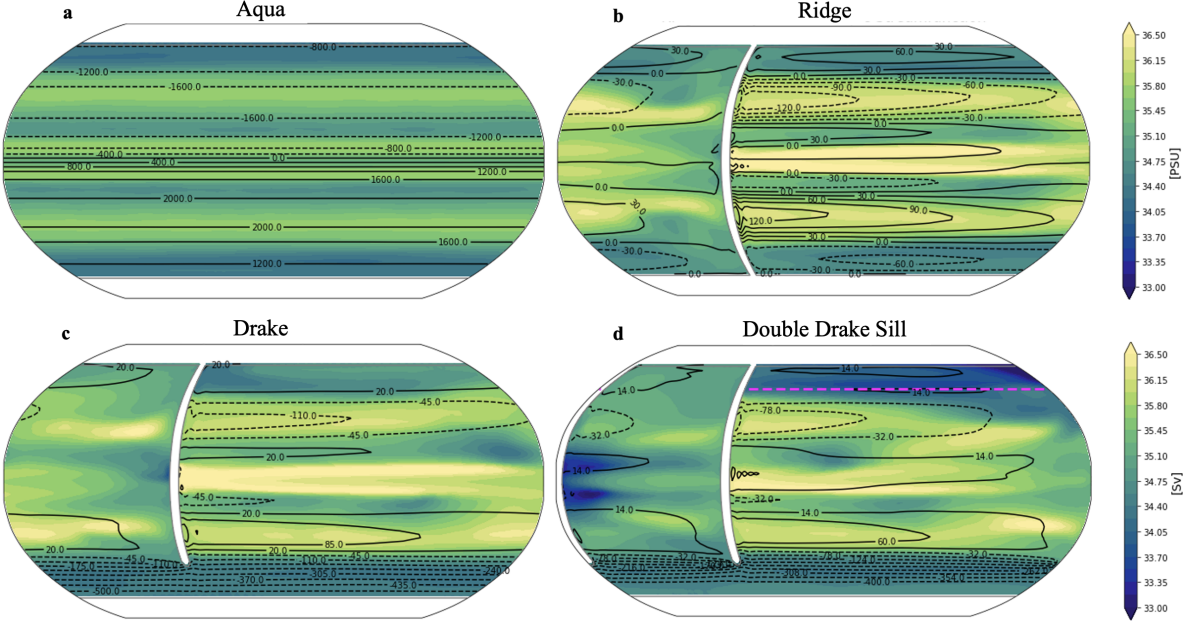


Figure 5.1: Sea surface salinity for each configuration is plotted as filled contours. On top, the barotropic streamfunction is contoured in black. The latitude of the zonal sill in *Double Drake Sill* is indicated with the magenta dashed line.

balance and as such, there are no wind-driven gyres (Fig. 5.1a). Unlike in the real ocean, where the gyres are closed streamfunction pathways, the streamfunction lines in *Aqua* follow latitude lines and do not allow any mean meridional mass transport. At the equator, there is a local surface salinity minima due to strong equatorial upwelling. In the mid to high latitudes, the sea surface salinity reflects the pattern of evaporation minus precipitation.

The sea surface salinity in *Aqua* reflects the lack of the gyres with minima and maxima arranged in zonal bands that are symmetric about the equator. In *Ridge*, the introduction of a meridional ridge creates a barrier to zonal flow in the ocean supporting Sverdrup balance that results in western-intensified gyre circulation (Fig. 5.1b). The subtropical gyres are strong, over 140 Sv in certain regions, reflecting the scale of the global ocean basin and the long wind fetch. This ocean circulation results in more zonal variation in the sea surface salinity.

The removal of the ridge in the Southern Ocean, as in *Drake*, creates hemispheric asymmetry in the ocean circulation and sea surface conditions (Fig. 5.1c). The Northern Hemisphere in *Drake* looks much the same as that in *Ridge*, but without a barrier in the southern high latitudes, there is very little poleward meridional flow in the southern ocean. This acts to isolate the southern polar region from the midlatitudes. As such, the ocean is fresher at high latitudes in the Southern Hemisphere than at the respective latitudes in the Northern Hemisphere. Creating two ocean basins (*Double Drake Sill*) adds further complexity to the structure of the barotropic streamfunction and the surface salinity; there is asymmetry in

### Sea Surface Temperature and Sea Ice Extent

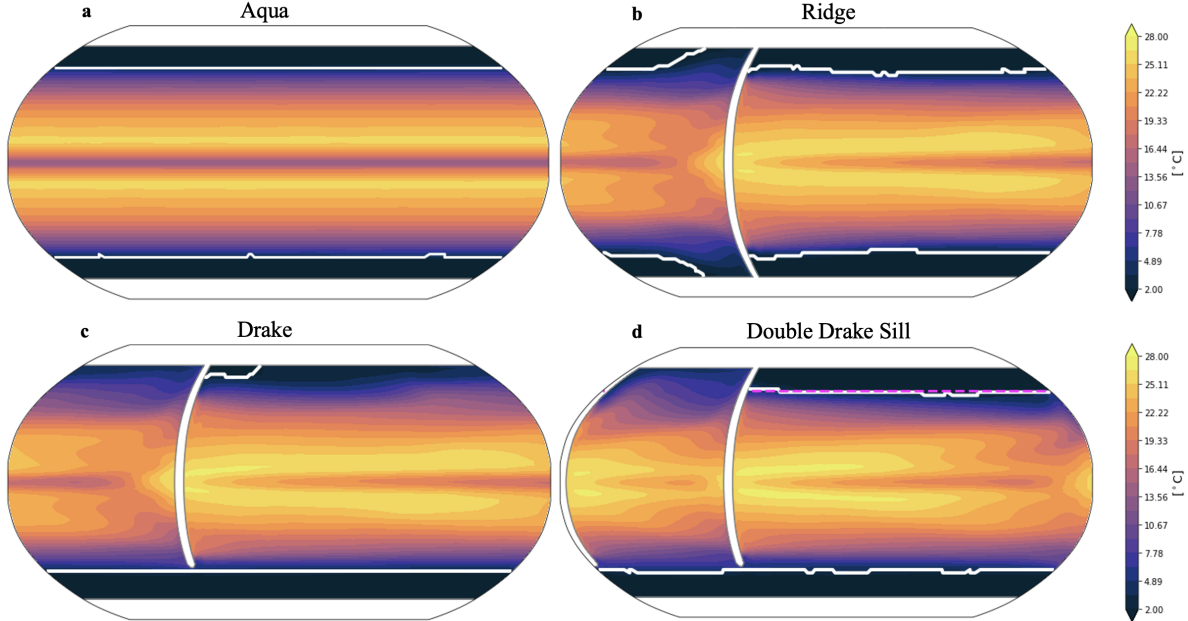


Figure 5.2: SST for each of the continental configurations – *Aqua*, *Ridge*, *Drake*, *Double Drake Sill* – is shown in filled contours. The white contour indicates maximum sea ice extent for at least 15% of the averaging period of 100 years.

the strength of gyres and the sea surface salinity between the two ocean basins more zonal structure in the surface salinity. In *Double Drake Sill*, the wider basin's maximum gyre transport is stronger than the narrow basin by about a factor of 4, reflecting the width of the ocean basins (Fig. 5.1d). The presence of the Southern Ocean acts in *Drake*, acts to isolate the southern high latitudes. The narrower basin has higher surface salinity at northern high latitudes than the wide basin with the sill.

In the absence of any meridional boundaries, the pattern of sea surface temperature (SST) in *Aqua* arranges into zonal bands (Fig. 5.2a). Opening a southern ocean, as in *Drake*, results in lower temperatures in the Southern Ocean, but elsewhere the pattern of SST is similar to that of *Ridge* (Fig. 5.2c). The meridional barrier in the north allows for warmer waters to travel farther poleward whereas in the south, the absence of a ridge isolates the southern high latitudes from warm subtropical waters. In addition, the presence of two ocean basins results in different SSTs between basins. In *Double Drake Sill*, the narrow basin is warmer than the wide, particularly at high northern latitudes (Fig. 5.2d).

These different patterns of SST across configurations are tightly linked to the distribution of sea ice. The sea ice in *Aqua* extends to around 50°N and 50°S for at least 15% of the 100-year averaging period. In *Ridge*, the SST displays more meridional structure, supported by the gyres that develop as a result of the meridional ridge (Fig. 5.2b). The sea ice extent is significantly reduced compared to that of *Aqua*, a difference connected to the farther poleward extinctions of warm water at the surface into the subtropics and beyond. In the

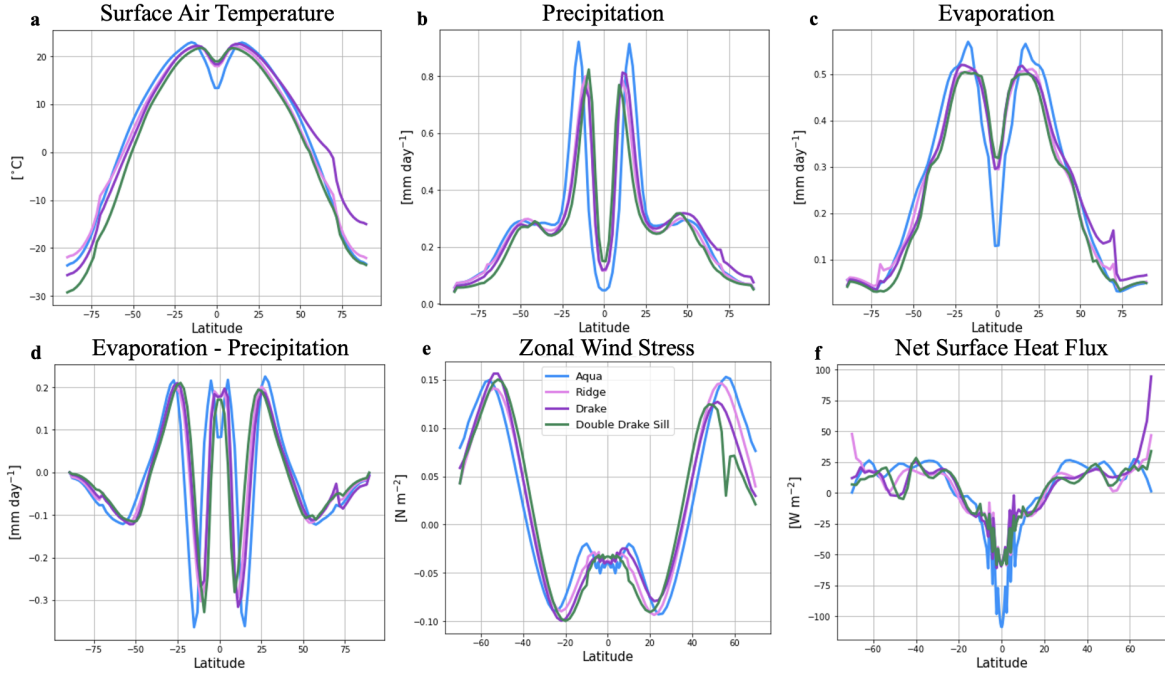


Figure 5.3: Zonal average a) SST, b) precipitation, c) evaporation, d) evaporation minus precipitation, e) wind stress, and f) surface heat flux for each configuration.

Southern Hemisphere, the sea ice extent in *Drake* is similar to that of *Aqua*, whereas in the Northern Hemisphere, the sea ice extent is much more similar to that of *Ridge*. In *Double Drake Sill*, the sea ice in the Southern Hemisphere is similar to that of *Aqua* and *Drake*, whereas in the Northern Hemisphere, the warm, narrow basin remains ice free while the wide basin grows sea ice in the northwestern part of the basin.

Next, we look at zonal mean surface climate in each continental configuration. In *Aqua*, the strong equatorial upwelling results in a local minimum in zonal mean near surface air temperature in the low latitudes. The temperature is hemispherically symmetric. The addition of the meridional barrier decreases the equator to pole near surface temperature gradient in *Ridge* compared to *Aqua* (Fig. 5.3a). The ridge prevents the strong upwelling in aqua from developing on the equator, and as a result, the equatorial temperature minimum is smaller in magnitude than in *Aqua*, and the gyre circulation acts to increase the polar temperature over that of *Aqua* (Fig. 5.3a). In *Drake*, without a barrier in the southern ocean, the zonal mean near surface temperature in the Southern Hemisphere is colder than in the Northern Hemisphere. This is due to the lack of meridional flow and thus small magnitude of poleward heat transport in the Southern Ocean, which is accomplished by gyre circulation that cannot exist without a meridional boundary.

*Aqua* has larger of zonal mean precipitation than the other configurations, but this is largely compensated by the zonal mean evaporation to create similar patterns for evaporation minus precipitation across different configurations (Fig. 5.3b-d). The presence of meridional boundaries reduces the strength of the wind stress in the midlatitudes (Fig. 5.3e). The con-

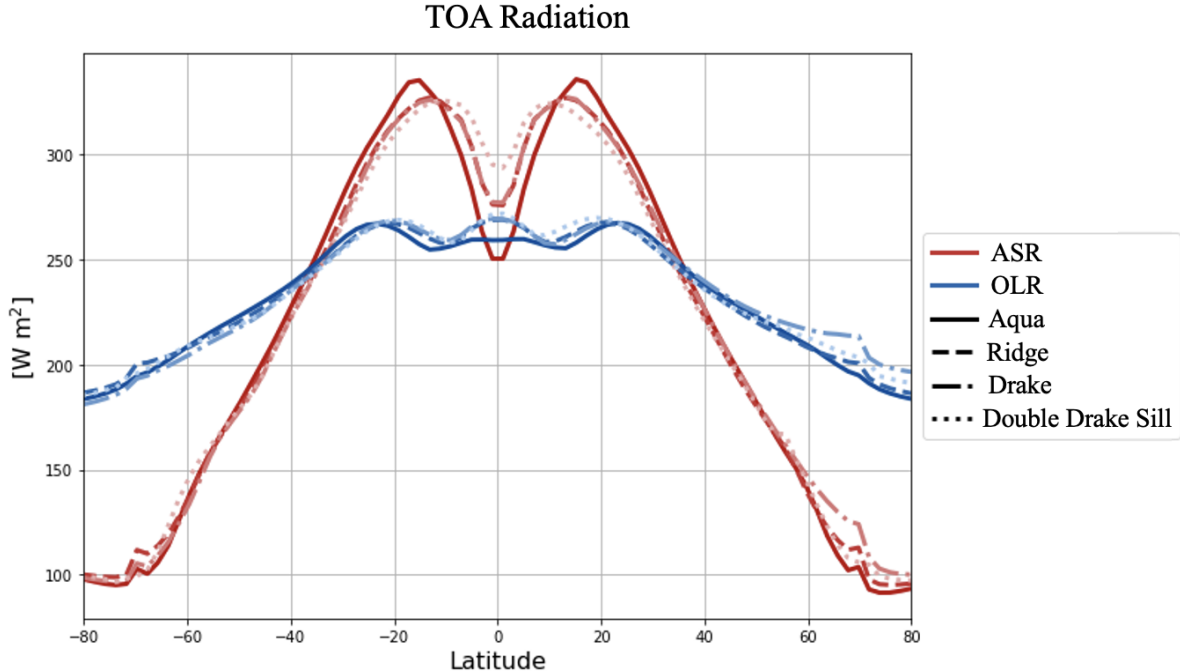


Figure 5.4: Zonal mean top of atmosphere (TOA) radiation for each configuration. Absorbed solar radiation (ASR) plotted in red colors and outgoing longwave radiation (OLR) in blue colors.

tinental boundaries increase outgoing surface heat flux at high latitudes (Fig. 5.3f). *Ridge* displays an increase in outward surface over that of *Aqua*. The outward heat flux of *Drake* is high in the northern high latitudes, as in *Ridge*, and low in the southern high latitudes, as in *Aqua*. The magnitude of the surface heat flux in *Double Drake Sill* sits between that of *Drake* and *Ridge*.

*Drake* and *Double Drake Sill* have climates marked by larger precipitation, evaporation minus precipitation, and wind stress in the Southern Hemisphere than the northern (Fig. 5.3b,d,e). There is also larger surface heat flux out of the ocean to the atmosphere in the Northern Hemisphere than the southern (Fig. 5.3f).

This symmetry across hemispheres is reflected in the radiation at the top of the atmosphere (TOA). The TOA radiation in *Aqua* and *Ridge* is hemispherically symmetric, while in the two configurations without any land barriers in the southern ocean, *Drake* and *Double Drake Sill*, both the absorbed solar radiation (ASR) and outgoing longwave radiation (OLR) are larger in the Northern Hemisphere than in the Southern Hemisphere (Fig. 5.4). There is larger magnitude of ASR in *Aqua* in the subtropics than in any other configuration as well and a smaller magnitude on the equator than in the other configurations (solid red line, Fig. 5.4).

A large influence on the structure of TOA radiation is the distribution of clouds in each configuration. In *Aqua*, there is greater than 80% cloud cover in the mid to high latitudes, a minimum in the subtropics, and another maximum on the equator (Fig 5.5a). The addition of

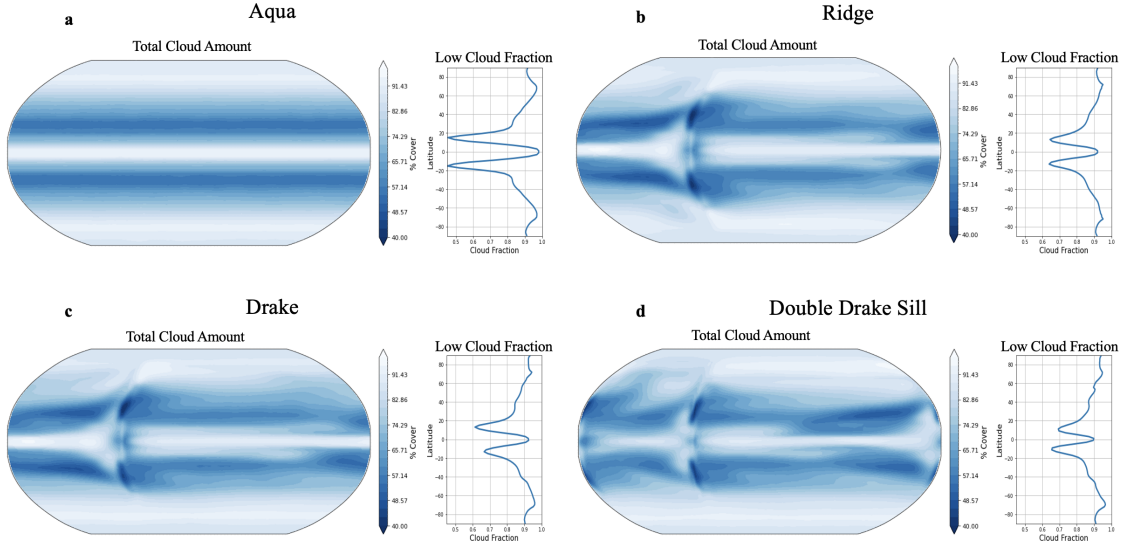


Figure 5.5: Maps showing the total cloud amount in a) *Aqua*, b) *Ridge*, c) *Drake*, and d) *Double Drake Sill*. Plots to the right of each map show the zonal mean fraction of the total cloud amount comprised of low clouds.

a pole-to-pole meridional boundary, as in *Ridge*, alters the distribution of clouds by creating a deck of low clouds west of the ridge that breaks the zonal structure of the clouds (Fig 5.5b). The opening of a channel in the southern high latitudes, as in *Drake*, results in a larger cloud amount in the Southern Hemisphere mid and high latitudes than in the Northern Hemisphere ((Fig 5.5c). Creating two ocean basins with a southern ocean, as in *Double Drake Sill*, results in greater complexity in the distribution of clouds (Fig 5.5d). Notably, the wide, Pacific-like basin is cloudier than the narrow, Atlantic-like basin. For each of the configurations, much of the cloud amount is composed of low clouds, with a larger fraction of low clouds to mid and high clouds in regions that have a larger total cloud amount in general. Moreover, the distribution of clouds echoes many of the patterns evident in the SSTs of each configuration (Fig. 5.2), with regions of lower SST displaying higher cloud amounts. The low clouds over the equator in *Aqua* (and to a lesser extent in the other configurations) reduces the absorbed solar radiation on the equator. In the mid-latitudes, differences in the storm track between configurations act to reduce the cloud cover and change the ASR.

### 5.2.2 Overturning Circulation

We next turn our attention to the meridional overturning circulation in each configuration, which informs the climatological potential temperature in the atmosphere and ocean. In *Aqua*, the low latitude atmospheric cells that span from  $0^\circ$  to  $15^\circ$ , rotate in the opposite direction from the Hadley cell in the real world, as implied by the atmospheric heat transport (Fig. 5.6a). These ‘reverse Hadley’ cells result from the strong equatorial upwelling and low SSTs at the equator in these configurations, particularly when compared to the temperatures of the real ocean. The low temperature on the equator, coupled with high cloud cover (Fig. 5.5), results in lower absorbed solar radiation on the equator than off the equator (Fig. 5.4),

driving down-gradient energy transport towards the equator.

Between  $15^\circ$  and  $40^\circ$  there are clockwise cells in the Northern Hemisphere and counterclockwise in the Southern Hemisphere. Poleward of  $40^\circ$  there is one more cell in each hemisphere, approximately matching the latitude and intensity of the Ferrell cell (Fig. 5.6a), top panel). In the ocean, the overturning circulation is correlated with the contours of potential temperature (Fig. 5.6a, bottom panel). The strong, deep overturning cells in the low latitudes to the subtropics help bring warm water to the intermediate depths and bring large amounts of heat to the mid-latitudes.

In *Ridge*, the oceanic equatorial cells are weaker and the poles are warmer than in *Aqua* (Fig. 5.6b, top panel). The ocean subtropical cells that transport warm water are much shallower but extend farther poleward than those in *Aqua* (Fig. 5.6b, lower panel). There is also deep overturning in the high latitudes transporting cold water from the surface to the intermediate depths and to mid latitudes below the subtropical cells. This is because the barrier in *Ridge* prevents the wind driven circulation from becoming as strong as in *Aqua*. *Drake* breaks the north-south hemispheric symmetry in the temperature and overturning that is present in *Aqua* and *Ridge*. In the Southern Hemisphere, the atmospheric polar potential temperatures are lower and the overturning circulation is weaker than in the Northern Hemisphere (Fig. 5.6c, top panel). The subtropical cells in *Drake* are similar to those in *Ridge*, but the intermediate and deep ocean overturning leads to a warmer Northern Hemisphere ocean than Southern Hemisphere (Fig. 5.6c, bottom panel). The cross-equatorial meridional circulation and the northern high latitude deep water formation brings warm water northward at the surface before it subducts near the northern polar land boundary. Zonal mean potential temperature and overturning circulation in *Double Drake Sill* is similar to that in *Drake*, though the presence of the zonal sill in the northern wide basin interrupts the overturning circulation in the wide basin, resulting in comparatively lower temperatures in the northern high latitudes (Fig. 5.6d, top panel).

In all these configurations, air ascends off the equator at about  $15^\circ$  and flows towards the equator, where there is subsidence. This is connected to the low SSTs on the equator. This circulation is most pronounced in *Aqua*, where the equatorial SSTs are lowest of all the configurations. In *Aqua*, the ocean overturning circulation is dominated by deep subtropical wind-driven cells which extend polewards of  $40^\circ$  and to the bottom of the ocean, bringing cold deep water up to the surface at the equator. These counter-rotating atmospheric meridional overturning cells weaken with the addition of meridional boundaries in the ocean, but they do not disappear, indicating that the subtropical ocean circulation brings more deep cold water to the surface in these simulations than in the real world.

The meridional overturning circulation in the ocean in the *Aqua* configuration exhibits strong, deep subtropical cells that extend the full depth of the ocean, with magnitudes larger than 60 Sv (Fig. 5.7a). Adding a ridge shoals the vertical penetration and weakens the magnitude of the subtropical overturning cells by about 2000 m and 20 Sv compared to those in *Aqua*. The ridge also creates conditions for deep overturning near both poles (Fig. 5.7b). Opening a passage, as in *Drake*, creates hemispheric asymmetry in the deep water formation, primarily relegating it to the Northern Hemisphere and generating a cross-equatorial overturning circulation (Fig. 5.7c). The addition of a second ridge to create two

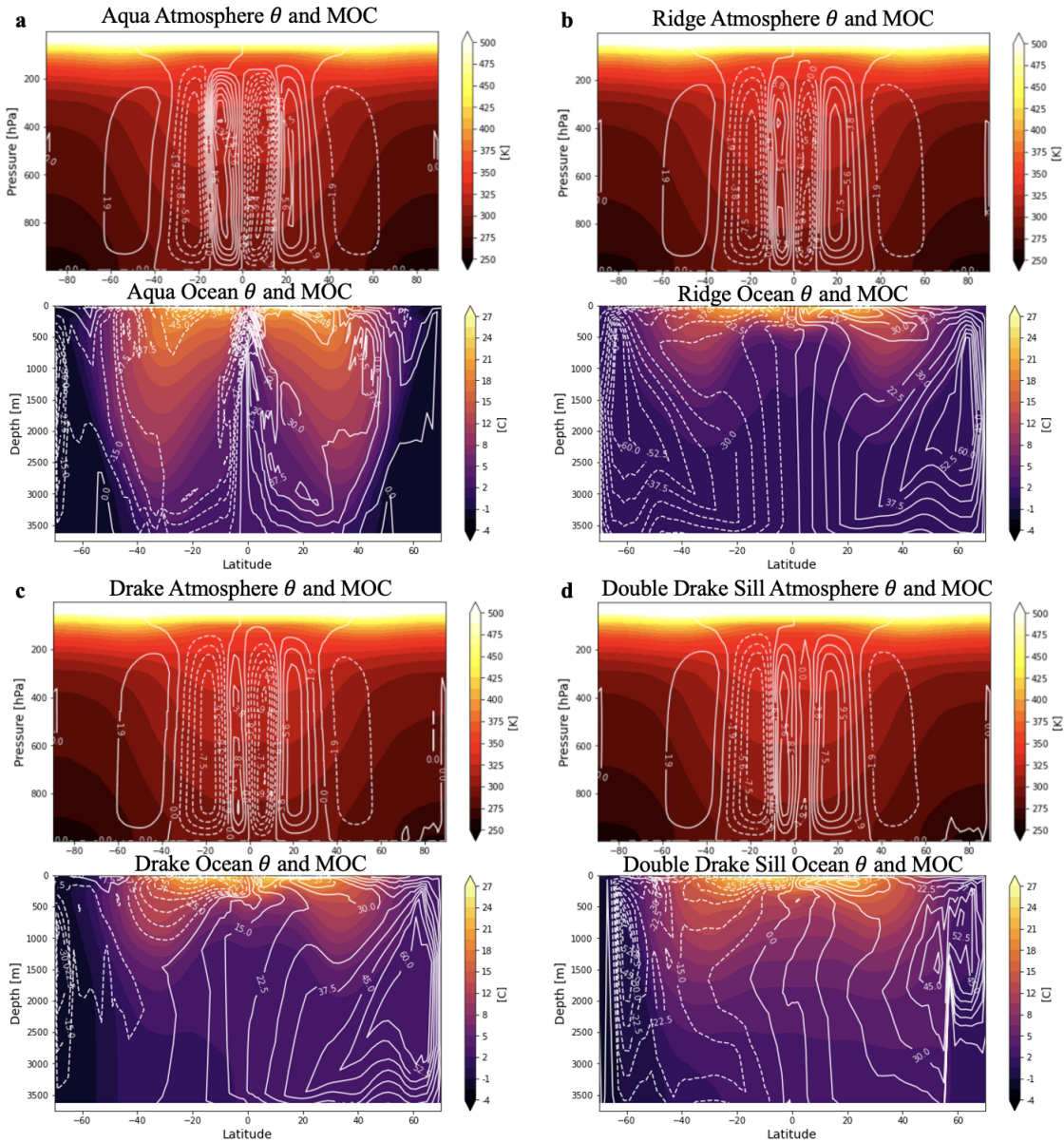


Figure 5.6: Potential temperature and mean meridional overturning circulation in the ocean and the atmosphere.

## Meridional Overturning Circulation

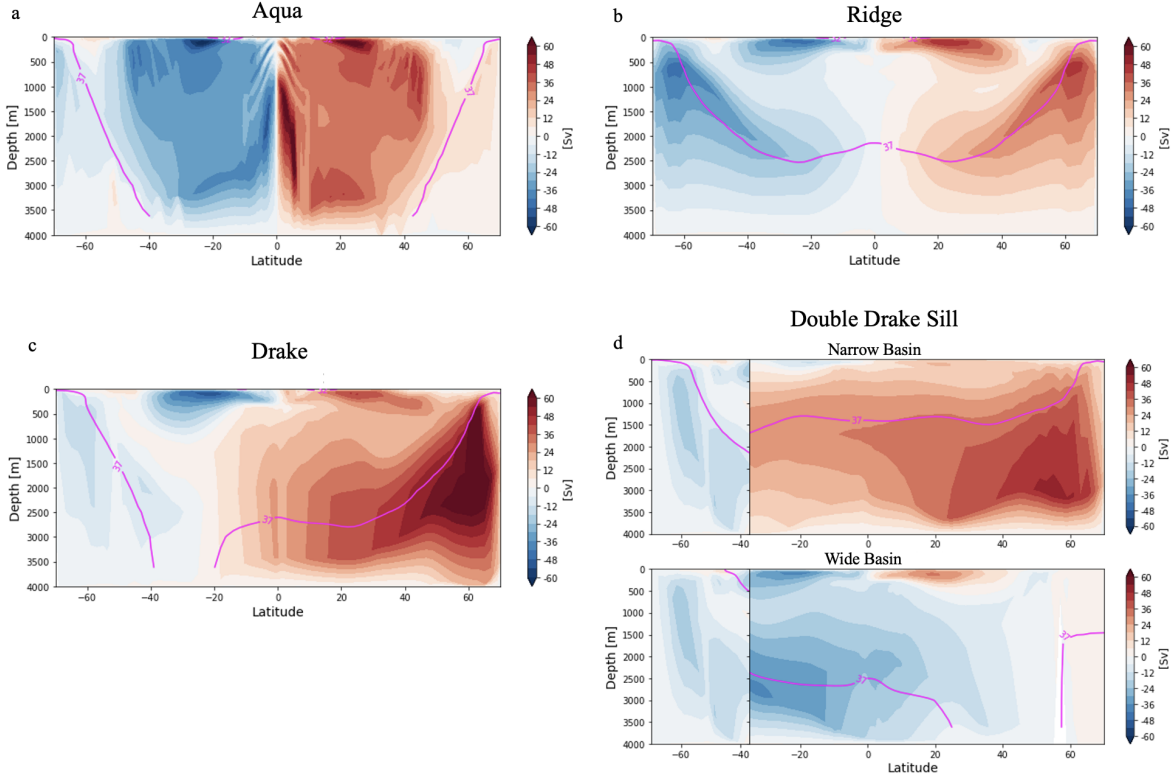


Figure 5.7: Meridional overturning circulation in the ocean for each configuration. MOC is plotted for each ocean basin in *Double Drake Sill* (d). Filled contours indicate volume streamlines. Magenta contours trace the  $\sigma = 37 \text{ kg m}^{-3}$  isopycnal.

ocean basins leads to the localization of deep cross-equatorial overturning circulation and deep water formation to one of the basins. In the *Double Drake Sill* configuration, the deep water formation occurs in the narrow basin, not in the wide basin with the zonal sill (Fig. 5.7d). With two ocean basins, the strength of the shallow subtropical cells is about 24 Sv stronger in the wide basin than the narrow basin.

We examined an additional configuration similar to *that of Double Drake Sill* zonal sill in the northern wide basin (*Double Drake*). In that run, the deep water formation and associated cross-equatorial MOC occurs in the wide basin. This is discussed in detail in chapter 2. In brief, the coupled model developed for this dissertation preferentially develops a meridional overturning circulation and deep water formation in the wider of the two ocean basins, contrary to findings from previous idealized aquaplanet-type studies (Enderton and Marshall 2009; Nilsson et al. 2003; Ferreira et al. 2018). The addition of the sill in the northern wide basin interrupts the meridional flow in the ocean, keeping dense isopycnals from outcropping in the northern high latitudes, where relatively cold air temperatures create large air-sea temperature gradients, which act to reduce the buoyancy of the water at the surface enough for it to sink (Chapter 5).

### 5.2.3 Heat Transport

The total meridional heat transport remains remarkably similar across different configurations (black lines, Fig. 5.8), despite differences in sea ice distribution, and thus zonal mean surface albedo (Fig. 1). In the low latitudes, between about 25 degrees north and south of the equator, the ocean (blue lines, Fig. 5.8) transports more heat than the atmosphere (red lines, Fig. 5.8) does. The ocean heat transport varies across simulations as with the ocean circulation, which responds to changes in idealized continental configuration. In *Aqua*, the ocean transports a maximum of about 3 PW at 20° and less than 0.5 PW at 60° (Fig. 5.8a). The maximum heat transport in *Ridge*, *Drake*, and *Double Drake Sill* is shifted poleward compared to *Aqua*, and is closer to 2 PW. These simulations also show an increased ocean heat transport at higher latitudes; *Ridge*, *Drake*, and *Double Drake Sill* all transport about 1 PW at 60°N. *Ridge*, like *Aqua*, has hemispherically symmetric heat transport. This symmetry is broken in *Drake* and *Double Drake Sill*, however. In *Drake*, more heat is transported northward than southward by the ocean, and the ocean transports heat north across the equator (Fig. 5.8c). Both of these features of the ocean heat transport in *Drake* are due to the presence of a ridge with an open southern passage.

In response to changes in ocean heat transport, the atmosphere compensates, shifting the pattern and magnitude of atmospheric heat transport to maintain a similar total meridional (atmosphere plus ocean) heat transport across simulations. The magnitude of atmospheric heat transport adjustments are larger than those in the ocean across the configurations. There is equatorward heat transport by the atmosphere in the deep tropics, consistent with the ‘reverse Hadley’ circulation identified in Fig. 5.6. This acts to make the total meridional heat transport in these simulations different than that in nature at low latitudes.

Adding ridges to the ocean results in reduced ocean heat transport at low latitudes, which also reduces the magnitude of the counter-rotating reverse Hadley cell in the configurations with idealized continents. The reverse Hadley cells never fully disappear, however, and are present in the *Ridge*, *Drake*, and *Double Drake Sill* simulations, though with a smaller magnitude than *Aqua*. Also, in simulations with hemispherically asymmetric continental distribution and northward ocean heat transport at the equator (*Drake* and *Double Drake Sill*), the atmosphere transports heat southward across the equator, acting to keep the total meridional heat transport symmetric in both the northern and Southern Hemisphere.

While the addition of idealized ridges does reduce the magnitude of the reverse Hadley cells in *Ridge*, *Drake*, and *Double Drake Sill* compared to *Aqua*, the cells are never eliminated. This is because the ocean is transporting a large amount of heat in the low latitudes, particularly in the shallow subtropical cells, which are stronger than that in nature due to the larger wind fetch of the basins in these idealized configurations. This results in a lower SST at the equator than in the real ocean. Since the ocean is transporting so much heat with a relatively constant top of atmosphere radiation, the atmospheric heat transport needs to compensate in order to balance these changes, often referred to as Bjerknes compensation (Bjerknes 1964; Liu et al. 2016).

While the ocean meridional heat transport changes between configurations in response to the different continental barriers to flow, it is not immediately obvious what processes drive

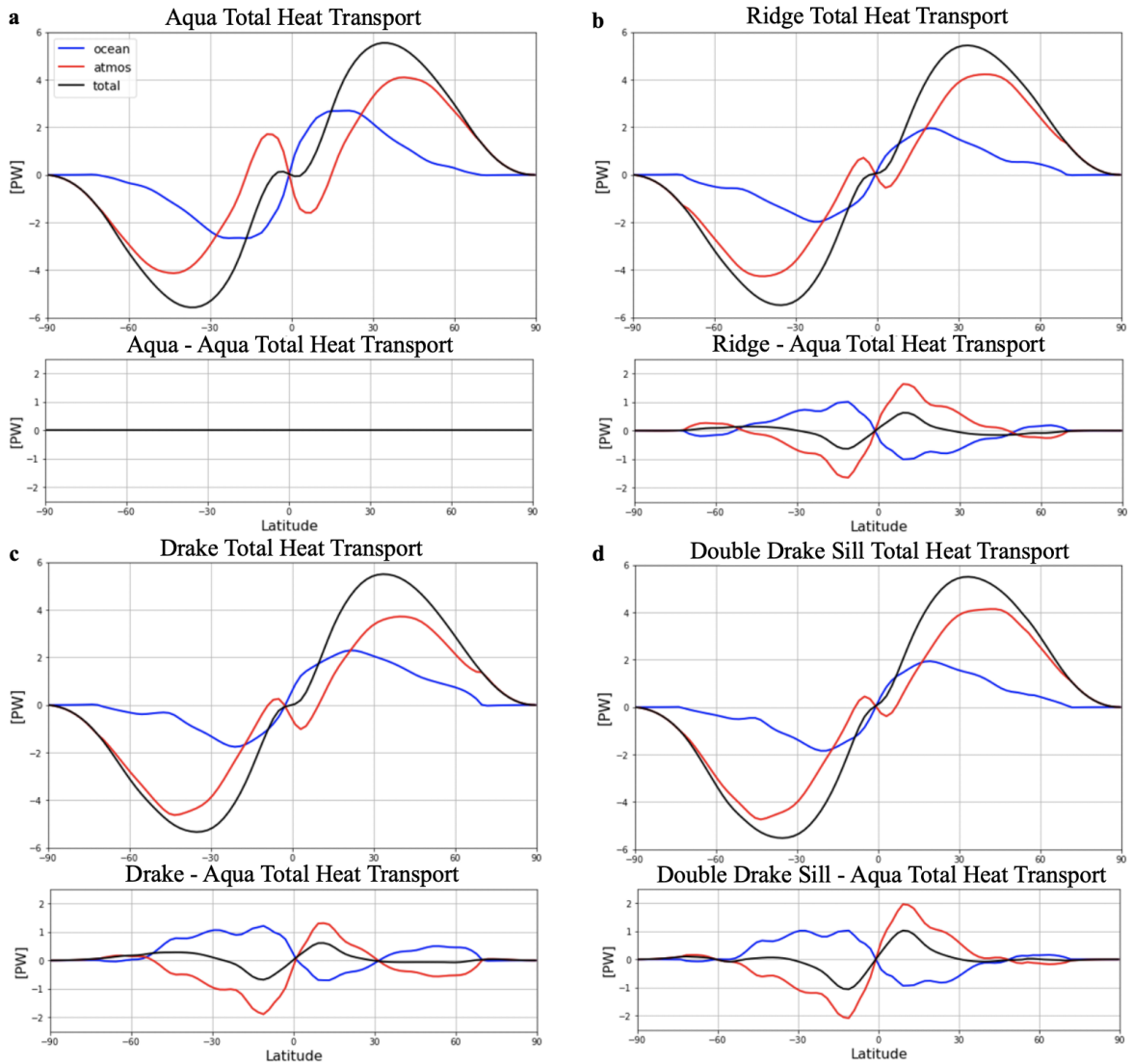


Figure 5.8: Meridional heat transport for a) *Aqua*, b) *Ridge* c) *Drake* d) *Double Drake Sill*. Plots show total meridional heat transport (black lines), atmospheric heat transport (red lines), and oceanic heat transport (blue lines). Top panels show total transport while lower panels display each configuration's anomaly from *Aqua*.

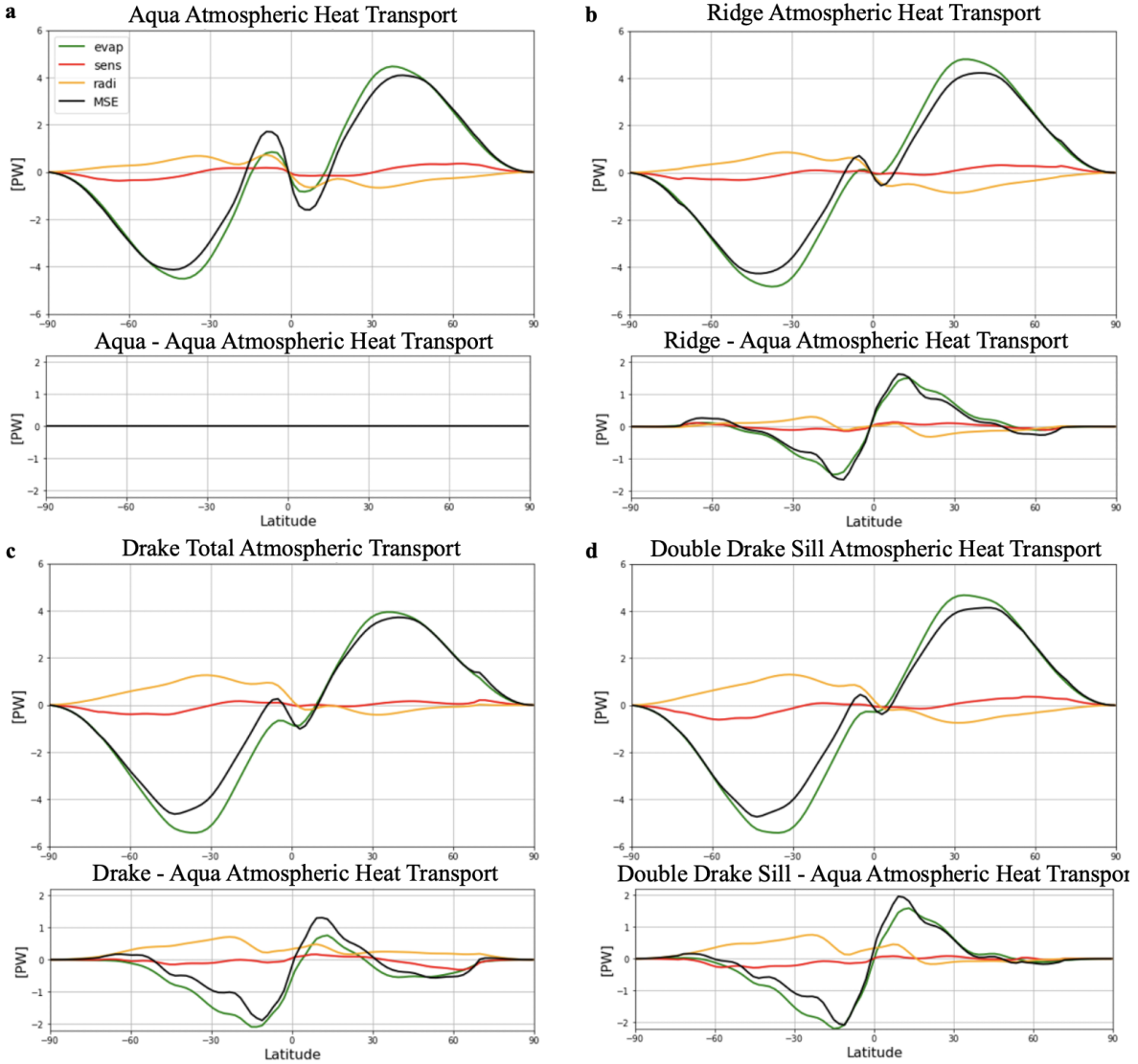


Figure 5.9: Atmospheric heat transport and its partitioning for a) *Aqua*, b) *Ridge* c) *Drake* d) *Double Drake Sill*. Plots show total atmospheric heat transport (black lines), implied atmospheric heat transport from evaporative fluxes (green lines), implied atmospheric heat transport from sensible fluxes (red lines), and implied atmospheric heat transport from radiative fluxes (yellow lines). Top panels show total transport while lower panels display each configuration's anomaly from *Aqua*.

the compensation in atmospheric heat transport. In order to identify the mechanisms coupling the ocean and atmosphere heat transport together, we decompose the atmospheric heat transport into evaporative, sensible and radiative components (Fajber et al. 2023). Outside the deep tropics, the differences in atmospheric heat transport are almost entirely evaporation driven. This explains the tight coupling between the ocean and atmosphere heat transports, since evaporation removes energy from the ocean and adds it to the atmosphere. Changes in evaporation therefore create compensating changes in oceanic and atmospheric heat transports, and are a primary mechanism for coupling atmospheric and oceanic heat transport together. The total heat transport in each of the four configurations (black lines, Fig. 5.9) aligns closely with the heat transport from the evaporative fluxes (green lines, Fig. 5.9). However, equatorward of  $15^{\circ}$ , within the reverse Hadley cells, the radiative fluxes (yellow lines, Fig. 5.9) play an order one role in driving the total heat transport.

The compensation between atmospheric and oceanic heat transport is imperfect, however, and the heat transport changes are of a larger magnitude than the ocean heat transport changes, particularly in the low latitudes. This super Bjerknes compensation is observed locally in regions with positive climate feedbacks (Liu et al. 2016).

Here, the positive feedbacks in the low latitudes result from cloud changes (Fig. 5.5). The overturning circulation in the atmosphere of our model configuration features cells that counter-rotate as compared to the real world Hadley Cell. These counter-rotating cells suppress clouds on the equator, particularly in *Aqua*. Changing the ocean heat transport results in a change in the ITCZ, which in turn changes the clouds, the cloud radiative effects, the evaporation, and the amount of heat transported by the atmosphere.

### 5.3 Discussion & Conclusions

This study describes the climatology of a series of different idealized aquaplanet-like simulations. The addition of meridional barriers to the ocean alters the ocean circulation by creating gyres and meridional overturning circulations. This has the effect of substantially modifying the distribution of sea surface salinity and SST, which then change the patterns of atmospheric circulation. The addition of gyres and meridional overturning circulations also modifies the heat transport of the ocean, transporting more heat to the poles in the low to mid latitudes, reducing the extent of sea ice (Fig. 5.2, 5.1) and warming the climate in general (Fig. 5.3a).

Despite the simplicity of its continental configurations, the climatology of the *Double Drake Sill* configuration shows strong resemblance to the present climate. There is hemispheric asymmetry driven by the presence of a Southern Ocean without any meridional barriers to ocean flow. The presence of two ridges that support barotropic gyres in a narrow basin and a wide basin result in an ocean circulation that maintains a warmer Northern Hemisphere than Southern Hemisphere. The storm track is stronger in the Southern mid latitudes than in the Northern, as shown in the precipitation and wind stress fields (Fig. 5.3b,e). While the atmosphere meridional overturning supports a reverse Hadley cell in the tropics, it is weaker than that of the *Aqua* configuration (Fig. 5.6a,d).

Our study affirms the key role of continental boundaries in creating hemispheric asymmetry

in climate. In particular, the ocean meridional overturning circulation develops asymmetry in *Drake* and *Double Drake Sill*, both configurations with Southern Oceans (Fig. 5.7c,d). This results in northward heat transport across the equator in both the *Drake* and *Double Drake Sill* configurations (Fig. 5.8c,d)

The heat transport changes in the ocean are balanced by changes in atmospheric heat transport, leaving the total meridional heat transport in each continental configuration remarkably similar (Fig. 5.8). This finding corroborates past work, which identifies a lack of sensitivity of meridional heat transport to the particulars of ocean and atmosphere dynamics (Stone 1978; Enderton and Marshall 2009). Here, however, there are differences in total meridional heat transport in the deep tropics, where the addition of meridional barriers reduces the strength of the subtropical overturning cells in the ocean (Fig. 5.6). The atmospheric heat transport over-compensates this change in ocean heat transport. In other words, the ocean transports less heat poleward in the tropical latitudes with the addition of meridional boundaries. The atmosphere compensates by transporting less heat equatorward in the reverse Hadley cells; however, the change in atmospheric heat transport is larger than the change in ocean heat transport, resulting in a change in the total meridional heat transport in the deep tropics (Fig. 5.8). Most of the change in atmospheric heat transport between configurations is caused by changes in evaporation. The evaporative component of the heat transport drives both the mean state atmospheric heat transport as well as the difference between configurations (Fig. 5.9).

In previous coupled model studies of idealized continental configurations, the atmospheric model component is SPEEDY, which does not include realistic representations of clouds or cloud feedbacks (Molteni 2003). In contrast, this model uses AM2, which includes fully prognostic cloud parameterizations. Adding simple meridional boundaries to the ocean results in different SST and atmospheric circulation patterns, which imprint on the distribution of clouds and thus the TOA radiative fluxes and the meridional heat transport. In *Aqua*, there is close to full cloud cover on the equator. Adding meridional boundaries to the ocean results in cloud changes, and in particular, a reduction of low clouds over the equator. Cloud amount differences between the continental configurations result in a positive local feedback whereby a reduction of overturning strength in the tropics in the ocean and atmosphere results in warmer SSTs and near surface air temperature on the equator. As such, there are fewer clouds on the equator in *Ridge*, *Drake*, and *Double Drake Sill* compared to *Aqua*, allowing for larger absorbed solar radiation in the low latitudes (Fig. 5.4). In SPEEDY, because the clouds are diagnostic, adding meridional boundaries to the ocean does not result in a significant change in TOA radiation in the tropical regions. This lack of realistic clouds leads to Bjerknes under-compensation. In contrast, the abundance of low clouds in the tropics in these simulations means that changing the ocean and atmosphere circulation by adding meridional boundaries can result in large cloud cover changes. The differences in local feedbacks control the degree to which the atmosphere can compensate the ocean heat transport changes (Liu et al. 2016).

It is worth noting that the total meridional heat transport does not change much in the high latitudes, despite changes in sea ice cover between configurations. Past results suggest that differences in sea ice distribution can result in differences in total meridional heat transport

(Enderton and Marshall 2009), through changes in surface fluxes that arise from albedo differences between configurations. Here, however, we see that though sea ice distribution changes as a result of different boundaries to ocean flow, the radiative effect of clouds plays a larger role in maintaining similar total heat transports between configurations, particularly in the mid to high latitudes.

## 6 Conclusions

This dissertation aims to contribute to our understanding of the role of ocean basin geometry in shaping the Earth’s climate. We build on a rich landscape of previous literature that makes use of idealized continental configurations to better understand the fundamental physics of the climate system (e.g., Marshall et al. 2007; Enderton and Marshall 2009; Ferreira et al. 2010; Nilsson et al. 2013; Wolfe and Cessi 2011; Jones and Cessi 2017; Cessi and Jones 2017; Nadeau and Jansen 2020).

Our planet’s climate is incredibly complex, which can lead to a drive to better simulate its dynamics by continually increasing the number of processes included in our models. However, there is a difference between simulation and understanding. A hierarchy of models of different complexities can be incredibly useful in testing the validity of physical theories of the dynamics and features of the Earth’s climate. There is, however, a need for care when taking the results of more simplified models and applying the findings to understand the full coupled system.

For instance, modeling studies that use MITgcm or MITgcm coupled to SPEEDY show that MOC localization should occur in the narrow ocean basin when a planet has two ocean basins, one narrow and one wide (Ferreira et al. 2010; Jones and Cessi 2017). Here, we find that the story is more nuanced. In Chapter 3, we find that overturning circulation changes that result from widening the Atlantic basin by changing the coastline shape (*Both Coast*) are distinct from changes resulting from widening the Atlantic basin without modifying the coastline shape (*Wide Coast*). These are distinct responses to coastline shape; the average basin widths and areas increase by the same amount. While northern deep ventilation and associated cross-equatorial overturning circulation is confined to the narrower of two ocean basins, MOC strength increases with an increase in basin width. This is inconsistent with the results of Jones and Cessi 2017, who found that widening the Atlantic-like basin leads to a small decrease in MOC strength.

In Chapter 4, we find that our coupled ocean-sea-ice-atmosphere configuration results in deep sinking and a cross-equatorial overturning circulation in the wide ocean basin (Fig. 4.1). This runs counter to previous studies. In this chapter, I tested several previous theories for MOC localization, but could not produce an AMOC. In order to get an AMOC-like circulation with deep sinking in the narrow basin, we added a below surface zonal ridge at the latitude of the Aleutians. Restricting the ocean’s access to the northern high latitudes in the wide basin forces the deep ventilation into the northern high latitudes in the narrow basin. The sill interrupts dense isopycnals that outcrop in the southern ocean from returning to the surface at high latitudes in the wide basin. Thus, it is potentially not just the shape of

the ocean basins, but the bathymetry of the seafloor that exerts first order control on the location of deep water formation.

We also find that the sinking basin does not need higher basin-average sea surface salinities than the non-sinking basin, but rather that the subpolar gyre salinities in the sinking basin should be higher. In particular, the salinity must be high enough at high latitudes in the sinking basin where surface water is exposed to cold air temperatures that drive negative enough surface buoyancy fluxes for watermass transformation to occur.

Based on these results, this thesis concludes that many of the most important characteristics of the Earth's climate depend on ocean basin geometry. The addition of simple meridional boundaries to the ocean supports the development of gyres, which move around tracers like temperature and salinity in the ocean. Hemispheric asymmetries in the continental boundaries, namely, opening a channel for the Southern ocean, leads to hemispheric asymmetries in the climatologies of the configurations. This is another piece of evidence pointing to the importance of ocean basin geometry in determining the large scale patterns of temperature, precipitation, evaporation, and circulation in the ocean and the atmosphere.

Previous work that employs idealized representations of the continents offered many important insights to the physics of the global circulation of the atmosphere and the ocean. Prior studies generally make use of the same models, MITgcm for the ocean and SPEEDY for the atmosphere, both of which are limited by process complexity and resolution. In particular, we posit that the stark differences between the results in this thesis and those studies can be attributed to the representation of clouds. Clouds and cloud feedbacks are a large source of uncertainty in climate modeling, so better understanding the role of clouds in generating the climatologies and dynamics of the Earth's ocean and atmosphere is an important line of research. SPEEDY sacrifices realistic representation of clouds and cloud feedbacks for computational efficiency. Here, we use MOM6 coupled to AM2, which is much improved in its simulation of clouds compared to SPEEDY.

In Chapter 5, we found that including more realistic physical representations of clouds in our modeling studies results in surprising heat transport responses to the addition of meridional boundaries in the ocean. For instance, total heat transport in the tropics changes by about half a petawatt across configurations. We affirm the key role of evaporation in coupling atmospheric heat transport changes to changes in ocean heat transport. Differences in cloud amount that arise from changes in atmospheric circulation responding to different SST patterns in different continental configurations lead to local feedbacks that cause Bjerknes overcompensation of the atmosphere in our model. The radiative effect of clouds and cloud changes exerts a large role in the degree of compensation between atmospheric and ocean meridional heat transport.

A large aspect of this dissertation is the creation of a framework for changing continental configurations in a new coupled model configuration. This model development work can be harnessed to test outstanding questions about the physics of the climate system. There are myriad directions for future work with this modeling setup.

One logical extension of this work which is already underway is subjecting the configurations in Chapter 5 to greenhouse gas forcing. Using these idealized continental configurations to

see how a simplified coupled climate system responds to a doubling of CO<sub>2</sub> can shed light on how the ocean takes up and stores heat, how the SSTs change with an increase of atmospheric CO<sub>2</sub>, and how overturning circulation responds to climate forcing. There are two major ways in which the ocean shapes the climate's transient response to greenhouse gas forcing. The first is through the vertical transport of heat to depth, away from the surface, thus slowing global warming. The second is through the pattern effect (Armour et al. 2013; Zhou et al. 2016; Stevens et al. 2016; Dong et al. 2019). This project would aim to better understand and explore possible answers to the following questions: How does the ocean circulation and its modulation of climate change depend on ocean basin geometry? How robust is the finding that regions with more positive climate feedbacks are also regions of slower surface warming, which leads to an increase in climate sensitivity over time?

Other future directions include delving more deeply into paleoclimate-inspired modeling studies. One could imagine creating idealized continental configurations based on land distributions of the geologic past. Another direction could be to look into the dual sinking exhibited by the *Rockies Wideland* configuration in Chapter 4. With the exception of *Rockies Wideland*, all the continental configurations detailed in this dissertation lack topography on land. Future work could follow past work (Maroon et al. 2015) to explore the impacts of idealized mountain ranges on climate. This model could also be used to test the climate's sensitivity to different ocean passageways, like the Tasman Seaway, or the Panama Seaway (Ferreira et al. 2018).

The wide range of possible directions speaks to the contribution of this dissertation to the field of climate dynamics. The work done here to develop a novel coupled model configuration with the capacity to create idealized continental configurations can be extended to answer a whole host of fundamental questions about how geometry shapes ocean circulation and climate. Moreover, the work presented in this dissertation challenges the idea that findings from more idealized climate models can be applied directly to the behavior of full complexity models and, by extension, to nature. Here we see that model findings must be considered carefully, and that simplified representations do not necessarily provide theories that can easily disentangle the complex physics of the full climate system. After all, the multiple spheres of the global climate can interact in surprising ways. While this thesis helps elucidate many key features of the climate system, it also highlights that there is no end in sight to the mysteries of our planet.

## References

- Adcroft, Alistair et al. (2019). "The GFDL global ocean and sea ice model OM4. 0: Model description and simulation features". In: *Journal of Advances in Modeling Earth Systems* 11.10, pp. 3167–3211.
- Armour, Kyle C (2017). "Energy budget constraints on climate sensitivity in light of inconstant climate feedbacks". In: *Nature Climate Change* 7.5, pp. 331–335.
- Armour, Kyle C, Cecilia M Bitz, and Gerard H Roe (2013). "Time-varying climate sensitivity from regional feedbacks". In: *Journal of Climate* 26.13, pp. 4518–4534.
- Balaji, V (2012). "The flexible modeling system". In: *Earth System Modelling- Volume 3*. Springer, pp. 33–41.
- Bell, Michael J (2015). "Meridional overturning circulations driven by surface wind and buoyancy forcing". In: *Journal of Physical Oceanography* 45.11, pp. 2701–2714.
- Bjerknes, Jacob (1964). "Atlantic air-sea interaction". In: *Advances in geophysics*. Vol. 10. Elsevier, pp. 1–82.
- Bryan, Frank (1987). "Parameter sensitivity of primitive equation ocean general circulation models". In: *Journal of Physical Oceanography* 17.7, pp. 970–985.
- Buckley, Martha W and John Marshall (2016). "Observations, inferences, and mechanisms of the Atlantic Meridional Overturning Circulation: A review". In: *Reviews of Geophysics* 54.1, pp. 5–63.
- Butler, ED et al. (2016). "Reconstructing global overturning from meridional density gradients". In: *Climate Dynamics* 46.7-8, pp. 2593–2610.
- Cessi, Paola and CS Jones (2017). "Warm-route versus cold-route interbasin exchange in the meridional overturning circulation". In: *Journal of Physical Oceanography* 47.8, pp. 1981–1997.
- Czaja, Arnaud (2009). "Atmospheric control on the thermohaline circulation". In: *Journal of physical oceanography* 39.1, pp. 234–247.
- Czaja, Arnaud and J Marshall (2006). "The partitioning of poleward heat transport between the atmosphere and ocean". In: *Journal of the atmospheric sciences* 63.5, pp. 1498–1511.
- De Boer, Agatha M et al. (2010). "Meridional density gradients do not control the Atlantic overturning circulation". In: *Journal of Physical Oceanography* 40.2, pp. 368–380.
- De Boer, AM, JR Toggweiler, and DM Sigman (2008). "Atlantic dominance of the meridional overturning circulation". In: *Journal of Physical Oceanography* 38.2, pp. 435–450.
- Delworth, Thomas L and Keith W Dixon (2006). "Have anthropogenic aerosols delayed a greenhouse gas-induced weakening of the North Atlantic thermohaline circulation?" In: *Geophysical Research Letters* 33.2.
- Dong, Yue et al. (2019). "Attributing historical and future evolution of radiative feedbacks to regional warming patterns using a Green's function approach: The preeminence of the western Pacific". In: *Journal of Climate* 32.17, pp. 5471–5491.
- Donohoe, Aaron et al. (2013). "The relationship between ITCZ location and cross-equatorial atmospheric heat transport: From the seasonal cycle to the Last Glacial Maximum". In: *Journal of Climate* 26.11, pp. 3597–3618.
- Drijfhout, Sybren, Geert Jan Van Oldenborgh, and Andrea Cimatoribus (2012). "Is a decline of AMOC causing the warming hole above the North Atlantic in observed and modeled warming patterns?" In: *Journal of Climate* 25.24, pp. 8373–8379.

- Emile-Geay, Julien et al. (2003). "Warren revisited: Atmospheric freshwater fluxes and "Why is no deep water formed in the North Pacific"?". In: *Journal of Geophysical Research: Oceans* 108.C6.
- Enderton, Daniel and J Marshall (2009). "Explorations of atmosphere–ocean–ice climates on an aquaplanet and their meridional energy transports". In: *Journal of Atmospheric Sciences* 66.6, pp. 1593–1611.
- Fairall, Chris W et al. (2003). "Bulk parameterization of air–sea fluxes: Updates and verification for the COARE algorithm". In: *Journal of climate* 16.4, pp. 571–591.
- Fajber, Robert et al. (2023). "Atmospheric heat transport is governed by meridional gradients in surface evaporation in modern-day earth-like climates". In: *Proceedings of the National Academy of Sciences* 120.25, e2217202120.
- Ferrari, Raffaele and David Ferreira (2011). "What processes drive the ocean heat transport?" In: *Ocean Modelling* 38.3-4, pp. 171–186.
- Ferreira, David, J Marshall, and Jean-Michel Campin (2010). "Localization of Deep Water Formation: Role of Atmospheric Moisture Transport and Geometrical Constraints on Ocean Circulation". In: *Journal of Climate* 23.6, pp. 1456–1476.
- Ferreira, David et al. (2018). "Atlantic-Pacific asymmetry in deep water formation". In: *Annual Review of Earth and Planetary Sciences*.
- Frierson, Dargan MW et al. (2013). "Contribution of ocean overturning circulation to tropical rainfall peak in the Northern Hemisphere". In: *Nature Geoscience* 6.11, pp. 940–944.
- Ganachaud, Alexandre and Carl Wunsch (2000). "Improved estimates of global ocean circulation, heat transport and mixing from hydrographic data". In: *Nature* 408.6811, pp. 453–457.
- Gent, Peter R and James C McWilliams (1990). "Isopycnal mixing in ocean circulation models". In: *Journal of Physical Oceanography* 20.1, pp. 150–155.
- GFDL, Global Atmospheric Model Development Team et al. (2004). "The new GFDL global atmosphere and land model AM2–LM2: Evaluation with prescribed SST simulations". In: *Journal of Climate* 17.24, pp. 4641–4673.
- Gnanadesikan, Anand (1999). "A simple predictive model for the structure of the oceanic pycnocline". In: *Science* 283.5410, pp. 2077–2079.
- Green, Brian, J Marshall, and A Donohoe (2017). "Twentieth century correlations between extratropical SST variability and ITCZ shifts". In: *Geophysical Research Letters* 44.17, pp. 9039–9047.
- Griesel, Alexa and Miguel Angel Morales Maqueda (2006). "The relation of meridional pressure gradients to North Atlantic deep water volume transport in an ocean general circulation model". In: *Climate Dynamics* 26.7–8, pp. 781–799.
- Held, IM et al. (2019). "Structure and performance of GFDL's CM4. 0 climate model". In: *Journal of Advances in Modeling Earth Systems* 11.11, pp. 3691–3727.
- Held, Isaac M (2005). "The gap between simulation and understanding in climate modeling". In: *Bulletin of the American Meteorological Society* 86.11, pp. 1609–1614.
- Hu, Aixue et al. (2015). "Effects of the Bering Strait closure on AMOC and global climate under different background climates". In: *Progress in Oceanography* 132, pp. 174–196.
- Jackson, L, R Hallberg, and S Legg (2008). "A parameterization of shear-driven turbulence for ocean climate models". In: *Journal of Physical Oceanography* 38.5, pp. 1033–1053.

- Jeevanjee, Nadir et al. (2017). "A perspective on climate model hierarchies". In: *Journal of Advances in Modeling Earth Systems* 9.4, pp. 1760–1771.
- Johnson, Helen L and David P Marshall (2002). "A theory for the surface Atlantic response to thermohaline variability". In: *Journal of Physical Oceanography* 32.4, pp. 1121–1132.
- Johnson, Helen L et al. (2019). "Recent contributions of theory to our understanding of the Atlantic Meridional Overturning Circulation". In: *Journal of Geophysical Research: Oceans* 124.8, pp. 5376–5399.
- Jones, C Spencer and Paola Cessi (2016). "Interbasin transport of the meridional overturning circulation". In: *Journal of Physical Oceanography* 46.4, pp. 1157–1169.
- Jones, CS and Paola Cessi (2017). "Size matters: Another reason why the Atlantic is saltier than the Pacific". In: *Journal of Physical Oceanography* 47.11, pp. 2843–2859.
- Kaspi, Yohai and Tapio Schneider (2011). "Winter cold of eastern continental boundaries induced by warm ocean waters". In: *Nature* 471.7340, pp. 621–624.
- Kostov, Yavor, Kyle C Armour, and J Marshall (2014). "Impact of the Atlantic meridional overturning circulation on ocean heat storage and transient climate change". In: *Geophysical Research Letters* 41.6, pp. 2108–2116.
- Kuhlbrodt, Till et al. (2007). "On the driving processes of the Atlantic meridional overturning circulation". In: *Reviews of Geophysics* 45.2.
- Large, WG and SG Yeager (2004). "Diurnal to decadal global forcing for ocean and sea-ice models: the data sets and flux climatologies. NCAR Technical Note". In: *National Center for Atmospheric Research* 11, pp. 324–336.
- Liu, Zhengyu et al. (2016). "A theory for Bjerknes compensation: The role of climate feedback". In: *Journal of Climate* 29.1, pp. 191–208.
- Lumpkin, Rick and Kevin Speer (2007). "Global ocean meridional overturning". In: *Journal of Physical Oceanography* 37.10, pp. 2550–2562.
- Maroon, Elizabeth (2016). "The Roles of Land and Orography on Precipitation and Ocean Circulation in Global Climate Models". PhD thesis. University of Washington.
- Maroon, Elizabeth A, Dargan MW Frierson, and David S Battisti (2015). "The tropical precipitation response to Andes topography and ocean heat fluxes in an aquaplanet model". In: *Journal of Climate* 28.1, pp. 381–398.
- Marotzke, Jochem (1997). "Boundary mixing and the dynamics of three-dimensional thermohaline circulations". In: *Journal of Physical Oceanography* 27.8, pp. 1713–1728.
- Marshall, J and T Radko (2003). "Residual-mean solutions for the Antarctic Circumpolar Current and its associated overturning circulation". In: *Journal of Physical Oceanography* 33.11, pp. 2341–2354.
- Marshall, J et al. (2007). "Mean climate and variability of the atmosphere and ocean on an aquaplanet". In: *Journal of the Atmospheric Sciences* 64.12, pp. 4270–4286.
- Marshall, J et al. (2014). "The ocean's role in setting the mean position of the Inter-Tropical Convergence Zone". In: *Climate Dynamics* 42.7-8, pp. 1967–1979.
- Marshall, John and Kevin Speer (2012). "Closure of the meridional overturning circulation through Southern Ocean upwelling". In: *Nature Geoscience* 5.3, pp. 171–180.
- Molteni, Franco (2003). "Atmospheric simulations using a GCM with simplified physical parametrizations. I: Model climatology and variability in multi-decadal experiments". In: *Climate Dynamics* 20.2, pp. 175–191.

- Nadeau, Louis-Philippe and Malte F Jansen (2020). “Overturning circulation pathways in a two-basin ocean model”. In: *Journal of Physical Oceanography* 50.8, pp. 2105–2122.
- Newsom, Emily R and Andrew F Thompson (2018). “Reassessing the role of the Indo-Pacific in the ocean’s global overturning circulation”. In: *Geophysical Research Letters* 45.22, pp. 12–422.
- Nilsson, Johan, Göran Broström, and Gösta Walin (2003). “The thermohaline circulation and vertical mixing: Does weaker density stratification give stronger overturning?” In: *Journal of Physical Oceanography* 33.12, pp. 2781–2795.
- Nilsson, Johan et al. (2013). “Ocean basin geometry and the salinification of the Atlantic Ocean”. In: *Journal of climate* 26.16, pp. 6163–6184.
- Nilsson, Johan et al. (2021). “Is the Surface Salinity Difference between the Atlantic and Indo-Pacific a Signature of the Atlantic Meridional Overturning Circulation?” In: *Journal of Physical Oceanography* 51.3, pp. 769–787.
- Oldenburg, Dylan et al. (2021). “Mechanisms of low-frequency variability in North Atlantic Ocean heat transport and AMOC”. In: *Journal of Climate* 34.12, pp. 4733–4755.
- Palter, Jaime B (2015). “The role of the Gulf Stream in European climate”. In: *Annual review of marine science* 7, pp. 113–137.
- Park, Young-Gyu and Kirk Bryan (2000). “Comparison of thermally driven circulations from a depth-coordinate model and an isopycnal-layer model. Part I: Scaling-law sensitivity to vertical diffusivity”. In: *Journal of Physical Oceanography* 30.3, pp. 590–605.
- Ragen, Zho et al. (Mar. 2024). *MOM6 Topography*. Version 1.0.0. URL: [https://github.com/s-ragen/MOM6\\_topography.git](https://github.com/s-ragen/MOM6_topography.git).
- Rahmstorf, Stefan (1996). “On the freshwater forcing and transport of the Atlantic thermohaline circulation”. In: *Climate Dynamics* 12.12, pp. 799–811.
- Reed, RK and PJ Stabeno (1997). “Long-term measurements of flow near the Aleutian Islands”. In: *Journal of Marine Research* 55.3, pp. 565–575.
- Reichl, Brandon G and R Hallberg (2018). “A simplified energetics based planetary boundary layer (ePBL) approach for ocean climate simulations.” In: *Ocean Modelling* 132, pp. 112–129.
- Reid Jr, Joseph L (1961). “On the temperature, salinity, and density differences between the Atlantic and Pacific oceans in the upper kilometre”. In: *Deep Sea Research (1953)* 7.4, pp. 265–275.
- Robinson, Allan and Henry Stommel (1959). “The oceanic thermocline and the associated thermohaline circulation 1”. In: *Tellus* 11.3, pp. 295–308.
- Rose, Brian EJ and J Marshall (2009). “Ocean heat transport, sea ice, and multiple climate states: Insights from energy balance models”. In: *Journal of the atmospheric sciences* 66.9, pp. 2828–2843.
- Rotstayn, Leon D (1997). “A physically based scheme for the treatment of stratiform clouds and precipitation in large-scale models. I: Description and evaluation of the microphysical processes”. In: *Quarterly Journal of the Royal Meteorological Society* 123.541, pp. 1227–1282.
- Sabine, Christopher L et al. (2004). “The oceanic sink for anthropogenic CO<sub>2</sub>”. In: *science* 305.5682, pp. 367–371.

- Schmittner, Andreas, Mojib Latif, and Birgit Schneider (2005). “Model projections of the North Atlantic thermohaline circulation for the 21st century assessed by observations”. In: *Geophysical research letters* 32.23.
- Shao, Andrew E et al. (2020). “A General-Coordinate, Nonlocal Neutral Diffusion Operator”. In: *Journal of Advances in Modeling Earth Systems* 12.12, e2019MS001992.
- Sijp, Willem P and Matthew H England (2009). “Southern Hemisphere westerly wind control over the ocean’s thermohaline circulation”. In: *Journal of Climate* 22.5, pp. 1277–1286.
- Sijp, Willem P et al. (2012). “The key role of the western boundary in linking the AMOC strength to the north–south pressure gradient”. In: *Journal of physical oceanography* 42.4, pp. 628–643.
- Sinha, Bablu et al. (2012). “Mountain ranges favour vigorous Atlantic meridional overturning”. In: *Geophysical Research Letters* 39.2.
- Smethie Jr, William M and Rana A Fine (2001). “Rates of North Atlantic Deep Water formation calculated from chlorofluorocarbon inventories”. In: *Deep Sea Research Part I: Oceanographic Research Papers* 48.1, pp. 189–215.
- Speer, Kevin and Eli Tziperman (1992). “Rates of water mass formation in the North Atlantic Ocean”. In: *Journal of Physical Oceanography* 22.1, pp. 93–104.
- Stevens, Bjorn et al. (2016). “Prospects for narrowing bounds on Earth’s equilibrium climate sensitivity”. In: *Earth’s Future* 4.11, pp. 512–522.
- Stommel, Henry (1961). “Thermohaline convection with two stable regimes of flow”. In: *Tellus* 13.2, pp. 224–230.
- Stone, Peter H (1978). “Constraints on dynamical transports of energy on a spherical planet”. In: *Dynamics of atmospheres and oceans* 2.2, pp. 123–139.
- Straneo, Fiammetta (2006). “On the connection between dense water formation, overturning, and poleward heat transport in a convective basin”. In: *Journal of Physical Oceanography* 36.9, pp. 1822–1840.
- Sun, Shantong, Andrew F Thompson, and Ian Eisenman (2020). “Transient overturning compensation between Atlantic and Indo-Pacific basins”. In: *Journal of Physical Oceanography* 50.8, pp. 2151–2172.
- Sutton, Rowan T and Daniel LR Hodson (2005). “Atlantic Ocean forcing of North American and European summer climate”. In: *science* 309.5731, pp. 115–118.
- Sverdrup, Harald Ulrich (1947). “Wind-driven currents in a baroclinic ocean; with application to the equatorial currents of the eastern Pacific”. In: *Proceedings of the National Academy of Sciences of the United States of America* 33.11, p. 318.
- Talley, Lynne D (2003). “Shallow, intermediate, and deep overturning components of the global heat budget”. In: *Journal of Physical oceanography* 33.3, pp. 530–560.
- (2008). “Freshwater transport estimates and the global overturning circulation: Shallow, deep and throughflow components”. In: *Progress in Oceanography* 78.4, pp. 257–303.
- Thorpe, RB et al. (2001). “Mechanisms determining the Atlantic thermohaline circulation response to greenhouse gas forcing in a non-flux-adjusted coupled climate model”. In: *Journal of Climate* 14.14, pp. 3102–3116.
- Tiedtke, M (1993). “Representation of clouds in large-scale models”. In: *Monthly Weather Review* 121.11, pp. 3040–3061.
- Trenberth, Kevin E and Julie M Caron (2001). “Estimates of meridional atmosphere and ocean heat transports”. In: *Journal of Climate* 14.16, pp. 3433–3443.

- Vellinga, Michael and Richard A Wood (2002). "Global climatic impacts of a collapse of the Atlantic thermohaline circulation". In: *Climatic change* 54.3, pp. 251–267.
- Wang, Xiaoli, Peter H Stone, and Jochem Marotzke (1995). "Poleward heat transport in a barotropic ocean model". In: *Journal of physical oceanography* 25.2, pp. 256–265.
- Warren, Bruce A (1983). "Why is no deep water formed in the North Pacific?" In: *Journal of Marine Research* 41.2, pp. 327–347.
- Watson, Andrew J, Geoffrey K Vallis, and Maxim Nikurashin (2015). "Southern Ocean buoyancy forcing of ocean ventilation and glacial atmospheric CO<sub>2</sub>". In: *Nature Geoscience* 8.11, pp. 861–864.
- Weijer, Wilbert et al. (1999). "Impact of interbasin exchange on the Atlantic overturning circulation". In: *Journal of Physical Oceanography* 29.9, pp. 2266–2284.
- Wijffels, Susan E et al. (1992). "Transport of freshwater by the oceans". In: *J. Phys. Oceanogr.* 22.2, pp. 155–162.
- Winton, Michael et al. (2013). "Connecting changing ocean circulation with changing climate". In: *Journal of climate* 26.7, pp. 2268–2278.
- Wolfe, Christopher L and Paola Cessi (2010). "What sets the strength of the middepth stratification and overturning circulation in eddying ocean models?" In: *Journal of Physical Oceanography* 40.7, pp. 1520–1538.
- (2011). "The adiabatic pole-to-pole overturning circulation". In: *Journal of Physical Oceanography* 41.9, pp. 1795–1810.
  - (2014). "Salt feedback in the adiabatic overturning circulation". In: *Journal of Physical Oceanography* 44.4, pp. 1175–1194.
- Woollings, Tim et al. (2012). "Response of the North Atlantic storm track to climate change shaped by ocean–atmosphere coupling". In: *Nature Geoscience* 5.5, pp. 313–317.
- Wright, Daniel G (1997). "An equation of state for use in ocean models: Eckart's formula revisited". In: *Journal of Atmospheric and Oceanic Technology* 14.3, pp. 735–740.
- Yang, Haijun and Qin Wen (2020). "Investigating the role of the Tibetan Plateau in the formation of Atlantic meridional overturning circulation". In: *Journal of Climate* 33.9, pp. 3585–3601.
- Youngs, Madeleine K, Raffaele Ferrari, and Glenn R Flierl (2020). "Basin-Width Dependence of Northern Deep Convection". In: *Geophysical Research Letters* 47.15, e2020GL089135.
- Zelinka, Mark D et al. (2017). "Clearing clouds of uncertainty". In: *Nature Climate Change* 7.10, pp. 674–678.
- Zelinka, Mark D et al. (2020). "Causes of higher climate sensitivity in CMIP6 models". In: *Geophysical Research Letters* 47.1, e2019GL085782.
- Zhou, Chen, Mark D Zelinka, and Stephen A Klein (2016). "Impact of decadal cloud variations on the Earth's energy budget". In: *Nature Geoscience* 9.12, pp. 871–874.